

University of Windsor

Scholarship at UWindor

Electronic Theses and Dissertations

Theses, Dissertations, and Major Papers

1-31-2023

Numerical Thermal Performance Analysis of a Phase Change Material-Air-Liquid Heat Exchanger Using Latent Heat Thermal Energy Storage

Mahdi Momeni
University of Windsor

Follow this and additional works at: <https://scholar.uwindsor.ca/etd>



Part of the [Mechanical Engineering Commons](#)

Recommended Citation

Momeni, Mahdi, "Numerical Thermal Performance Analysis of a Phase Change Material-Air-Liquid Heat Exchanger Using Latent Heat Thermal Energy Storage" (2023). *Electronic Theses and Dissertations*. 8936. <https://scholar.uwindsor.ca/etd/8936>

This online database contains the full-text of PhD dissertations and Masters' theses of University of Windsor students from 1954 forward. These documents are made available for personal study and research purposes only, in accordance with the Canadian Copyright Act and the Creative Commons license—CC BY-NC-ND (Attribution, Non-Commercial, No Derivative Works). Under this license, works must always be attributed to the copyright holder (original author), cannot be used for any commercial purposes, and may not be altered. Any other use would require the permission of the copyright holder. Students may inquire about withdrawing their dissertation and/or thesis from this database. For additional inquiries, please contact the repository administrator via email (scholarship@uwindsor.ca) or by telephone at 519-253-3000ext. 3208.

Numerical thermal performance analysis of a phase change material-air-liquid heat exchanger using latent heat thermal energy storage.

By

Mahdi Momeni

A Thesis
Submitted to the Faculty of Graduate Studies
through the Department of Mechanical, Automotive, and Materials Engineering
in Partial Fulfillment of the Requirements for
the Degree of Master of Applied Science
at the University of Windsor

Windsor, Ontario, Canada

2023

© 2023 Mahdi Momeni

Numerical thermal performance analysis of a phase change material-air-liquid heat exchanger using latent heat thermal energy storage.

By

Mahdi Momeni

APPROVED BY:

B. Balasingam
Department of Electrical and Computer Engineering

O. Jianu
Department of Mechanical, Automotive, and Materials Engineering

A. Fartaj, Advisor
Department of Mechanical, Automotive, and Materials Engineering

January 18, 2023

DECLARATION OF CO-AUTHORSHIP / PREVIOUS PUBLICATION

I. Co-Authorship

I hereby declare that this thesis incorporates the findings of a numerical research with the supervision of Professor A. Fartaj at the University of Windsor. This work is a collaboration with Dr. S. Askar and Mr. S. Jalilian. I confirm that I am the primary author and have the credit authorship contribution in conceptualization, methodology, software, investigation, validation, visualization, writing - original draft, writing - review & editing, data analysis, and graphing. Professor Fartaj contributed to supervision, conceptualization, visualization, methodology, writing - review & editing. The contributions of Dr. Askar was in the assistance in result description and review in the journal paper providing comments and suggestions for the third journal paper which is in under review process. Mr. Jalilian's contribution is in the review and editing of the second paper (accepted) with comments and suggestions.

I am aware of the University of Windsor Senate Policy on Authorship, and I certify that I have properly acknowledged the contribution of other researchers to my thesis and have obtained written permission from each of the co-author(s) to include the above material(s) in my thesis.

I certify that, with the above qualification, this thesis, and the research to which it refers, is the product of my own work.

II. Previous Publication

This thesis includes [3] original papers that have been previously published/submitted to journals for publication, as follows:

Publication title	Publication status
<p>Mahdi Momeni, Amir Fartaj, 2023, “Numerical thermal performance analysis of a phase change material-to-air and liquid heat exchanger implementing latent heat thermal energy storage”. Journal of Energy Storage, Volume 58, 106363, ISSN2352-152X, https://doi.org/10.1016/j.est.2022.106363.</p>	<p>Published</p>
<p>Mahdi Momeni, Saman Jalilian, Amir Fartaj, 2022, “Heat Transfer Analysis of a Crossflow Minichannel Heat Exchanger Based on Air and Liquid Flow Implementing PCM as Latent Heat Thermal Energy Storage”. Proceedings of the 10th International Conference on Fluid Flow, Heat and Mass Transfer.</p>	<p>Accepted</p>
<p>Mahdi Momeni, Serena Askar, Amir Fartaj, “Thermal performance enhancement of a compact two-fluid phase change material heat exchanger using latent heat cold thermal energy storage”. Applied Thermal Engineering, ATE-S-22-08392.</p>	<p>Under review</p>

I certify that I have obtained a written permission from the copyright owner(s) to include the above published material(s) in my thesis. I certify that the above material describes work completed during my registration as a graduate student at the University of Windsor.

III. General

I declare that, to the best of my knowledge, my thesis does not infringe upon anyone’s copyright nor violate any proprietary rights and that any ideas, techniques, quotations, or any other material from the work of other people included in my thesis, published or

otherwise, are fully acknowledged in accordance with the standard referencing practices. Furthermore, to the extent that I have included copyrighted material that surpasses the bounds of fair dealing within the meaning of the Canada Copyright Act, I certify that I have obtained a written permission from the copyright owner(s) to include such material(s) in my thesis.

I declare that this is a true copy of my thesis, including any final revisions, as approved by my thesis committee and the Graduate Studies office, and that this thesis has not been submitted for a higher degree to any other University or Institution.

ABSTRACT

Due to the mismatches in energy supply and demand in thermal systems, employing latent heat thermal energy storage using phase change materials (PCMs) is a reliable and effective solution. Compact heat exchangers are an essential component of thermal management systems in several industries, such as the HVAC industry, automotive, and many others. In this regard, this paper introduces a novel PCM-air-liquid heat exchanger to increase thermal system performance by providing a hybrid heat source to the airside. A novel numerical work based on multiphysics coupling of heat transfer and double fluid flow and phase change within a complex geometry is represented. Numerical heat transfer analysis is performed on the model based on three-dimensional computational fluid dynamics (CFD) simulation. In order to make a thorough thermal performance assessment, the dynamic behavior of the system is investigated for the heat exchanger in two studies of air heating and cooling mode and conducted for the PCM charging and discharging processes. Furthermore, the effect of airside flow variation on the thermal response of the system is studied, and the results are discussed based on the fluids temperature, heat transfer rate, and the PCM phase transition procedure. It is demonstrated from the results attained that the PCM can store excess thermal energy from the working fluid during the charging process and releases it to the airside during the discharging process. It is observed that the heating load of 323 kJ for the air-heating study and cooling load of 188 kJ for the air-cooling study is stored during the PCM charging process. This thermal energy provides up to 6 and 9 minutes of extra airside heating and cooling time during the PCM discharging process for the studies, respectively. The share of PCM latent component of the airside heat transfer is determined to be at an average of 51% between all simulation cases. It is also observed that by increasing the airflow rate, the discharged heating/cooling load is decreased slightly, and the heating/cooling time is reduced notably. The presented thermal energy storage system offers a unique solution for the start-stop function implemented in many hybrid and electric vehicles. During short periods of engine shutdown, the system could provide passenger thermal comfort and enable effective energy savings.

DEDICATION

*Dedicated to
my family,
who offers me a continuous support*

ACKNOWLEDGEMENTS

As a first and foremost, I would like to express my gratitude to the Lord who has enabled me to deal with all the challenging tasks of completing this dissertation thanks to his grace, mercy, and strength.

I would like to express my sincere gratitude and appreciation to my advisor, Prof. Amir Fartaj, for all of his guidance, feedback, and patience during the preparation of my MASc thesis. With the assistance of his vast knowledge and expert guidance, I was able to complete my dissertation successfully.

I extend my gratitude to my advisory committee members, Dr. Jianu and Dr. Balasingam their time, insightful comments and suggestions, and commitment. Special thanks to the chair of defense for facilitating the defense process.

I gratefully acknowledge Dr. Askar for all her time and support during my program and for an effective analysis and feedback during collaborating in our paper publications. I would like to recognize the help of her for her suggestions, comments and kind dedication.

I would like to express my gratitude to the University of Windsor for its support through the Natural Sciences and Engineering Research Council of Canada, NSERC, grant. I would like to express my gratitude to the technical team and secretary of the department of Mechanical engineering for their assistance.

Words cannot express how grateful I am for the support of my mother and father. With all their sincere sacrifices and efforts they made to help me reach to the current position I have in life. I would be unable to accomplish this endeavor without their tremendous understanding, patience, and encouragement.

TABLE OF CONTENTS

DECLARATION OF CO-AUTHORSHIP / PREVIOUS PUBLICATION.....	iii
ABSTRACT	vi
DEDICATION	vii
ACKNOWLEDGEMENTS	viii
LIST OF TABLES	xii
LIST OF FIGURES.....	xiii
NOMENCLATURE / ABBREVIATIONS	xvi
CHAPTER 1 INTRODUCTION	1
1.1 Thermal Analysis of Heat Exchangers	3
1.2 Thermal Energy Storage.....	4
1.2.1. PCM Classification	6
1.2.2. PCM Applications.....	8
1.3 Motivation	10
1.4 Objectives	11
CHAPTER 2 LITERATURE SURVEY.....	13
2.1. Heat Transfer Enhancement of Heat Exchangers.....	13
2.1.1. Enhancement Methods	13
2.1.2. Thermal Analysis of Heat Exchangers.....	14
2.2. Thermal Energy Storage.....	17
2.2.1 Thermal Energy Storage in Heat Exchangers	18
2.3. Scope of the Current Work.....	21
CHAPTER 3 DESIGN AND NUMERICAL MODELING	23
3.1. System Description.....	23
3.1.1. Single Slabbed PCM Heat Exchanger.....	23
3.1.2. Five Slabbed PCM Heat Exchanger.....	25
3.2. Operating Conditions and Assumptions	27

3.3.	PCM Selection	30
3.4.	Numerical Procedure and Boundary Conditions	31
3.5.	Governing Equations	34
CHAPTER 4 GRID INDEPENDENCE STUDY AND MODEL VALIDATION		37
4.1.	Grid Independence Study	37
4.2.	Model Validation	39
4.2.1.	Step 1: Model Validation for Air Heating Heat Exchanger	39
4.2.2.	Step 2: Model Validation for PCM Heat Exchanger	40
CHAPTER 5 RESULTS AND DISCUSSION		43
5.1.	Single Slab PCM Heat Exchanger Air Heating Response	43
5.1.1.	Dynamic Simulation Results	43
5.1.2.	PCM Phase Transition Procedure	46
5.2.	PCM Heat Exchanger Air Heating Results	47
5.2.1.	Transient Simulation Results	47
5.2.1.1.	Fluids Outlet Temperature and PCM Phase Plots	48
5.2.1.2.	Fluids Heat Transfer Rate	57
5.2.1.3.	Share of PCM Latent Heat During Discharging Process	59
5.2.2.	PCM Phase Transition Procedure	61
5.2.3.	Energy Gain Through PCM Passive Air Heating	64
5.3.	PCM Heat Exchanger Air-Cooling Results	66
5.3.1.	Dynamic Thermal Performance Analysis	66
5.3.1.1.	Fluids and PCM Temperature Response	66
5.3.1.2.	Fluids Heat Transfer Rates	73
5.3.2.	PCM Phase Transition Process	75
5.3.3.	Effective Passive Air Cooling Through PCM CTES	77
5.3.3.1.	PCM air cooling performance	78
5.3.3.2.	Latent heat transfer analysis	80
CHAPTER 6 CONCLUSIONS AND RECOMMENDATIONS		83

6.1. Conclusions	83
6.1.1. Air heating study	83
6.1.2. Air cooling study	84
6.2. Recommendations	84
REFERENCES	86
VITA AUCTORIS	91

LIST OF TABLES

Table 3.1: Design specifications of the single slabbed PCM-air-liquid heat exchanger based on [28].	24
Table 3.2. Detailed modeling design specifications for the five-slabbed PCM-air-liquid liquid heat exchanger [28, 60].	26
Table 3.3. Study 1 operating conditions.	27
Table 3.4. Study 2 operating conditions.	28
Table 3.5. Study 3 operating conditions.	29
Table 3.6. Thermophysical properties of the selected PCM for Study 1 and 2 [61].	30
Table 3.7. PCM thermophysical properties for Study 3 [15].	31
Table 4.1. Grid independence study results.	38
Table 5.1. Comparison of crucial results attained from the simulation cases.	66
Table 5.2. Key PCM air cooling results attained during the discharging process for different simulation cases.	80

LIST OF FIGURES

Figure 1.1. Energy use in primary and secondary sectors, 2018 [2].	1
Figure 1.2. Heating process of PCMs [13].	6
Figure 1.3. PCM classification [14].	6
Figure 1.4. Melting temperatures for different PCM groups [16].	7
Figure 1.5. Variuos applications of PCMs [12].	9
Figure 3.1: CAD design of the single-slabbed PCM heat exchanger.	24
Figure 3.2: Circular minnichannels inside HEX slab [6].	24
Figure 3.3. View of the laboratory experimental setup.	25
Figure 3.4. The five slabbed PCM-air-liquid heat exchanger proposed in this study (a) experimental model [60], (b) modeling schematic.	26
Figure 4.1. Generated computational meshes for the five-slabbed PCM-HEX.	38
Figure 4.2: Mesh grid generated for the single-slabbed PCM heat exchanger.	38
Figure 4.3. Model validation for the compact heat exchanger with results attained by Fotowat et al. [28].	40
Figure 4.4. Comparison of transient numerical results with experimental study by Askar et al. [60]	41
Figure 4.5. Model validation plot with experimental Error bars applied.	42
Figure 5.1. Dynamic plots for the operation fluids and PCM for (a) charging process (b) discharging process.	44
Figure 5.2: Fluids heat transfer rates (a) airside heat transfer for charging and discharging process (b) waterside heat transfer for charging process.	46
Figure 5.3: Phase fraction contours of the PCM melting and solidification process.	47
Figure 5.4. Fluids temperature and PCM phase fraction plots for charging and discharging processes for simulation (a) Case 1 (b) Case 2 (c) Case 3.	51
Figure 5.5. 3D illustration of airside and water flow temperature distribution and PCM solid fraction for different times of the charging process for Case 1 simulation.	52

Figure 5.6. Steady state temperature distribution for the heat exchanger charging process for Case 1 (a) slabs, fins and PCM domain (b) air streamlines passing through the fins.	54
Figure 5.7. Fins temperature distribution by the end of the charging process for Case 1 (a) frontal view (b) backside view.	55
Figure 5.8. Hot heat transfer fluid minichannels temperature distribution by the end of the charging process for Case 1 (a) frontal view (b) backside view.	56
Figure 5.9. 2D Temperature distribution of the cut plain through the middle of the heat exchanger by the end of the charging process for Case 1.	57
Figure 5.10. Airside heat transfer rate during the charging and discharging process.	58
Figure 5.11. Water side heat transfer rate for the charging process.	59
Figure 5.12. Release of the stored latent heat in the discharge process for different simulation cases.	60
Figure 5.13. Latent and sensible heat rate trends through the discharge process for simulation Case 1.	61
Figure 5.14. 2D solid phase contours of the PCM melting and solidification for Case 1 simulation.	63
Figure 5.15. 2D PCM temperature contours for Case 1 simulation (a) charging process (b) discharging process.	63
Figure 5.16. Discharge heat transfer comparison between cases with and without PCMs.	65
Figure 5.17. Dynamic air outlet temperature responses during the charging and discharging processes for three simulation cases.	68
Figure 5.18. Cold fluid outlet temperature.	68
Figure 5.19. PCM average temperature.	69
Figure 5.20. PCM average solid phase fraction transition.	69
Figure 5.21. Graphic temperature distribution of the PCM-HEX at the end of the charging process for simulation Case 1.	70
Figure 5.22. Fins temperature distribution by the end of the charging process for Case 1 (a) frontal view (b) backside view.	71
Figure 5.23. Cold heat transfer fluid minichannels temperature distribution by the end of the charging process for Case 1 (a) frontal view (b) backside view.	72

Figure 5.24. Airside heat transfer rates during the charging and discharging processes. .	74
Figure 5.25. Cold fluid heat transfer rate during the charging process.	75
Figure 5.26. Phase fraction contours of the PCM domain during the charging and discharging processes for Case1.....	76
Figure 5.27. Temperature distribution through the PCM block for Case1.....	77
Figure 5.28. Discharged air outlet temperature comparison for Case 1 of with and without PCM.	78
Figure 5.29. PCM effect on the discharged air-cooling rate for Case 1.....	79
Figure 5.30. Trends of PCM sensible and latent heat rates in Case 1 discharging process.	81

NOMENCLATURE / ABBREVIATIONS

A_m	Mushy zone constant
C_p	Specific heat capacity (J/kg.K)
\vec{g}	Gravitational acceleration (m/s ²)
h	Enthalpy (J)
H	Total enthalpy (J)
k	Thermal conductivity (W/m ² .K)
\vec{n}	Normal boundary vector
P	Pressure (Pa)
\vec{q}	Heat flux vector
\vec{S}	Source term of momentum (m/s)
T	Temperature (°c)
\vec{V}	Velocity vector (m/s)

Abbreviations

CAD	Computer-aided design
CFD	Computational fluid dynamics
CTES	Cold thermal energy storage
HTF	Heat transfer fluid
HVAC	Heating, ventilation, and air conditioning
LHTES	Latent heat thermal energy storage
PCM	Phase change material
PCM-HEX	PCM heat exchanger
TES	Thermal energy storage

Greek symbols

α_m	Mass fraction
β	Thermal expansion coefficient (1/K)
ε	Numerical constant
ρ	Density (kg/m ³)
θ	Liquid fraction
μ	Dynamic viscosity (Pa/s)

∇	Gradient operator
Γ	Corresponding latent heat (J)

Subscripts

0	Initial state
atm	Atmosphere
m	Melting point
ref	Reference state

CHAPTER 1

INTRODUCTION

Strong demand for energy supply is resulting from the continuous growth of the global economy. It has been projected that world energy consumption will increase by 50% between the years 2020 and 2050 according to the International Energy Outlook [1] published by the U.S. Energy Information Administration (EIA). Due to the current limitations of energy resources, fluctuating prices of energy resources, and the significant effect of energy use on global warming, researchers have developed alternative energy sources and developed alternatives to technologies with high environmental impact or high costs in order to avoid these challenges. The reason for this is due to the potential risk of global warming and climate change posed by the increase in energy use. A major factor in these risks is the release of greenhouse gases (GHG) as a result of the burning of fossil fuels, such as in the transportation sector. In Canada, the transportation sector is the second largest consumer of energy after industry, Figure 1.1. It contributes significantly to greenhouse gas emissions, with a 28% increase between 2000 and 2019 [2].

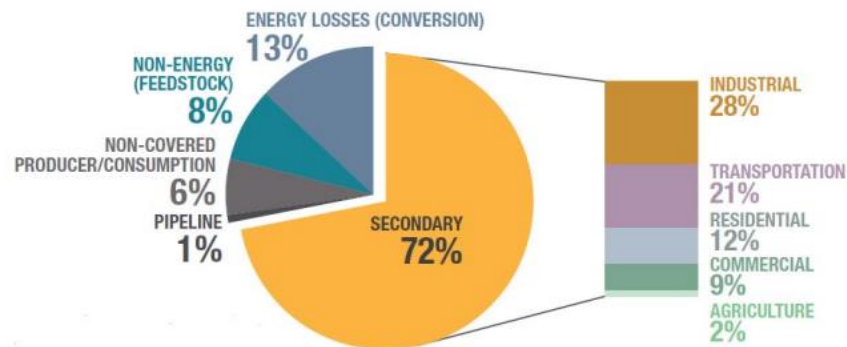


Figure 1.1. Energy use in primary and secondary sectors, 2018 [2].

The continuous increase in energy consumption is a challenge to the availability of many energy resources. As a result, it is highly recommended that existing energy resources be utilized efficiently. Some automotive systems, such as the Heating, Ventilation, and Air Conditioning (HVAC) system, consume considerable amounts of energy and contribute to

greenhouse gas emissions. An air conditioner installed in a vehicle is referred to as Mobile Air Conditioning (MAC). The energy use from MAC systems is expected to exceed 5.7 million barrels of oil per day by 2050 [3]. Additionally, the MAC contributes to GHG emissions through its energy consumption, reducing the driving range of electric vehicles. However, MAC systems are essential for the comfort of vehicle occupants due to their thermal properties. Enhancing the thermal management system of a vehicle can have a significant impact on the safety of the vehicle, its fuel consumption, its range, as well as the thermal comfort of the passengers. To achieve a balance between the thermal comfort required by passengers and the energy consumption of the MAC system, efficient thermal management and control are necessary. The technology of today has not yet reached a point where it is possible to completely eliminate the need for fossil fuels. As a result, it is essential to perform good energy management to ensure long-term fuel reserves, especially with the increasing concern over the environment.

Over the years, vehicle thermal management, represented by a MAC system, has gained increasing interest in terms of its enhancements and new technologies. This is due to concerns regarding energy consumption, environmental impact, weight and size reductions, as well as an increase in the demand for electric vehicles. The thermal management system in a vehicle ensures that the occupants are comfortable in terms of temperature. Humans are typically satisfied with their thermal environment when they are in thermal comfort. In order to attain thermal comfort, a variety of factors must be considered, including measurable factors, such as air temperature, relative humidity, air velocity, and radiant temperature, as well as personal factors, such as clothing and activity level [4]. Increasing thermal comfort for passengers is a top priority for automotive manufacturers. They are responsible for providing heating, cooling, and ventilation of air through the use of an air conditioning system. An important role played by HVAC technology is to facilitate a comfortable environment for passengers.

1.1 Thermal Analysis of Heat Exchangers

Thermal management systems utilize a heat exchanger as one of the key components for transferring heat between fluids at different temperatures, which is designed to perform a variety of functions. There are a variety of purposes for heat exchangers in a system, including the heat transfer of heat, the cooling of heat, the recovery of heat, the evaporation and condensation of heat, the control of a fluid in a process, etc. Different types of heat exchangers are commonly used in current systems, including shell and tube, automotive radiators, condensers, and heater cores. According to Shah and Sekulic [5], heat exchangers can be classified according to the transfer process, the number of fluids, the compactness of the surface, the construction, the flow arrangement, and the mechanism for transferring heat.

The term surface compactness is used to describe a class of heat exchangers that has a high area density as defined by the amount of surface area available for heat transfer per unit volume. The combination of a high surface area density and a small hydraulic diameter, which allows the fluid to flow into the exchanger, results in an enhanced efficiency within a smaller volume than conventional heat exchangers. Heat exchangers with compact liquid-gas surfaces have a density of $400 \text{ m}^2/\text{m}^3$ or greater. Conversely, a meso heat exchanger is defined as one whose surface area density exceeds $3000 \text{ m}^2/\text{m}^3$ and whose hydraulic diameter is between 100 mm and 1 mm. There are many applications for these types of compact heat exchangers, such as aerospace, cryogenics, power plants, automobiles, and others. They offer many advantages over conventional heat exchangers [6].

Dynamic analysis of heat exchangers has gained considerable attention in recent years for applications that primarily involve heating or cooling for studying the control of fluid outlet temperature. It is necessary to investigate a heat exchanger under variations of inlet conditions for several main reasons. Firstly, to measure reaching the final steady state of the heat exchanger fluids. Secondly, analyzing the heat exchanger's performance after any operation step change is imposed on the system and controlling the fluid's outlet temperature [7]. It is vital to perform a transient analysis to ensure optimal heat transfer and energy efficiency from the heat exchanger [8]. Among different heat exchanger types,

the cross flow heat exchanger is frequently used among various tubular heat exchangers in the industry, and numerous experimental and numerical studies have been conducted [9].

While the heat exchanger is considered the most crucial device for thermal systems, and its performance influences the whole functioning of the thermal system, research has focused on improving the thermal characteristics of heat exchangers [10]. As heat exchangers are indispensable to many industries, it has become a necessity to improve their efficiency and reduce their cost and energy consumption. Researchers have reported different methods of enhancing heat transfer, including extended surfaces, nanofluids, turbulence promoters, surface fluid vibrations, etc. Efficient heat exchanger design such as using minichannels in heat exchangers can improve thermal characteristics, compactness, and energy efficiency contrasted with conventional heat exchangers. As another significant method, enhancing heat exchangers by incorporating thermal energy storage (TES) is a viable solution and has attracted research studies [11]. Using effective methods for TES within a heat exchanger, thermal energy can be stored or released to alleviate peak energy demands or provide extra cooling and heating for thermal processes [10].

1.2 Thermal Energy Storage

In addition to providing an understanding of the transient behavior of the heat exchanger and predicting the temperature of the fluid at its outlet, a solution that is capable of sustaining the extra thermal energy load and dampening the temperature variations due to transient changes must be found. As a result of the search for innovative methods to provide sustainable thermal comfort, TES was developed [12]. The storage of thermal energy can be classified into three types: sensible, latent, and thermochemical. In thermochemical energy storage, the heat generated by a thermal reaction is stored, while sensible energy storage involves a temperature change without a phase change. By integrating phase change materials (PCMs) into heat exchangers, a latent heat thermal energy storage (LHTES), can alleviate a peak energy demand or provide additional cooling and heating for thermal processes.

The use of LHTES in conjunction with the PCM provides a cost-effective way to reduce energy consumption by releasing stored energy as a result of the exchange of heat between the PCM and the process fluid. The PCM is capable of extending the period of operation

when the main heat transfer fluid (HTF) is shut down for short periods, thereby reducing the need to use a power source or batteries in addition to reducing energy consumption. This type of application can be found in vehicles equipped with automatic start-stop function. As soon as a vehicle stops at a red light, the engine as well as the air conditioning compressor cease to operate. It is possible to use a PCM to provide the additional cooling/heating time to ensure that the passenger cabin is at a comfortable temperature during this short period of time while the vehicle is stopped.

A phase change material, also known as PCM, is a material that can change from liquid to solid at a constant temperature by absorbing and releasing thermal energy. A sensible heat transition is accompanied by a temperature change, whereas a latent heat transition does not involve a temperature change. The solid state of a PCM transforms to a liquid state as it absorbs heat and the bond between the atoms is loosened. During freezing, on the other hand, it is the opposite, the PCM releases energy and the molecules arrange themselves to form solids. The latent heat of fusion is the name given to this energy. The mass of each PCM is governed by a latent heat of fusion, which controls the amount of energy to be absorbed or released along with the amount of energy to be released. As for melting and freezing rates, they are determined by the operating conditions.

The heating process of a PCM is illustrated in Figure 1.2. Here, the process begins with a subcooled liquid that undergoes sensible heating until it reaches its melting point. At this point, the material continues to be heated and undergoes a phase change from solid to liquid at a constant temperature. After the liquid is heated, the material reaches its boiling point at an elevated temperature as a result of the liquid heating. The liquid undergoes a phase change to vapor when it reaches the boiling point. This phase change is, however, controlled by the latent heat of vaporization, and any further heating is considered sensible heating.

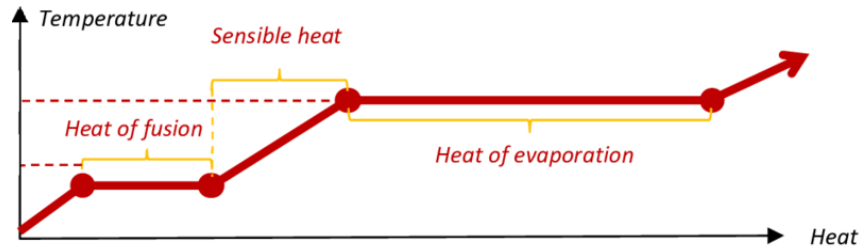


Figure 1.2. Heating process of PCMs [13].

1.2.1. PCM Classification

In spite of the fact that PCMs exist in a wide range of temperatures, all of them can be classified into three distinct groups: organic, inorganic, and eutectic. The following classification is provided by Sharma et al. [14] and can be found in Figure 1.3. The main categories of PCM are summarized below.

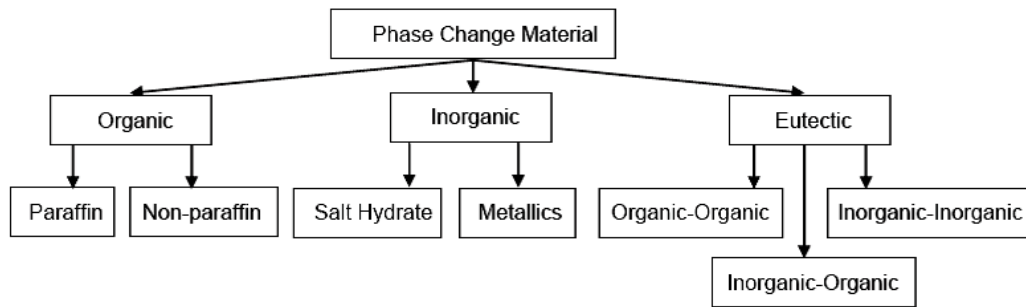


Figure 1.3. PCM classification [14].

The most common type of PCMs are organic PCMs, such as paraffin, fatty acids, and polyethylene glycol. As a result of its availability, affordability, and feasibility, paraffin has been extensively studied in thermal management applications. It is possible to store a large amount of energy using a small mass using organic PCMs due to their high latent heat. In addition, they are capable of being used with a wide variety of materials without deteriorating them and they have a good repeatability for multiple cycles without affecting their performance. In addition, they exhibit a high level of physical and chemical stability. Among the disadvantages of this type of PCM is the low thermal conductivity, which may reduce its effectiveness.

Inorganic PCMs consist of salt hydrates and metallic compounds. In applications requiring high melting temperatures, they are commonly used due to their thermal stability over

repeated cycles. PCMs made of inorganic substances have a higher thermal conductivity than PCMs made of organic substances, and their phase changes occur more rapidly than those made of organic substances. Inorganics are restricted by their irreversible phase change, which requires stirring or chemical addition. They can also corrode when exposed to the environment or interacting with the material of the housing [15].

Eutectic compounds consist of two or more PCM types, which can be organic, inorganic, or both, and possess a single melting point. This type of PCM has the advantage of being able to control its melting point by altering the weight percentage of the components. There is no phase separation or supercooling involved in their solidification or melting. Figure 1.4 represents the melting temperature and enthalpy range of various PCM groups.

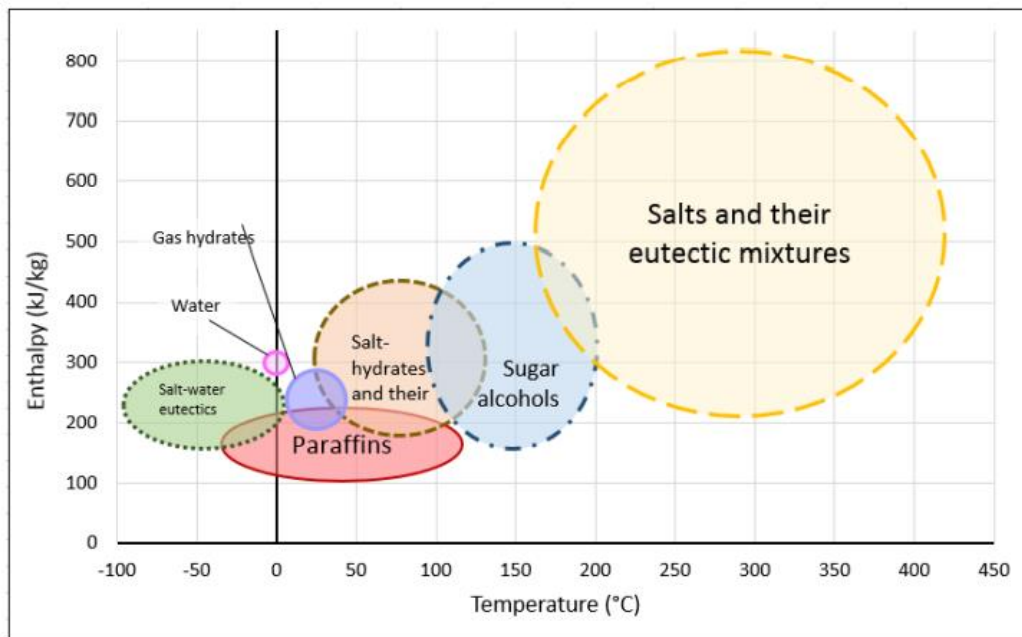


Figure 1.4. Melting temperatures for different PCM groups [16].

A PCM can be classified as one of the groups discussed above. Choosing a specific PCM will involve taking into consideration these characteristics, as well as the temperature range of the application and other factors. Each group of PCMs has its own advantages and disadvantages.

1.2.2. PCM Applications

PCM is gaining increasing interest for a number of reasons, including increased energy costs, environmental concerns, and weight and space limitations. Using PCM as a thermal energy storage device is beneficial in terms of energy efficiency as well as thermal comfort. As a result of the wide range of temperatures involved in many systems, PCM can be used as an energy storage medium for various thermal systems. The use of PCM as cooling storage in buildings is one of these applications. It is possible to use phase change materials to cool a building envelope, an HVAC system, and a solar system. This system stores energy and releases it at a later time, thereby reducing peak load and resulting in smaller HVAC units [17]. In solar systems, PCMs can be used as thermal energy storage devices to store thermal energy for later use. It is possible to apply PCM to the transportation of food, medical supplies, electronics, etc., at the desired temperature while they are being transported. This technology may also be used in the transportation of refrigerated trucks so as to minimize the peak heat transfer rate and maintain the refrigeration equipment for a longer period of time. A PCM can be integrated into an electronic system depending on the temperature range of the application. As a result of absorbing heat at peaks and emitting it at the bottom, the cooling system is minimized. In Figure 1.4, the various applications of PCMs in different thermal systems is shown.



Figure 1.5. Variuos applications of PCMs [12].

Phase change materials are available in a wide range of melting and freezing temperatures. When selecting a PCM for a specific application, it is important to consider its characteristics. A PCM can be selected based on three factors: thermal, chemical, and economic considerations. The important factor in selecting PCMs in numerical investigations is the thermal characteristics of the PCM. These characteristics can include latent heat of fusion, thermal conductivity, density, and melting temperature range. As the latent heat of fusion is measured in (J/g), it is an important factor to consider when selecting a PCM. In order to store a greater amount of thermal energy, a material with a higher energy storage capacity is required. Researchers are continuously investigating different methods to enhance the thermal conductivity of PCMs, since a high thermal conductivity is important for heat transfer performance. The selection of a suitable PCM with suitable characteristics is a significant factor in applying the PCM to thermal management applications.

1.3 Motivation

The availability of energy sources is limited, while the demand for energy is growing continuously. Therefore, many industries require thermal system equipment that can provide a high level of thermal management system performance. Using PCM as a latent heat storage device to reduce energy consumption is an economical way to release the stored energy through the heat exchange from the PCM to the desired fluid. When the main fluid must be shut off for a short time during shutdown time, the PCM reliably extends the operating period, minimizing the need for a power source or batteries.

A comprehensive CFD analysis of a PCM heat exchanger (PCM-HEX) used for air heating and cooling application in this study is motivated by the following reasons:

- Most of the published research focus on PCM heat exchangers based on single fluid flow operation.
- Studies regarding the implementation of thermal energy storage in compact heat exchangers for real-world thermal management applications to provide a sustainable energy storage medium for heating and cooling purposes are scarce in the open literature.
- No numerical study has yet to be introduced in the open literature to investigate hybrid heating for the airside in a compact PCM-air-liquid heat exchanger which implements thermal energy storage and operates based on two operational fluids.
- Due to experimental challenges in constructing and compiling a well-equipped experimental setup to investigate the use of PCM in compact heat exchangers and obtain in-depth thermal performance results, the need for numerical studies is realized and motivates this research.
- The previous experimental setup is conducted numerically to provide a deep insight in the thermal performance analysis of the PCM-air-liquid heat exchanger.
- For the first time, to efficaciously simulate a complex PCM heat exchanger based on multiphysics coupling of heat transfer and fluid flow is highly precious. This study aims to simulate a novel model of two operational fluids and a PCM within a complex geometry having minichannel liquid flow, and fin implementation.

- The increased demand for electric and hybrid vehicles, the incorporation of climate control features such as start-stop operations, and the need to enhance thermal comfort during short periods of vehicle shutdown.

Considering all the reasons above, this numerical work is important and necessary since it provides insight and a solution to real-life problems, resulting in savings on energy and power in heat exchanger systems based on two operational fluids.

1.4 Objectives

By using a PCM to enhance and maintain a sustainable energy system, we can improve the efficiency of our energy system. As a result, the PCM is capable of managing heat and providing thermal energy in an effective manner. Hence, the current study proposes the use of a PCM as a reliable thermal energy storage device. Despite significant effort being put into developing and presenting different thermal energy storages in the published literature, there remains a scarcity of numerical studies that deal with the incorporation of PCM into a compact crossflow heat exchanger. A solution for the thermal comfort of occupants is presented by using the following objectives in the present study in order to address the lack of available numerical works:

- Numerically design and investigate a 3D compact crossflow PCM-air-liquid heat exchanger based on computational fluid dynamics.
- Validate the model with experimental results with the same geometry and operational conditions setup with two experimental data.
- Analyze the dynamic behavior of the PCM heat exchanger for air cooling and heating using different air inlet mass velocity ratios.
- Examine the effect of airside flowrate variation on charging and discharging of the PCM.
- Carry out a complete thermal performance analysis of the heat exchanger response on the fluids and PCM charging/discharging processes for both air heating and cooling application.
- Examine the melting and solidification procedure of the PCM during the charging and discharging processes.

- Compare the thermal comfort provided by PCM when compared to air cooling/heating without PCM.
- Analyze the main factors corresponding to PCM heat exchanger thermal performance.
- Assess the dynamic share of latent heat during the PCM discharging process.

In order to achieve the study objectives, the numerical simulations are conducted by the commercial software COMSOL Multiphysics® 6.0, using 3D CFD by the finite element method.

CHAPTER 2

LITERATURE SURVEY

Heat exchangers are employed in a wide range of applications for the purpose of accomplishing thermal management and maintaining thermal comfort. Due to the importance of performance enhancement of heat exchangers on the overall thermal system functioning, it is necessary to study various methods of heat transfer enhancement methods in these devices. In this chapter, a review of these methods is represented with the focus on thermal energy storage as a viable solution for these systems. A variety of numerical, analytical, and experimental investigations are presented on several types of heat exchangers. This is followed by discussing the summary of the literature with presenting the scope of the current study.

2.1. Heat Transfer Enhancement of Heat Exchangers

2.1.1. Enhancement Methods

Heat exchangers are widely used in a variety of engineering applications. In order to improve the performance of compact heat exchangers, numerous extensive studies have been conducted. Over the past decade, researchers have been searching for compact, energy-efficient, and environmentally friendly heat exchangers. Studies have been conducted on the thermal performance of heat exchangers, which include modifying the properties of the working fluid, using different orientations of the heat exchanger, changing the geometry surfaces, and varying the fin parameters of the extended surfaces. Addition of another piece of equipment that requires an additional source of energy to improve heat transfer and thermal performance in a heat exchanger is considered costly and increases the size and weight of the thermal unit. There have therefore been suggestions for alternative methods. Among enhancement methods is the use of nanofluids in cross-flow heat exchangers to improve heat transfer [18]. A review study of nanofluids in heat exchangers was recently presented by Humnic and Humnic [19]. A summary of the enhancements in fluid properties and Nusselt number is presented in the first section of their paper. The other section examines how nanofluids can be used in different types of heat exchangers.

Increasing heat transfer can also be achieved by considering the size and shape of tubes and channels of the heat exchanger. The effects of different channel diameters on a thin slab have been studied by Ismail et al. [20]. It has been demonstrated that the heat transfer coefficient, pressure drop, and Nusselt number are affected by the ratio of slab length to channel diameter. Heat transfer has been demonstrated to be increased by adding extended surfaces (fins) to the heat exchanger. In studies conducted by Moorthy et al. [21], Basavarajappa et al. [22], and Altwieb et al. [23], the shape, size, and orientation of fins are examined with respect to their impact on heat transfer in a heat exchanger. Other studies by Kuehndel et al. [24] and Erec et al. [25] examined the effects of geometrical parameters on heat exchanger thermal performance.

Efficient heat exchanger design such as using minichannels in heat exchangers can improve thermal characteristics, compactness, and energy efficiency contrasted with conventional heat exchangers [26]. Fotowat et al. [27] experimentally compared the transient response of a conventional and meso heat exchanger subjected to step changes in the inlet operation conditions. It was found that the meso heat exchanger exhibited a significantly higher thermal efficiency and achieved a steady state earlier than the typical heat exchanger. In another study by the author [28], an experimental study was performed on the transient air heating performance of a compact liquid-air cross flow heat exchanger with an optimum design consisting of multipass serpentine and minichannel flow. Due to their study, it is concluded that effective air-liquid heat exchanger design by fins, liquid flow in minichannel liquid flow in multiple slabs has significant effect on heat exchanger heat transfer performance.

2.1.2. Thermal Analysis of Heat Exchangers

Dynamic analysis of air-liquid heat exchangers has gained considerable attention in recent years for applications that primarily involve heating or cooling for studying the control of fluid outlet temperature. Among different heat exchanger types, the crossflow heat exchanger is frequently used among various tubular heat exchangers in the industry, and numerous experimental and numerical studies have been conducted on their thermal behavior [9]. Most of these studies examined the effects of variations in the fluid's inlet temperature and channel/tube mass flow rate on the dynamic performance of the heat

exchanger. According to Abdallah and Rooke [29], the liquid-gas crossflow heat exchanger's thermal response to a step change in liquid temperature was examined, and analytical expressions for the liquid and gas outlet temperatures were derived. It was found that their analytical solution was in good agreement with the numerical methods available. Using numerical and experimental approaches, Gogus and Ataer [30] examined the transient response of a crossflow heat exchanger to a step change in liquid temperature. In order to predict the thermal behavior of a crossflow heat exchanger incorporating fins, a model was developed and verified. An analysis of the transient performance of a multi-pass cross flow heat exchanger by Silaipillayarputhur and Idem [31] was conducted numerically. The effects of a change in inlet temperature and flow rate of the minimum capacity rate fluid were studied. Both fluids as well as the wall have been solved, and their responses have been discussed. As a result of comparing these results with those published in for different flow arrangements, the authors concluded that adding more passes to cross and counter flow arrangements improved steady state transfer performance. Additionally, when three or more passes were used, the crossflow arrangement showed a faster thermal response time.

Early efforts to improve crossflow heat exchanger control capability using transient analysis were undertaken in the mid-sixties with applications in HVAC and automotive. Researchers investigated the effect of variations in the inlet flow rate of the fluid inside the tube on both the fluid's outlet temperatures and the response time. Pearson et al. [32] investigated the dynamic response of the air outlet temperature to changes in water flow rate in a conventional crossflow heat exchanger. Their results were compared to those obtained through experimentation and numerical simulation of a first-order dynamic model. An experiment by Fotowat et al. [7] investigated the transient response of a minichannel cross flow heat exchanger when the channel flow rate is subjected to step changes. In their study, different step magnitudes have been examined and their effects on the outlet temperature response of both fluids have been evaluated. An experimental study published by Askar et al. [33] examined the effects of air mass flow rate step changes on the performance of a compact crossflow heat exchanger for air heating. Based on different air mass flow rate steps imposed on the heat exchanger, they determined the thermal response and derived an empirical correlation for Nusselt number prediction.

An investigation by Mishra et al. [34] has been conducted into the transient thermal response of a CFHX as a result of variations in fluid temperature and flow rate. As part of their numerical analysis, step and ramp changes were taken into account for the flow rate of hot fluid. As a result, they found that the exit temperatures increased when the hot fluid flow rate changes were greater and decreased when the cold fluid flow rate changes were greater. According to Del Valle and Ortega [35], a cross flow heat exchanger with liquid and air temperatures and flow rates perturbed was characterized experimentally during transient operation. According to their findings, an increase in water flow rate raises the temperature of the outlet water. Additionally, there was no delay in the response of exit temperatures to perturbations in water flow rate.

Gao et al. [36] studied the prediction of transient responses for a crossflow heat exchanger using a numerical thermal dynamic model. Various combinations of variations have been studied, including changes in air inlet temperature and water flow rate, changes in air inlet temperature and air flow rate, changes in air inlet temperature in combination with changes in air and water mass flow rates, as well as changes in both fluid inlet mass flow rates. Based on their findings, it has been demonstrated that the effect of mass flow rate variation on outlet temperature response is much faster than the effect of temperature variation. Furthermore, the combination cases resulted in unexpected thermal performance, including overshoots at the outlet temperature response.

It is noted from the literature the dynamic analysis provides insight into the thermal behavior of the heat exchanger whenever there is a change in the inlet conditions. It could also predict the temperature response of fluid outlet trends regarding the change imposed. However, innovative technologies could be adapted to enhance conventional heat exchangers and provide sustainable thermal management for energy systems [37]. A passive heating or cooling system such as TES using PCMs is proposed to minimize the shocks caused by changes in inlet conditions. This type of storage allows the thermal system to be designed for average heat loads instead of peak loads. When undergoing a phase change, a PCM is characterized by a high storage capacity, allowing it to absorb or release a significant amount of thermal energy. Due to the ability of PCM in heat management and providing adequate thermal energy, the implementation could enhance

and provide a sustainable energy system and improve overall efficiency [38]. Accordingly, the next section intends to present the literature survey of the use latent heat storage using PCM as a viable TES solution for heat exchangers.

2.2. Thermal Energy Storage

Thermal energy storage uses a medium to store energy that can then be released when needed by transferring heat with a fluid. They offer a number of advantages over traditional cooling or heating systems as well as the ability to store large amounts of energy in a small space. Sarbu and Sebarchievici [39] reviewed several different thermal energy storage technologies, including sensible and latent. Chavan et al [40] examined and reviewed various applications of thermal energy storage for both heating and cooling.

Phase change materials are materials that can store a large amount of thermal energy and have a high energy density. Various enhancement techniques have been reported by researchers in order to improve the thermal properties of PCMs. Wang et al. [41] developed a phase change material that was enhanced in thermal conductivity by the addition of aluminum nitride. By storing and releasing thermal energy, they examined the thermal energy storage performance. A PCM with a high thermal conductivity and a reduced latent heat was developed as a result of their experiments. According to Fan and Khodadadi [42], experimentally and numerically based studies have been conducted on ways to improve the thermal conductivity of PCMs. Several metal inserts were evaluated as promoters on a variety of PCMs. The use of different types of additives into an organic PCM to improve its thermal performance has been investigated experimentally by Teng and Yu [43]. As a result of the use of titania in a PCM, they have found that the storage performance is enhanced, and the phase change temperature range is extended.

By increasing the thermal conductivity of a PCM, Ji et al. [44] studied the storage of thermal energy more efficiently. A PCM with enhanced thermal conductivity has been developed using graphite foams, which can be applied to a wide range of applications, including automotive and building construction. Sivasamy et al [45] have discussed various enhancement techniques for improving energy storage's thermal performance. There has been a discussion of several types of thermal conductivity enhancement methods as well as applications of thermal energy storage.

2.2.1 Thermal Energy Storage in Heat Exchangers

Research has shown interest in both experimental and numerical studies toward incorporating PCM in different heat exchangers as a TES solution for various thermal management applications. Kalapala and Devanuri [11] presented a comprehensive review of the effects of design and operating conditions on the performance of a PCM heat exchanger. They concluded that TES systems based on latent heat are influenced by the design of the heat exchanger. Shell and tube heat exchangers are most used for this application. Rana et al. [46] performed a two-dimensional CFD comparison study of the melting process and heat transfer phenomenon of a shell and tube PCM heat exchanger using an elliptical tube, a circular tube, and a rectangular tube. The PCM melting time, liquid fraction, and temperature distribution were studied. According to the results, the heat exchanger with rectangular tubes obtained the lowest melting time. This was followed by cylindrical and elliptical tubes. Rahimi et al. [47] experimentally examined the charge and discharge processes for a commercial PCM by varying the hot fluid's inlet temperatures and flow rates. They demonstrated that fins enhance melting and solidification processes. Moreover, the melting time decreases as the flow regime changes from laminar to turbulent, and the temperature of the water inlet increases. Further, the amount of mass flow rate influences the solidification time. Akgün et al. [48] examined the impact of increasing heat transfer fluids' flow rate and temperature according to the processes of charging and discharging. Due to their research, melting time decreases as inlet temperature increases. Reduced fluid mass flow rates have also been suggested to lower energy consumption. The impact of adding copper nanoparticles to a multi-tube PCM heat exchanger was studied by Gorzin et al. [49]. The increase in the nanoparticle volume fractions leads to a reduction in solidification time.

As a major issue, the low thermal conductivities of PCMs have led to the focus of studies on improving the thermal properties of PCM in order to enhance heat transfer characteristics using various methods. Li et al. [10] have numerically investigated the effect of the fin number and location during the melting process in a horizontally positioned double tube PCM-HEX. It was found that the heat transfer and the heat exchanger performance are enhanced significantly by the fin position rather than the fin number. Moreover, the existence of fins and their positioning resulted in a 24% reduction in the

PCM melting time. Leong et al. [50] performed a state-of-the-art review on a PCM heat exchanger using a triplex tube configuration to identify the factors that affect the melting and solidification characteristics. They found that this type of heat exchanger offers higher TES compared to a shell and tube design. Besides, a combination of fins and nanoparticles enhanced the solidification and melting of PCM. In addition, optimized fins and pure PCM exhibited better phase transition properties than using nanoparticles alone. As for further solutions to improve PCM thermal behavior, using nanoparticles and multiple PCM configurations have been applied in several studies. Mozafari et al. [51] numerically studied the effect of nanoparticle addition with multiple PCM inside a triplex-tube PCM-HEX. Based on their results, the stored latent energy was increased by at least 40% using two or more PCMs. By combining multiple PCMs with nanoparticles, the energy storage and recovery times could be accelerated by up to 2 and 5 times, respectively, compared to the PCM without nanoparticle model. Gorzin et al. [49] investigated the effect of combining copper nanoparticles with a multi-tube PCM-HEX. It has been shown that a decrease in solidification time can be achieved when the volume fractions of nanoparticles increase. The use of extended surfaces and metal foams as well as a combination of both were reviewed by Teggari et al. [52] as ways to enhance PCM thermal conductivity. PCM performance was significantly enhanced by using metal foams, but extended surfaces were widely used due to their simplicity and cost-effectiveness.

Research trends on experimental or numerical works are increasing towards topics related to improving the thermal performance of heat exchangers incorporating PCMs [53]. It is observed from the literature that the studies mainly focused on incorporating PCMs in a single fluid heat exchanger for PCM thermal behavior analysis. Various studies focused on melting and solidification procedures of the PCM using a liquid flow tube with different tube and fin shapes and positions with variation PCM type and heat transfer fluid (HTF) operating conditions. In an experiment, Rahimi et al. [47] examined the charging and discharging processes of a commercial PCM by varying the inlet temperature and flow rate of the hot fluid. They concluded that the fins existence has enhanced the melting and solidification processes. Further, the melting time of the hot fluid decreased due to the change from laminar to turbulent flow regime and with an increase in the temperature of the water inlet. On the other hand, the PCM solidification time was also influenced by the

mass flow rate. Akgün et al. [48] have studied the effect of an increase in the flow rate and temperature of heat transfer fluids on the charging and discharging processes of the PCM. Their research showed that the melting time decreased with the increase in the inlet temperature, which is found to be in agreement with other studies. The reduction of fluid mass flow rates has also been suggested as a means of reducing energy consumption.

The compact PCM heat exchanger has been asserted to have higher thermal power and area-to-volume values than other heat exchangers [54]. Incorporating LHTES systems in compact finned heat exchangers based on fluid flow is a demanding topic for practical thermal performance enhancement of heat exchangers. Accordingly, studies mostly focused on a single fluid PCM-HEX based on liquid or air flow for thermal management of various applications. In this regard, Amagour et al. [55] performed a numerical study on a compact finned-tube PCM-HEX storage tank (PCM-liquid heat exchanger). Navier-Stokes equations and the enthalpy-porosity technique were used to solve the heat transfer problem during the phase change process using computational fluid dynamics (CFD). The TES efficiency and phase change transition were investigated by analyzing the impact of HTF flow rate. Based on their findings, the HTF flow rate had a greater influence on TES than fluid inlet temperature. Additionally, higher flow rates resulted in a faster phase change process and a reduced effectiveness of the system. In another similar numerical study by the author [56] based on an operation parametric study, they concluded that increasing the mass flow rate of the hot HTF reduces both the charging and discharging times in a similar manner. In addition, increasing the temperature difference between the hot HTF and PCM accelerated the melting and solidification processes. Due to their findings, fins increased to a certain extent and were found to accelerate the melting process and increase storage capacity.

He et al. [57] designed and presented a compact latent heat exchanger based on plate liquid flow for solar water heating systems with varying number of tube passes. They concluded that heat transfer rates were poor with tubes with fewer passes, and tubes with more passes have not achieved heat transfer improvements to and were more difficult to manufacture. Regarding PCM-HEXs working with airflow (PCM-air heat exchanger), Ouzzane and Bady [58] developed an innovative air-PCM-HEX used in hot climates in which the PCM

was based on frozen water and ethylene glycol used for air cooling. In their study, they demonstrated that lowering the PCM freezing temperature to around 10 °C results in an air temperature drop of only 1 °C. Also, they concluded that the cases that attained higher air cooling were observed to have a lower operation period. Finite element numerical analysis has been used to investigate a PCM-to-air heat exchanger as a TES system in HVAC applications by Herbingner et al. [59]. They found that the rate of heat transfer is dependent on temperature, velocity, and channel diameter on the airside. As a result of the decreased channel size and higher inlet air temperature, the heat transfer is increased. Recently, Serena et al. [15] studied an experimental PCM-air-liquid heat exchanger which operates based on liquid and airflow simultaneously for hybrid air cooling using air or PCM. It was demonstrated that using PCM in the air-liquid heat exchanger could provide around 120 kJ of additional cooling load while the coolant flow is shutdown. Furthermore, the cumulative energy transferred to the air decreased by 29 % when the air mass flow rate was doubled.

2.3. Scope of the Current Work

The above literature survey shows that the research path on thermal analysis of heat exchangers is attaining interest towards their performance enhancement using thermal energy storage. Numerous experimental and numerical works are conducted incorporating PCM in heat exchangers. However, most of the published research focus on PCM-HEXs based on single fluid flow operation. Studies regarding the implementation of thermal energy storage in compact heat exchangers for real-world thermal management applications to provide a sustainable energy storage medium for heating and cooling purposes are scarce in the open literature. This paper aims to present a novel numerical work of an effective compact crossflow PCM-air-liquid heat exchanger to provide hybrid source for air cooling/heating using PCM as thermal energy storage for times when the system coolant is shutdown. The model is validated with experimental results with the same geometry and operational conditions setup. A comprehensive heat transfer thermal performance analysis is performed on the system.

No numerical study has yet to be introduced in the open literature to investigate hybrid heating for the airside in a compact PCM-to-air and liquid heat exchanger based on two operational fluids. As the main novelties of this work, for the first time, this study has

overcome the numerical modeling challenges and been able to efficaciously simulate a complex PCM heat exchanger based on multiphysics coupling of heat transfer and fluid flow. This study has simulated two operational fluids and a PCM within a complex geometry having minichannel liquid flow, and fin implementation. Furthermore, this study aims to continue the previous experimental work with the same geometry conducted by Serena et al. [15] by presenting a numerical work. Due to experimental limitations in presenting deep insight into the thermal response of the system and having construction and operation challenges, this study aims to advance and fulfill the gap in the previous experimental study by performing numerical work to attain a clear insight into the thermal performance analysis of PCM-air-liquid heat exchangers. Extended surfaces (fins) are distributed inside the PCM medium and integrated throughout the whole heat exchanger to effectively transfer the thermal energy between the PCM and the two working fluids.

Equipping heat exchangers with PCM as a latent heat storage source to reduce energy consumption is an economical way to release the stored energy through the heat exchange from the PCM to the desired fluid. When the main fluid must be shut off for a short time during shutdown time, the PCM reliably extends the operating period, minimizing the need for a power source or batteries. A real-world application of the study is for the vehicle standby mode or a stop at a red light where the vehicle's source of power is shut down, thereby the hot liquid in the heat exchanger. During this short time, a PCM can provide additional air heating time, ensuring the passenger cabin is at a comfortable temperature. The presented thermal energy storage system offers a unique solution for the start-stop function of the power source in many hybrid and electric vehicles as a valuable real-world application of the study. The results achieved in this study will shed light on the development of PCM-air-liquid heat exchangers and provide a deep insight into their thermal performance.

CHAPTER 3

DESIGN AND NUMERICAL MODELING

The numerical work conducted in this study is thermal analysis of two PCM-air-liquid heat exchangers used for air heating and cooling applications. The design of the heat exchangers is based on previous designs and experimental works carried out in the Thermal Management Laboratory at the University of Windsor. The focus of this study was to equip the previously studied heat exchanger with PCM to act as a TES method for air heating and cooling purposes. Two heat exchanger designs based on single slabbed and five slabbed are modeled and studied. The single slab heat exchanger is conducted for air heating to evaluate the effect on PCM in a simple slabbed and finned based heat exchanger. After this stage, the five-slab heat exchanger, which is considered the practical model of this study, is designed and comprehensively studied for air heating and cooling applications. In the following, the design and numerical modeling of the system is thoroughly presented.

3.1. System Description

In this section, the design specifications of the two PCM heat exchangers proposed are presented into detail.

3.1.1. Single Slabbed PCM Heat Exchanger

The single-slabbed PCM heat exchanger model is based on a slab and finned air-liquid heat exchanger equipped with minichannel liquid flow operation and PCM. The computer-aided design (CAD) model of the system is represented in Figure 3.1. The heat exchanger material is aluminum for the body and has two rows of fins above and under the main slab. The PCM is placed through the top row of the heat exchanger between the fins. Hot water inserts the heat exchanger liquid side and distributes through 68 minichannels inside the slab represented in Figure 3.2. The heat exchanger is placed inside the air channel domain seen in Figure 3.1 (b), which allows the air to pass through the heat exchanger slabs through the bottom fins row and exchange heat with the hot water and the PCM domain. Effective extensive surfaces (fins) are distributed within the PCM domain and between the heat

exchanger slabs to enhance the PCM's thermal performance and ensure an efficient heat transfer to the fluids. The design specifications of the PCM heat exchanger are presented in Table 3.1.

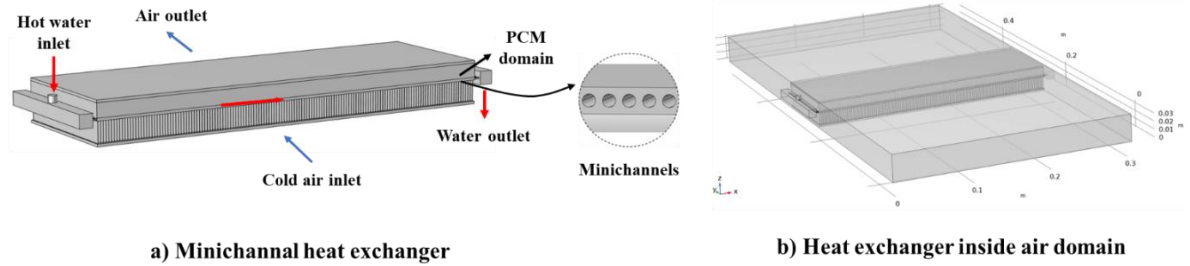


Figure 3.1: CAD design of the single-slatted PCM heat exchanger.

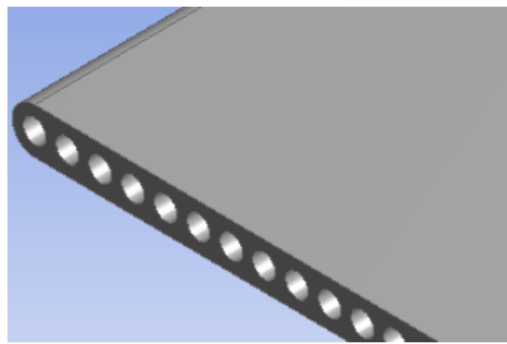


Figure 3.2: Circular minnichannels inside HEX slab [6].

Table 3.1: Design specifications of the single slatted PCM-air-liquid heat exchanger based on [28].

Specifications	Value	Specifications	Value
Number of channels in the slab	68	Fin height – top row (mm)	10.65
Slab length (mm)	305	Fin height – bottom row (mm)	15.79
Slab width (mm)	100	Fin thickness (mm)	1.85
Slab height (mm)	2	Number of fins per row	144
Channel diameter (mm)	1	Air channel dimensions (mm)	34 × 305 × 600
Fin density (fins per inch)	12	Heat exchanger material	Aluminum

3.1.2. Five Slabbed PCM Heat Exchanger

The five slabbed PCM-air-liquid HEX proposed in this study is a compact-finned cross flow minichannel heat exchanger. This heat exchanger was previously studied through several experiments by Fotowat et al. [7] and Askar et al. [33] in the Thermal Management Research Laboratory at the University of Windsor. A view of the experimental setup conducted is seen in Figure 3.3. The 3D CAD version of the model was redesigned in this study based on the experimental model and appears in Figure 3.4.



Figure 3.3. View of the laboratory experimental setup.

The heat exchanger is made of aluminum and has 5 slabs with 4 serpentine. Inside the slabs, 68 minichannel at 1 mm diameter are distributed along the length for the liquid HTF flow. Liquid enters the system through an inlet header and manifold and passes through the minichannels inside the slabs. The top and bottom of the heat exchanger are confined with dummy slabs for better heat distribution from the fins. Compact thin surfaces of fins are placed in 6 rows between the slabs to improve heat transfer performance between air, liquid and PCM. The PCM domain is modeled as the volume block between the two top slabs of the heat exchanger. This design was selected due to the feasibility of construction in the experimental environment [60]. The heat exchanger is placed inside a wind tunnel where air flows and passes through the fins and slabs of the heat exchanger. The fins inside the PCM domain work on improving the heat transfer performance among the liquid, and air, and to the PCM and offer uniform melting and solidification. The detailed design dimensions of the PCM-air-liquid heat exchanger are listed in Table 3.2.

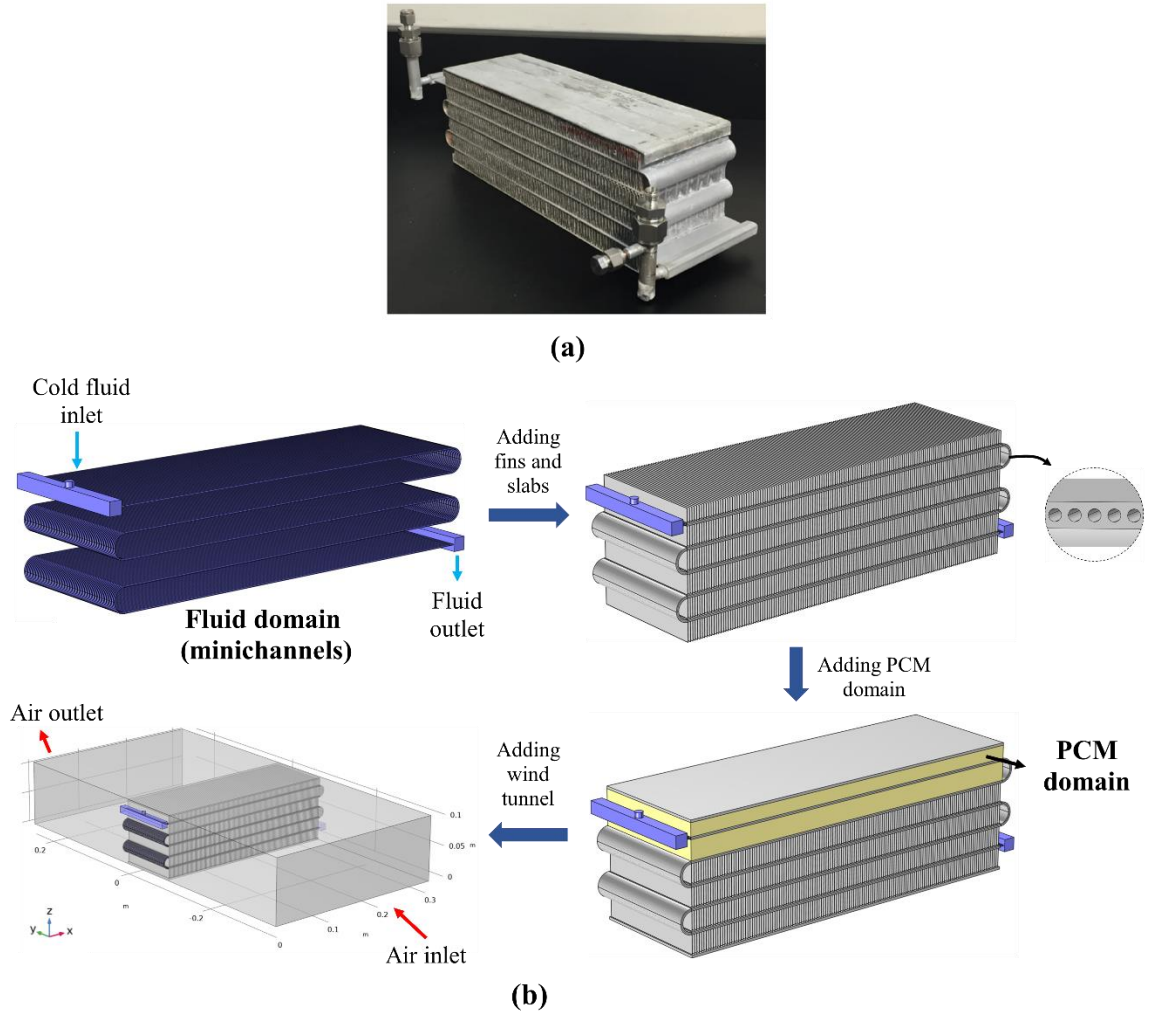


Figure 3.4. The five slatted PCM-air-liquid heat exchanger proposed in this study (a) experimental model [60], (b) modeling schematic.

Table 3.2. Detailed modeling design specifications for the five-slatted PCM-air-liquid liquid heat exchanger [28, 60].

Specifications	Value	Specifications	Value
Number of liquid flow slabs	5	Fin density (fins per inch)	12
Number of dummy slabs	2	Fin height (mm)	15.79
Number of channels inside slabs	68	Fin thickness (mm)	1.85
Slab length (mm)	305	Number of fins per row	144
Slab width (mm)	100	PCM block dimensions (mm)	100 × 305 × 26.4
Slab height (mm)	2	Air channel dimensions (mm)	600 × 305 × 105.6
Channel diameter (mm)	1	Body material	Aluminum

3.2. Operating Conditions and Assumptions

To set the operating conditions for the two designed PCM heat exchangers, the simulation operations were set based on the real experimental models conducted [15]. Three different studies were performed on the heat exchanger models. The five-slab heat exchanger model was conducted for both air heating and cooling application and the effect variation of three air mass flow rates were studied. The three studies conducted along with their operating conditions are described in Tables 3.1 to 3.3.

For Study 1 operation, the presented single slabbed PCM heat exchanger based on two operational fluids and PCM storage is designed to provide heating for the airside based on hybrid heat sources of water and the PCM. The hot fluid material is selected water, with an inlet temperature of 70 °C and a mass flow rate of 0.03 kg/s. In the airside, constant inlet temperature and air stream velocity are selected at 13 °C and 6 m/s, respectively. The initial temperature of the model simulation was selected at 20 °C. Table 3.3 represents the operating conditions for Study 1 as below:

Table 3.3. Study 1 operating conditions.

Study 1: Single slab PCM-HEX - Air heating			
<u>Airside</u>		<u>Liquid side</u>	
Inlet temperature	13 °C	Fluid type	Water
Mass flow rate	0.077 kg/s	Inlet temperature	70 °C
		Mass flow rate	0.03 kg/s

Regarding Study 2, the five-slabbed PCM-air-liquid heat exchanger is performed based on an experimental operational procedure conducted by Fotowat et al. for air heating [7]. Hot water at 70 °C and cold air at 13 °C is selected for the inlet of the liquid and air domain of the heat exchanger, respectively. The heat exchanger setup was conducted with the aim of real-world application for vehicle cabin heating based on previous experimental designs. The selection of air temperature was based on the ambient temperature of a typical fall day and the hot fluid operating conditions were selected according to a standard condition for its supply from a vehicle radiator. The inlet mass flow rate of water was selected as 0.03 kg/s, and several mass flow rates of air were studied with values of 0.08, 0.15, and 0.30

kg/s. To perform a transient study, the effect of changes in the inlet condition of the mass flow rates of the liquid side is studied. Thus, the inlet temperature of the water and its flow rate were kept constant, and a parametric study was performed with the inlet change in the air mass flow rate and studied at 0.08, 0.15, 0.30 kg/s. Initially, the whole system is considered at a stable initial condition temperature of 13 °C. Table 3.4 summarizes the operating conditions for Study 2:

Table 3.4. Study 2 operating conditions.

Study 2: Five-slab PCM-HEX - Air heating			
<u>Airside</u>		<u>Liquid side</u>	
Inlet temperature	13 °C	Fluid type	Water
Mass flow rate	Case 1: 0.08 kg/s	Inlet temperature	70 °C
	Case 2: 0.15 kg/s Case 3: 0.30 kg/s	Mass flow rate	0.03 kg/s

Study 3 is conducted for the five-slabbed PCM-air-liquid heat exchanger used for CTES application for air cooling. Regarding the fluids selection and operating conditions, 50-50% mixture of cold water/ethylene glycol with an inlet temperature of -2.5 °C was selected for the cold liquid HTF domain inside the channels. Hot air was selected for the air wind tunnel domain with an inlet temperature of 30 °C. The mass flow rate of the cold HTF was considered constant at 0.03 kg/s, and several airside mass flow rates of 0.08, 0.15, and 0.30 kg/s were studied. The goal was to perform air cooling using hybrid sources of cold HTF and PCM through cold thermal energy stored. An initial temperature for the whole system was selected at 30 °C. The main operation conditions for Study 3 are represented in Table 3.5:

Table 3.5. Study 3 operating conditions.

Study 3: Five-slab PCM-HEX - Air cooling			
<u>Airside</u>		<u>Liquid side</u>	
Inlet temperature	30 °C	Fluid type	Water/ethylene glycol 50/50%
Mass flow rate	Case 1: 0.08 kg/s	Inlet temperature	-2 °C
	Case 2: 0.15 kg/s Case 3: 0.30 kg/s	Mass flow rate	0.03 kg/s

The computational domain of the designed system consists of the air test chamber and the solid minichannel cross flow heat exchanger. For the simulation of the current work, four main domains and materials were designated for the whole system: aluminum for the heat exchanger domain consisting of the slabs and fins, HTF for the minichannels of the heat exchanger, air for the air channel, and the PCM for its designated domain.

Two simulations were performed for the PCM charging and discharging processes. During simulations for PCM-HEX air heating application of Study 1 and 2, regarding the PCM charging process, the hot water circulates through the heat exchanger, melting the solid PCM and heating the air simultaneously. During the PCM discharging process, the water circulation is shut down, allowing the air to extract the latent heat stored in the melted PCM, delaying the air temperature drop and maintaining a warm air outlet temperature. It is evident that the LTHES provided for the heat exchanger is a reliable and sustainable heat storage for later use during shutdown periods. For the air-cooling application in Study 3, for the charging process, cold HTF circulates through the heat exchanger, cooling the hot airflow and fully solidifying the liquid PCM. In the discharging process, the cold HTF is shutdown, enabling the airflow to extract the thermal energy stored in the solid PCM and resulting in passive air cooling, thus maintaining thermal comfort for a specific period of time.

The following assumptions were made for the system flows and boundary conditions to reduce some simulation complexity:

- Liquid phases of fluids and PCM are considered incompressible and Newtonian

- Changes in thermophysical properties of air, water, and PCM are neglected during a specific phase.
- The water fluid flow regime is selected as laminar, and the airflow is turbulent
- Uniform initial temperature is considered for all domains
- No volume change is considered during phase change
- Material properties remain constant with temperature change, and the Boussinesq approximation is used to define the density variation of PCM
- Uniform and homogeneous mass is assumed for the PCM domain
- The serpentine and manifold walls, and the air chamber, are thermally insulated; there is no heat transfer between these walls.
- The system considers negligible radiation heat transfer.
- There is no consideration of viscous dissipation or slip velocity.
- The HTF inlets exhibit negligible temperature variations.

3.3. PCM Selection

When studying the LHTES systems, the selection of the PCM to use is an essential factor because the PCM amount and properties influence the heating energy and time of discharge. Paraffin wax-based PCMs are explored and widely used in thermal management and TES applications due to their broad melting temperature ranges [61]. In this study, Docosane is used due to its appropriate melting temperature to work within the heat exchanger's air and liquid side temperatures for air heating purposes in Study 1 and 2. The thermophysical properties of the PCM are stated in Table 3.6.

Table 3.6. Thermophysical properties of the selected PCM for Study 1 and 2 [61].

Material properties	Value
Melting temperature (°C)	43.80
Latent heat of fusion (kJ/kg)	234
Average density (kg/m ³)	820
Specific heat (solid) (J/kg.°C)	1700
Specific heat (liquid) (J/kg.°C)	2200
Thermal conductivity (solid) (W/m.°C)	0.37
Thermal conductivity (liquid) (W/m.°C)	0.24

Regarding PCM selection for air cooling application for Study 3, the thermal characterization of the PCM chosen in this study was based on its melting temperatures that match the application considered in automotive thermal management systems for air cabin cooling. The commercial PCM was selected according to the experimental study conducted for the same PCM-HEX by Askar et al. [15]. Table 3.7 summarizes the thermophysical properties of the chosen commercial PCM.

Table 3.7. PCM thermophysical properties for Study 3 [15].

Material properties	Value
PCM type	Paraffin
Melting temperature (°C)	5.42
Latent heat of fusion (kJ/kg)	211
Density (kg/m ³)	760
Viscosity (m ² /s)	2.81×10^{-6}
Specific heat (J/kg.°C)	2170
Thermal conductivity (W/m.°C)	0.21

3.4. Numerical Procedure and Boundary Conditions

This study intends to analyze the heat transfer simulation of a PCM-air-liquid heat exchanger using the CFD method. To perform the numerical simulation, COMSOL Multiphysics® 6.0 software is used. This section details the methods and procedures adopted for the numerical simulation.

The 3D model was constructed in the commercial CFD software environment to perform an analysis of the numerical simulations conducted in this study [62]. Using the finite element method, the mathematical model is discretized [63]. To model the physics of the study, laminar flow for the water domain and turbulent flow for the airside is selected [64]. The physics of heat transfer in solids and liquids are utilized to simulate the phenomena of heat transfer of flows and the melting and solidification of the PCM inside the heat exchanger. Appropriate multiphysics coupling is established between heat transfer and flow physics [65]. This study has overcome the numerical modeling challenges and been able to efficaciously simulate a complex PCM heat exchanger based on multiphysics

coupling of heat transfer and double fluid flow. This study has simulated two operational fluids and a PCM within a complex geometry having minichannel liquid flow, and fin implementation. Symmetric Interior Penalty Galerkin (SIPG) was used to approximate the convective and diffusive terms [66], and Backward Differentiation (BDF) was used to approximate the time derivative [67].

Due to the model's complex geometry, a simulation procedure that reduces the time required for calculation is important for the 3D finned and tubed heat exchanger model. In the case of complete couplings between the PCM and the two fluids, resolution times would be very long. First, a steady-state simulation was completed for the fluid flows because the fluid flow rate is constant and reaches a steady state within a short period of time. A transient simulation was executed based on the result of the steady-state simulation to solve the energy and heat transfer equation. The one-way coupling is permitted since flow influences heat transfer, but temperature changes are insignificant to affect it. Regarding the steady-state solver, GMRES [68] is used with an iterative solver with a tolerance of 0.01 for the nonlinear momentum and continuity equations for fluids and PCM. PARADISO transient solver was employed [69], with a relative tolerance of 0.0001. The time-stepping method was applied with the backward differentiation formula without specifying the start and end times. Using either a first or a second-order backward differentiation method was required. Absolute tolerances were set at an appropriate value for pressure, temperature, and velocity.

Regarding the initial simulation conditions, the initial water velocity, air, and PCM were adjusted to zero. All domains were initially at the same temperature and were set as their initial values at the beginning of the charging process. In the air heating studies, the PCM was initially solid at its initial temperature at the start of the charging process and was liquid for the air-cooling simulation. During the charging process, the inlet of the air and water side were given at a constant temperature at a constant water mass flow rate. Several airside mass flow rates were simulated for both the charging and discharging processes for Study 2 and 3. The inlet velocities were determined from the inlet flow rates of the streams and the dimensions of the inner tube and air channel. The outer walls were insulated to prevent heat loss, and a no-slip boundary condition was applied. Outflow boundary

conditions were applied at the water and air outlet boundaries. For the discharging process, the water flow rate was set to zero, and all initial values were adopted from the final steady-state condition of the charging process.

The model's initial conditions and boundary conditions are defined mathematically as follows:

- For all $x, y,$ and z at $t = 0$: $\vec{V}(x, y, z, 0) = (0, 0, 0)$
- For all $x, y,$ and z at $t = 0$: $p(x, y, z, 0) = p_{\text{atm}}$
- For all $x, y,$ and z at $t = 0$: $T(x, y, z, 0) = T_0$
- At wall boundaries, for all $t > 0$: $\vec{V}(x, y, z, t) = (0, 0, 0)$
- At outer wall boundaries, for all $t > 0$: $-\vec{n} \cdot \vec{q} = 0$
- At flow inlet boundaries, for all $t > 0$: $\vec{V}(x, y, z, t) = -V_{\text{inlet}}\vec{n}$
- At flow inlet boundaries, for all $t > 0$: $T(x, y, z, t) = T_{\text{inlet}}$
- At flow outlet boundaries, for all $t > 0$: $\vec{V}(x, y, z, t) = -V_{\text{inlet}}\vec{n}$
- At flow outlet boundaries, for all $t > 0$: $-\vec{n} \cdot \vec{q} = 0$

Where \vec{n} represents the normal boundary vector, and \vec{q} represents the heat flux vector.

Based on CFD simulation, some limitations of the numerical modeling for the current work exist. Firstly, the numerical heat transfer analysis of a complicated system is conducted which is extremely heavy for simulation. This needs advanced computers to run besides making the simulation time-consuming for several design conditions. Secondly, the dissimilarity in geometry dimensions of the model design causes size differences in mesh elements distribution and is challenging to create a high-quality mesh grid throughout the domains. Thirdly, the PCM was considered to have a uniform mass throughout its volume, which is an ideal assumption and might differ in real experimental operation. Finally, in modeling PCMs in numerical simulation, an average phase change transition temperature range is assumed for the whole PCM domain. This assumption differs in the real world and the phase transition might not be the same throughout the PCM and differs due to the temperature conditions of the material.

3.5. Governing Equations

For the formulation of the PCM melting process domain, the enthalpy-porosity approach is applied [70]. By this method, melting PCM is considered a porous medium that contains both liquids and solids. Every computational cell's liquid fraction represents the cell's porosity. Consequently, the porosity value is assumed to be "0" for the solid region and "1" for the fully melted region. In the PCM domain, heat is transferred by convection and is modeled with negligible volume expansion. Thus, the PCM region uses the Boussinesq approximation to solve the buoyancy effect [71]. It is to be stated that in all simulations the liquid side flow is unsteady, incompressible, Newtonian, and laminar. Furthermore, viscous dissipation is ignored in simulations. Hence, the energy, momentum, and mass conservation equations for the modeled heat exchanger considering PCM, liquid and air fluids, and aluminum walls are formulated as follows [56]:

Mass conservation:

$$\frac{\partial \rho}{\partial t} + \nabla \cdot (\rho \vec{V}) = 0 \quad (1)$$

Momentum conservation:

$$\rho \frac{\partial \vec{V}}{\partial t} + \rho (\nabla \cdot \vec{V}) \vec{V} = -\nabla P + \mu (\nabla^2 \vec{V}) + \rho_{ref} \beta (T - T_{ref}) \vec{g} + \vec{S} \quad (2)$$

Energy conservation:

$$\frac{\partial (\rho H)}{\partial t} + \nabla \cdot (\rho H \vec{V}) = \nabla \cdot (k \nabla T) \quad (3)$$

Where in Eq. (2), \vec{S} is the Darcy source term that is calculated according to the variation in porosity of the mushy zone as follows [56]:

$$\vec{S} = A_m \frac{(1 - \theta)^2}{\theta^3 + \varepsilon} \vec{V} \quad (4)$$

The mushy zone coefficient [70] is represented by A_m in Eq. (4). The value is set to so that divide by zero is prevented while the PCM is solid. In these phases, \vec{S} will automatically become "0" when the PCM is fully melted and solid due to the values of θ being "1" and "0", respectively. The flow in the partially melted region depends on this

coefficient. The total latent heat (ΔH) and sensible heat of the particle is conveyed in terms of enthalpy (H),

$$H = h + \Delta H \quad (5)$$

According to this definition, the sensible heat share is:

$$h = \int_{T_0}^T C_P dT + h_0 \quad (6)$$

Additionally, the latent heat share that accounts for the phase change is described as:

$$\Delta H = \theta \Gamma \quad (7)$$

According to Eq. (7), θ presents the liquid fraction of the mushy zone, while Γ represents the subsequent latent heat of the utilized PCM. It is noted that the fraction of liquid in the expected porous zone can be changed from "0" to "1" to obtain from [72]:

$$\theta = \begin{cases} 0 & ; T < T_{Solidus} \\ \frac{T - T_{Solidus}}{T_{Liquidus} - T_{Solidus}} & ; T_{Solidus} < T < T_{Liquidus} \\ 1 & ; T_{Liquidus} < T \end{cases} \quad (8)$$

It is possible to solve the equation of energy using the apparent heat capacity method after defining the thermophysical properties of the PCM during phase change. Phase transitions are assumed to occur within a temperature range of $T_m - \frac{\Delta T_m}{2}$ and $T_m + \frac{\Delta T_m}{2}$ where T_m is the melting point and ΔT_m is the temperature range of the phase change. In terms of the two phases of the PCM, based on their densities and liquid fractions, the specific enthalpy of the PCM is calculated. The specific heat capacity is determined by the differentiation of the specific enthalpy concerning temperature, and the derivative of the mass fraction is found in Eq. (12).

$$\rho = \theta \rho_{liquid} + (1 - \theta) \rho_{solid} \quad (9)$$

$$k = \theta k_{liquid} + (1 - \theta) k_{solid} \quad (10)$$

$$C_P = \frac{\theta \rho_{liquid} C_{P,liquid} + (1 - \theta) \rho_{solid} C_{P,solid}}{\rho} + L \frac{\partial \alpha_m}{\partial T} \quad (11)$$

$$\alpha_m = \frac{1}{2} \frac{(1 - \theta) \rho_{solid} - \theta \rho_{liquid}}{\rho} \quad (12)$$

To assess the thermal performance of the fluids and PCM, the equations were taken into consideration and described below.

Heat transfer rate of the liquid:

$$\dot{Q}_l = \dot{m}_l c_P (T_{l,i} - T_{l,o}) \quad (13)$$

Airside heat transfer rate:

$$\dot{Q}_a = \dot{m}_a c_P (T_{a,o} - T_{a,i}) \quad (13)$$

The total latent heat stored in the PCM during the charging process is shown as:

$$\text{Total stored latent heat} = m_{PCM} \times (\text{PCM specific latent heat}) \quad (14)$$

Where the PCM mass is calculated by the volume integration throughout the PCM domain times the PCM density.

The share of latent heat transfer portion provided to the airside in the discharging process at each time is calculated above:

$$\text{Latent heat share} = \text{Total stored latent heat} \times \theta \quad (15)$$

The total share of latent heat in the discharging process is calculated as above:

$$\text{Total latent heat share} = \frac{\text{Total stored latent heat}}{\text{Total airside heat transfer}} \quad (16)$$

CHAPTER 4

GRID INDEPENDENCE STUDY AND MODEL VALIDATION

To ensure accuracy for the numerical model results, two steps are performed for strong model validation: (1) a mesh convergence test based on the comparison of steady state results with experimental data and (2) transient numerical model validation with two cases of experimental data results.

4.1. Grid Independence Study

In order to generate the mesh grid for the designed model, free tetrahedral meshes were used for the domains. The small geometry regions of the heat exchanger were discretized using more refined elements. For the liquid and air boundary inlets and outlets, two boundary layers were constructed. To determine the accuracy of the mesh and the model, a mesh convergence test is performed by changing the mesh quality to attain stable results. As 3D CFD simulation based on PCM operation is highly time consuming, the test was performed for the five slabbed heat exchanger with air and liquid flow without implementing PCM, and the final selected mesh size was implemented for the model. By decreasing the mesh element size and refining the mesh grid, five mesh cases with different element numbers were generated. Each case was simulated to compare the steady state results of the air outlet temperature with experimental data conducted for the same heat exchanger geometry used for air heating between air and liquid operation [28]. In Table 4.1, the mesh cases with their element numbers are represented, and temperature results are compared to obtain the relative Error between numerical and experimental results. The experimental data is based on the research conducted by Fotowat et al. [28] for the same HEX without PCM implementation used for air heating. The goal criterion of relative Error between numerical and experimental results of under 1% was targeted to achieve by refining mesh elements. It is seen that this target has been reached in mesh case 4 with a 0.74% Error. Despite increasing the mesh elements after this stage, the relative Error does not change significantly, yet in case 5, it is beginning to increase. Thus, the criterion for an accurate mesh is selected as case 4 and is implemented for the complete heat exchanger model.

Table 4.1. Grid independence study results.

Mesh case	Domain elements	Air outlet temperature (°C)	Relative Error (%)
1	2.25 million	32.14	5.11
2	3.89 million	32.72	3.40
3	5.10 million	33.47	1.19
4	6.13 million	33.62	0.74
5	8.54 million	33.60	0.78
Experimental data [28]	-	33.87	-

Figure 4.1 illustrates the final meshed geometry for the five slabbed PCM-HEX, including the air, PCM, slabs and fins, as well as the liquid channel domains. Accordingly, this mesh case 4 was adopted and the grid was constructed with the same element quality for the single slab PCM-HEX, which is evident in Figure 4.2. For this model, the total grid element number of 1.40 million is used with an average element quality of 0.31.

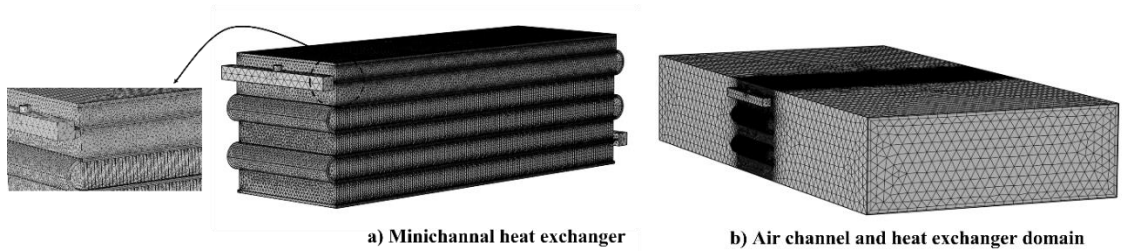


Figure 4.1. Generated computational meshes for the five-slabbed PCM-HEX.

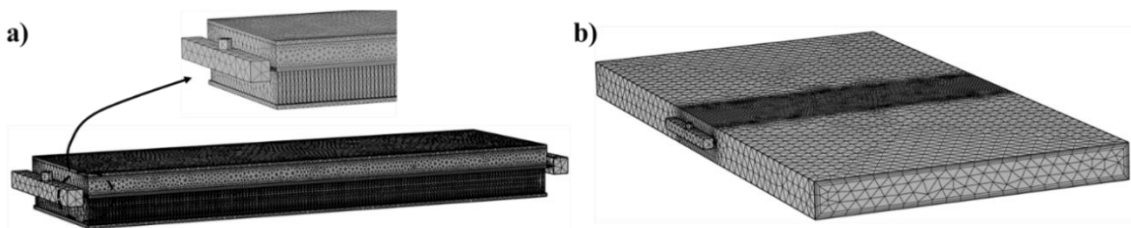


Figure 4.2: Mesh grid generated for the single-slabbed PCM heat exchanger.

4.2. Model Validation

To attain a precise CFD numerical model validation, after carefully developing the geometry model, and with the final high quality mesh implementation, the model is simulated, and the transient numerical result is compared with experimental results for two case studies for the five-slab model. Firstly, the simulation model is validated for the heat exchanger without implementing PCM used for air heating in the experiments. Secondly, the final model PCM heat exchanger is validated with PCM experimental results recently conducted. After a thorough model validation, the numerical setup is considered validated and accurate for further studies in this work. Therefore, the single slab heat exchanger is simulated with reliance to the model validation.

4.2.1. Step 1: Model Validation for Air Heating Heat Exchanger

The model is aimed to be validated with experimental research conducted for the same compact heat exchanger model constructed for air heating mode without implementing PCM. Figure 4.3 illustrates the comparison between the CFD numerical results with the previous experimental results of Fotowat et al. [28]. The transient air outlet temperature, which is the main outcome of the system is compared with the experimental results. The initial temperature for the numerical model was set equal to the experimental data and the transient trends are compared. It is to note that the airside velocity according to the experiments was set to 6 m/s and in the further results section, different mass flow rates were considered for the simulation. From comparing the verification results, an average relative error of 3.22% is attained with a maximum error of 4.26% during simulation time. Good numerical agreement with experimental data is observed. Overall, the average errors in numerical simulations and experiment results are minor as they are less than 5%. A similar trend can also be seen between the experimental and numerical curves. It may be concluded that the experimental and numerical data are in close agreement. Therefore, the model has been validated for the HEX without PCM implementation and can be used and further developed. After this, the heat exchanger model is extended by adding a PCM domain in the same heat exchanger geometry to conduct the numerical study on the model after the second step of model validation. Based on the model validation results in this step, with the relative error attained, a good degree of accuracy is predicted to be attained from the developed heat exchanger model integrated with PCM.

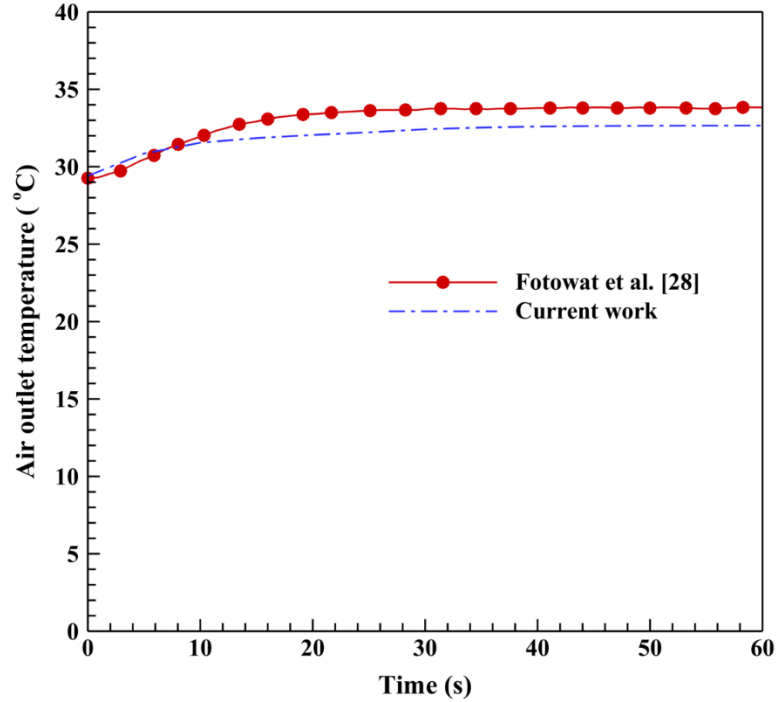


Figure 4.3. Model validation for the compact heat exchanger with results attained by Fotowat et al. [28].

4.2.2. Step 2: Model Validation for PCM Heat Exchanger

After performing model validation for the HEX without PCM implementation in the first step, to attain a more precise CFD numerical model validation, the PCM-HEX model is carefully developed and after the final mesh implementation, the model is simulated, and the transient numerical result is compared with experimental results attained by Askar et al. [60] using the same PCM-HEX. The PCM-HEX modeled in this study is based on the same geometry design and operating conditions as the experimental study. Figure 4.4 illustrates the comparison between the numerical results with the experimental data for the dynamic air outlet temperature for the discharging process. With the aim of PCM air cooling in the discharging process, the air outlet temperature is the main outcome product of the system and is valuable for model validation. The initial temperature condition of the model was set equal to the experimental data, and the results were compared for a 1000-second period. Comparing the plots, excellent numerical agreement with the experimental results is observed. The air outlet temperature trends between numerical and experimental curves are correlated, with low relative Errors attained during simulation time. An average relative Error of 3.30% with a maximum Error of 8.06% is obtained. Therefore, it is

concluded that the numerical model is strongly validated with real experimental data for the complete PCM-HEX system, and the model is validated and used for further numerical studies in this work.

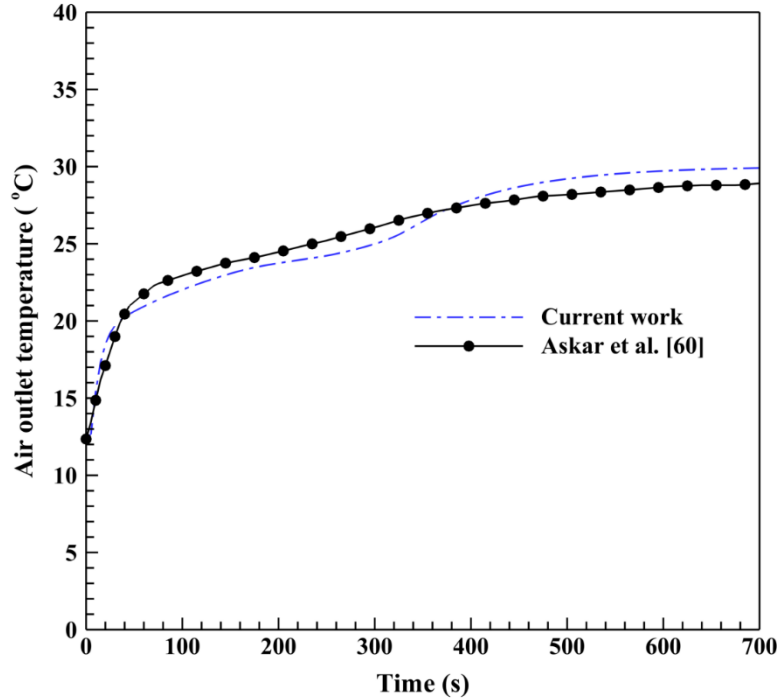


Figure 4.4. Comparison of transient numerical results with experimental study by Askar et al. [60]

Figure 4.5 shows the model validation plot for the comparison of numerical and experimental results while the experimental Error bars were considered. An average absolute deviation of 1.89% was applied to the experimental data based on the errors conducted [60].

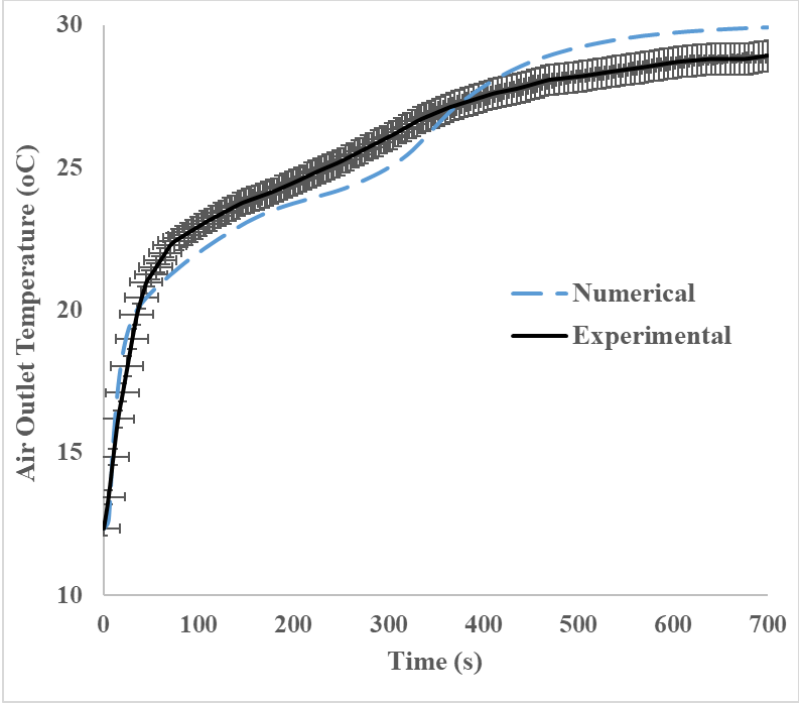


Figure 4.5. Model validation plot with experimental Error bars applied.

CHAPTER 5

RESULTS AND DISCUSSION

5.1. Single Slab PCM Heat Exchanger Air Heating Response

This section presents the numerical results of air heating integrated with TES using latent heat in a PCM heat exchanger. An analysis of the effects of the PCM inside the model is conducted using the operational conditions. The results provide an insight into the response of the charging and discharging processes and the effect of the PCM LHTES on extending the heating period to the airside. Several parameters, such as the fluids outlet temperature, the PCM average temperature, and the fluid heat transfer rate, are discussed in this section.

5.1.1. Dynamic Simulation Results

The CFD model simulated the charging and discharging processes dynamically for the mentioned operational conditions. The simulation was complete for 200 seconds for both the charging and discharging processes. For all results, the time of $t = 0 - 200$ s is devoted to the charging process and $t = 200 - 400$ s is considered for the discharge process. It was seen that this time interval was adequate for the system to reach a steady state situation for both processes.

Figure 5.1 represents the transient plots of fluids outlet temperature, PCM average temperature and solid fraction during the charging and discharging process. It is evident that all temperatures start from an initial value of $20\text{ }^{\circ}\text{C}$. During the charging process, the hot water heats the air while simultaneously melting the PCM. While the water inlet enters the heat exchanger at $70\text{ }^{\circ}\text{C}$, its outlet temperature rises in the charging process and is seen to reach around $54\text{ }^{\circ}\text{C}$ at the end of the process. From the heat transferred, the air and PCM domain temperatures rise, with the air outlet and the PCM average temperature reaching approximately 38 and $56\text{ }^{\circ}\text{C}$, respectively. It is evident that in this process, the system temperatures reach a steady state at around 120 seconds of operation time and the PCM is almost completely melted, reaching a solid fraction of 0.02.

The discharging process begins by shutting down the water inlet at $t = 200$ s after the charging process has reached a steady state condition. After the hot fluid shutdown, the

cool air remains flowing in the system, which allows the thermal energy stored in the PCM to be extracted, thus discharging the PCM and continuing the air heating process for the airside. It can be seen from the discharge process temperature plots that the air outlet and PCM average temperatures initially drop significantly with a sharp slope. During this duration, the PCM is above its solidification temperature, and sensible heat transfer occurs. Upon reaching its solidification temperature, the PCM's latent heat activates, allowing a high heat transfer rate to the air for a period of time, thus delaying the cooling of the airside. This is seen as a change of slope that occurred in the thermal plots of the air and PCM. During the hot fluid shutdown period, this delay time could provide additional heat for the air. Since the water outlet surface is outside the air channel during discharge, the temperature of the water outlet remains constant throughout the discharge process. Observing the PCM phase fraction plot for the discharge process, it is seen that the PCM is fully melted at around $t = 300$ s. At the final stage of the discharge process, the PCM and air outlet temperature reaches a steady state at 13°C . As the main outcome of the system thermal energy storage, it is observed that the LHTES in the discharge process could provide additional air heating for the airside and maintain the air outlet temperature in thermal comfort for around 150 seconds.

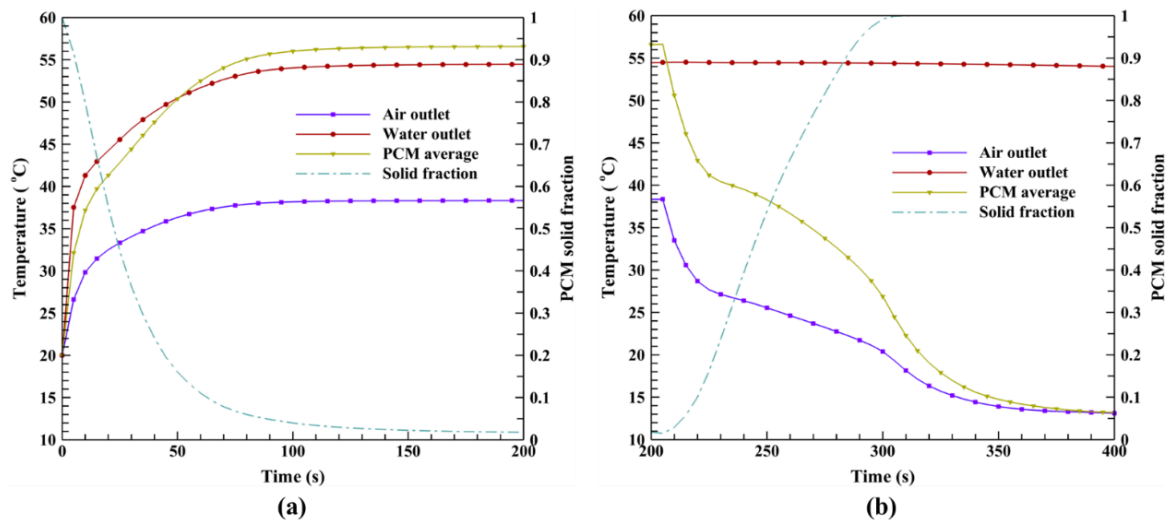


Figure 5.1. Dynamic plots for the operation fluids and PCM for (a) charging process (b) discharging process.

An illustration of the transient behavior of the airside heat transfer rate during the charging and discharging process along with the heat transfer rate of water during the charging process is provided in Figure 5.2. It is observed that the water side heat transfer drops in the charging process, starting from 6.3 kW and reaching to 1.9 kW at the final stage. This is because the water is cooled down during the charging process, heating up the air and melting the PCM to store latent heat. The integration through the heat rate plot of charging heat is provided, which is the total amount of heat transferred from the hot water to the cold air and PCM during the charging process. This amount is calculated and attained at 467.7 kJ. Observing the airside heat rate plot for the charging process, it is evident that the airside heat transfer starts at a low amount and increases to around 1.9 kW at the end of the process. This is because the air is heating in the charging process, and the air outlet temperature is increasing. The total heat that the airside attained from the hot fluid in the charging process is achieved at 364.9 kJ. By subtracting this amount from the total charging heat, 102.7 kJ of energy is attained. Considering no heat losses, this amount is the heat stored in the PCM during the charging process. This energy is later provided to heat the airside in the discharge process. Looking at the airside heat transfer during the discharge process, it is seen that the trend drops while the cold air fully resolidifies the PCM. The amount of energy the charged PCM and the heat exchanger body provide to the air in the discharge process is calculated as 117.9 kJ. This amount shows how much heat could be provided to the for the airside heating during the discharge process when the hot fluid is shut down and the effect of LHTES.

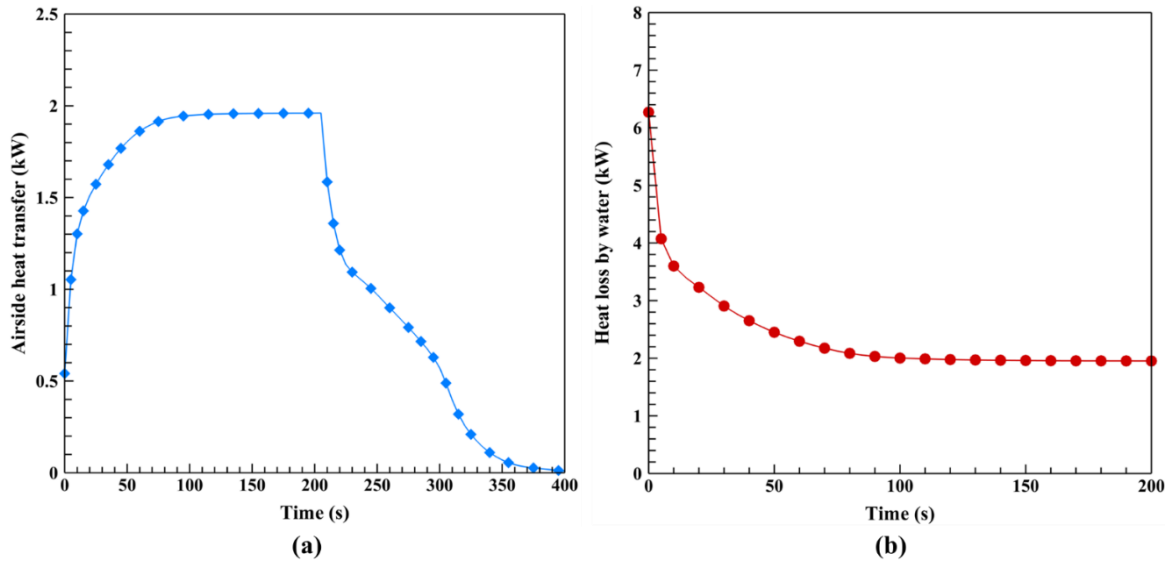


Figure 5.2: Fluids heat transfer rates (a) airside heat transfer for charging and discharging process (b) waterside heat transfer for charging process.

5.1.2. PCM Phase Transition Procedure

To represent the melting and solidification procedure of the PCM during the charging and discharging processes, the 2D phase fraction CFD results of the PCM during different simulation times are illustrated in Figure 5.3. Graphic solid fraction contours are provided for a cut plain in the middle section inside the PCM domain. It is observed from the charging process contours that the PCM melting phenomena is initially occurring faster around the inlet of the water, which is the left and under the PCM domain. The number of 144 thin fins distributed inside the PCM domain highly affects the melting and solidification procedure. Heat is distributed from the hot water by convective heat transfer through fins inside the PCM domain. The PCM plane is gradually melting in the charging process, reaching an almost fully melted position after 60 seconds of operation. The PCM domain's lower side is melting slower due to the cold air being in contact and passing underneath the PCM domain.

In the discharging process, it can be observed that while air is flowing underneath the PCM block, solidification occurs gradually from the lower to the higher regions of the domain. During convective heat transfer, cold energy from air facing beneath the domain is distributed inside the PCM block through the fins. The process of PCM solidification with airflow takes a higher time in contrast with the PCM melting with the liquid flow during

the charging process. After 80 seconds of discharge time, the PCM plane has reached an almost entirely solidified situation.

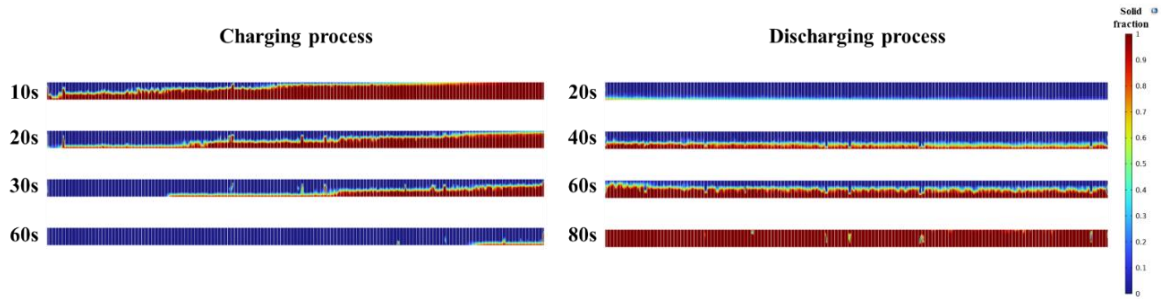


Figure 5.3: Phase fraction contours of the PCM melting and solidification process.

5.2. PCM Heat Exchanger Air Heating Results

This section pertains to the numerical results of air heating integrated TES and release using latent heat in the PCM heat exchanger. After validating results in the form of the compact heat exchanger, the PCM domain is constructed inside the heat exchanger model, as mentioned in the previous sections. The operational conditions are applied to study the effects of the presence of the PCM inside the model. The results provide an insight into the response of the charging and discharging processes and the effect of variation of airside mass flow rate on extending the heating period of the TES. Many parameters such as the fluids outlet temperature, PCM average temperature, heat transfer rates, and the thermal energy gained by the PCM are discussed in this section.

5.2.1. Transient Simulation Results

Using the CFD model, the charging and discharging processes were simulated for three different air mass flow rates. The mass flow rate selected for the simulation cases were Case 1: 0.08 kg/s, Case 2: 0.15 kg/s, and Case 3: 0.30 kg/s. Two lower air mass flow rates were selected to be studied to compare and achieve a flow rate of air that attains an effective passive air heating by the PCM and extend the heating period in the discharging process. The simulation was complete for 150 seconds of charging and 550 seconds of discharging process. For all results illustrated, the time interval of $t = 0 - 150$ s is dedicated to the charging process, and $t = 150 - 700$ s is for the discharge process. It was seen that this timing was adequate for the system to reach a steady state situation in all airflow rates and thus was an appropriate timeframe to report for the processes. In the following, the transient

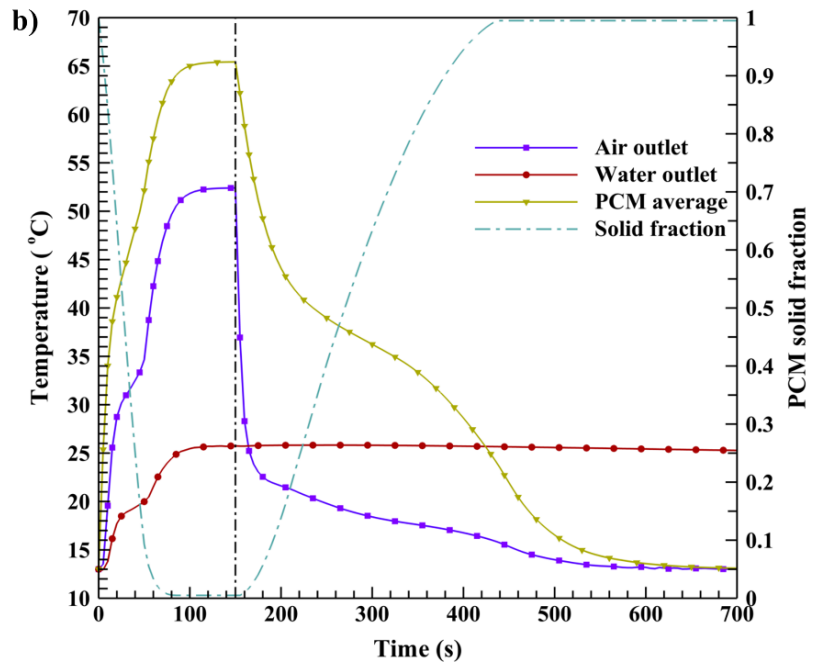
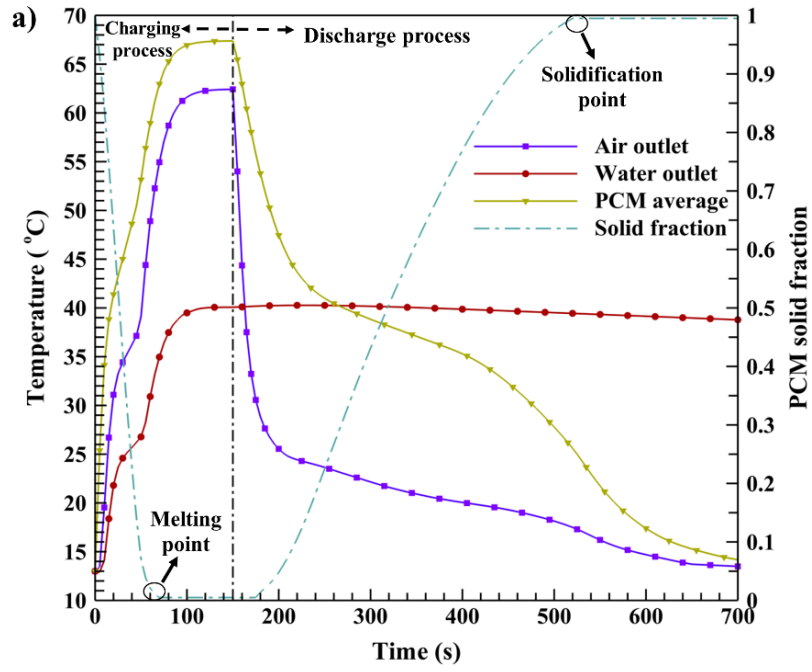
results of temperature, heat and PCM phase fraction, along with the share of latent heat, are discussed.

5.2.1.1. Fluids Outlet Temperature and PCM Phase Plots

The transient plots of the PCM charging and discharging process at three different simulation cases are represented and compared in Figure 5.4. The dynamic response of the air outlet temperature, water outlet temperature, PCM volume average temperature, and the PCM solid phase fraction are observed. The initial values for the temperature of the system model were assumed to be equal in all domains and were set to 13 °C. Generally, it is observed that the heat transfer and PCM melting in the charging process reaches to steady state faster than in the discharging process. This is because in the charging process, water flows in the heat exchanger channels throughout all the heat exchanger slabs, transferring its heat to air and PCM with the help of the fins between the slabs more effectively. While in the discharging process, water flow is off, resulting in a later equilibrium between the airflow and PCM due to slower heat transfer occurring between them. The PCM is located inside the volume of the top two slabs and thus has mostly indirect heat transfer with the airflow. The air transfers heat to the body of the heat exchanger by passing through the fins between the four lower slabs. The aluminum fins are uniformly connected to the heat exchanger's slabs and body, which could transfer heat from the airside section to the PCM domain. This way, the PCM is resolidified in the discharging process.

During the $t = 0 - 150$ s time interval for the charging process, the fluids outlet temperature sharply rises from the initial temperature to their steady state condition in all air mass flow rate cases. During this process, water melts the PCM and heats the air through heat transfer within the heat exchanger's fins. When the PCM starts melting within its melting temperature, latent heat capacity is activated, and the melting occurs at a constant temperature inside the PCM within the melting period. As seen in the figures, a slope change occurs concurrently within the PCM and fluid outlet temperatures while the PCM is within its melting temperature range. This is explained by the fact that in this transition, more water energy is extracted by the PCM due to the latent heat of fusion happening at a constant melting temperature. In the figure for simulation Case 1, due to the PCM average solid fraction trend, it is seen that the fraction reaches almost zero at around $t = 70$ s ,

which is the melting time of the PCM in the charging process. The phase fraction reaches a steady state at this time, and the PCM is fully melted with no effective latent heat. As other simulation figures show, the PCM melting time in the charging process increases with the air mass flow rate. This is because, in higher mass flow rates, the share of water heat transfer dedicated to the airside is increased. The melting time reaches around $t = 80$ s and $t = 100$ s for air mass flow rates of Case 2 and Case 3, respectively. Despite this, due to the temperature trends in all air mass flow rates, it is observed that the system temperature reaches a steady state slightly faster with the increase of the air mass flow rate. The system's steady state condition occurs when the temperatures reach a constant value with no further noticeable change with time. When the charging process is complete, it is visible that the average temperature of the PCM reaches higher than the temperatures of the fluids. This is because the PCM located at the beginning of the heat exchanger slabs extracts heat effectively from the inlet hot water. The final average temperature of the PCM in the charging process is mostly affected by the water inlet condition and is not seen to be affected significantly by the increase in air mass flow rate. This amount reaches around 65 °C, slightly reducing with the increased air mass flow rate. In contrast to the PCM average temperature, the final fluid outlet temperatures in the charging process, however, are considerably affected by the airside mass flow rate. Comparing trends between cases in Figure 5.4, it is seen that with the increase in air mass flow rate, the fluid's final outlet temperature is decreased in the charging process. These changes are explained by the fact that when the airside mass flow rate increases, the air has less time in direct surface contact with the heat exchanger fins to extract heat from the hot water and thus has resulted in a drop in the air outlet temperature. For the waterside, by raising the air mass flow rate, the temperature difference between the water inlet and outlet increases resulting in a larger temperature drop and a lower outlet temperature on the waterside. This is because the increase of air mass flow rate increases the airflow velocity inside the heat exchanger, resulting in a higher convective heat transfer coefficient for the airside. This is followed by a decrease in the temperature of the heat exchanger fins. To compensate for this temperature drop, the fins must extract more heat from the waterside, leading to a higher conduction heat transfer between the heat exchanger tubes and fins, leading to a drop in the waterside temperature.



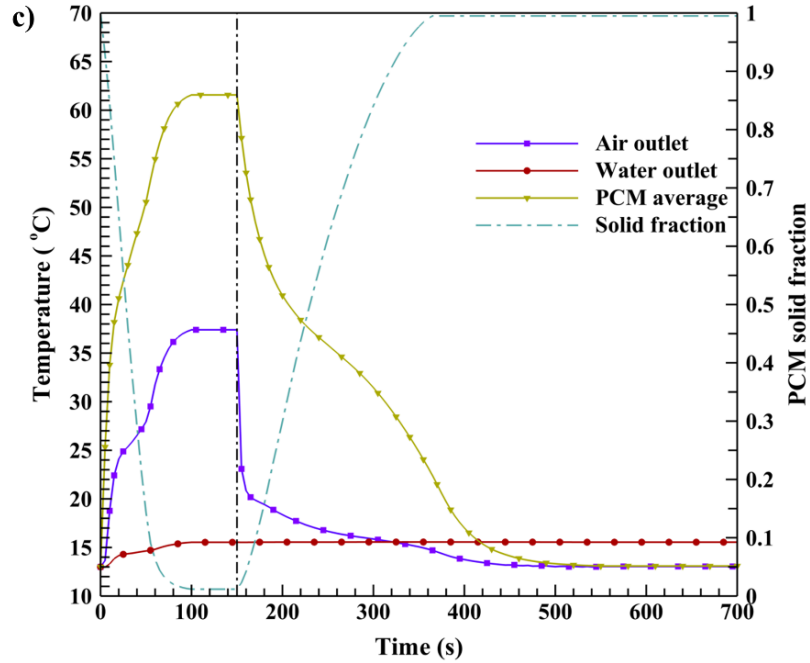


Figure 5.4. Fluids temperature and PCM phase fraction plots for charging and discharging processes for simulation (a) Case 1 (b) Case 2 (c) Case 3.

Presenting the graphic 3D contours of the temperature phase fraction would be highly valuable to further illustrate the heat exchanger behavior in the charging process. In this regard, Figure 5.5 represents the temperature distribution of the fluid's temperature and the PCM solid fraction with the pass of time for the charging process of the Case 1 simulation. The fluids, the water channels, the slabs domain, and the air path streamlines passing through the slabs are provided. The PCM solid fraction is illustrated with five cut planes through the PCM domain along the path of the slab. It is evident that initially, at $t = 0$ s, the system is in the primary state, with all domains at the initial temperature of $T_0 = 13$ °C and PCM being completely solid, with a solid fraction of "1". As time passes through the charging process, water gradually heats the slabs, and the air passes through while simultaneously melting the PCM between the slabs. With the passing of water through the minichannel inside the slabs, water gradually drops its temperature by its heat transfer with air and the PCM. This results in a temperature distribution throughout the slab's path. During the charging process, the higher slabs closer to the inlet of the water reaches higher temperatures, and the lower slabs possess lower temperatures. As cool air inserts the heat exchanger, the front of the slabs in contact with the air inlet streamlines are cooler than the back side where air exits the slabs. Due to the temperature contours, over time, the

temperature of the water inside the channels increases, resulting in the slabs heating up and an increase in the water and air outlet temperature. This is in agreement with Fig. 4 (a), as the water outlet temperature reaches 23.6, 26.7, and 39.5 °C at $t = 25$ s, $t = 50$ s, and $t = 100$ s, respectively. During these moments, the slabs' air outlet temperature was observed at 33.2, 39.1, and 61.6 °C in order. The air streamlines are seen to have uniform temperatures before and after passing through the heat exchanger. In observing the PCM phase fraction plane slices over time, it is evident that the PCM is generally melting and reaching a full melting phase within a short period of time. The time it takes for PCM to melt completely is shorter than the time it takes for the heat exchanger and fluid temperatures to reach a steady state. This trend is also visible in Figure 5.4. According to Figure 5.5, the PCM slices melt faster near the slabs and the water inlet. During the melting process, the PCM domain is supported by fins and slabs on both sides, which assist in uniform melting. During the melting transition, at $t = 25$ s, about half of the PCM is melted with an average solid fraction of 0.53. At $t = 50$ s, most of the PCM is melted with an average solid fraction of 0.07 and reaches a fully melted situation at $t = 100$ s. A more detailed description of the melting and solidification processes inside the PCM domain is provided in Section 5.2.2.

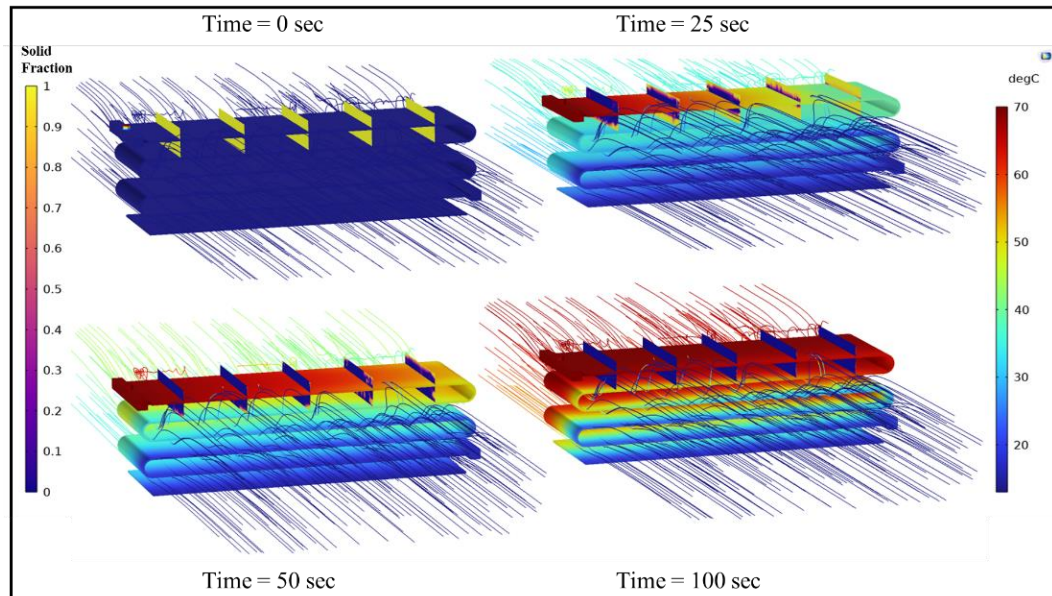


Figure 5.5. 3D illustration of airside and water flow temperature distribution and PCM solid fraction for different times of the charging process for Case 1 simulation.

A further illustration of the flow of air through the heat exchanger and the temperature distribution for the steady state of the charging process is provided in Figure 5.6. The heat exchanger is observed to possess a wide temperature distribution. According to Figure 5.6 (a), due to the airflow in contact with the slabs, fins, and PCM domain, the frontal area of these structures are cooler than the back. Figure 5.6 (b) shows that the airflow temperature and streamlines are uniform before passing through the heat exchanger. The flow of air produces vortices in the streamlines after it exits the heat exchanger at the top region. There is a difference in temperature between streamlines leaving lower slabs and fins and streamlines leaving higher slabs and fins when they exit. This is because the lower slabs and fins in contact with air are cooler due to the temperature drop on the water side.

Following the charging process, and reaching a fully steady state condition, the discharging process begins by shutting down the water inlet at $t = 150$ s . In this process, at fluid shutdown, the cool air remains flowing in the system, allowing to the extraction of the thermal energy stored from the charged PCM, thus discharging the PCM and continuing to provide air heating for the system. The cool air at 13 °C transfers heat with the hot melted PCM, which was shown to reach around 65 °C at the end of the charging process. As seen in the discharge process in Figure 5.4 in all simulation cases, the air outlet and the PCM average temperature initially drop significantly with a sharp slope. This is because the PCM is above its solidification temperature at this point, and there is sensible heat transfer occurring for the PCM. The PCM's latent heat is activated when it reaches its solidification temperature, enabling a high heat transfer to the air for a period of time, resulting in a delay time for the airside temperature drop. This delay time could provide additional heat for the air during the hot fluid shutdown period. This additional thermal comfort time provided by the heat exchanger for air heating is seen to be highly dependent on the air mass flow rate, decreasing in higher flows. During the discharge process, the water outlet temperature remains almost constant because the water outlet surface is outside the air channel and does not transfer heat with the surroundings. Looking at the PCM solidification plot, with the increase in air mass flow rate, the PCM reaches faster to its solidification point with a solid fraction of “1”. The PCM solidification time was observed as $t = 520$ s, $t = 440$ s, and $t = 360$ s for simulation Cases 1 to 3, respectively. Designing a PCM heat exchanger with

an effective air mass flow rate is highly necessary to provide sufficient heating time during the discharging process.

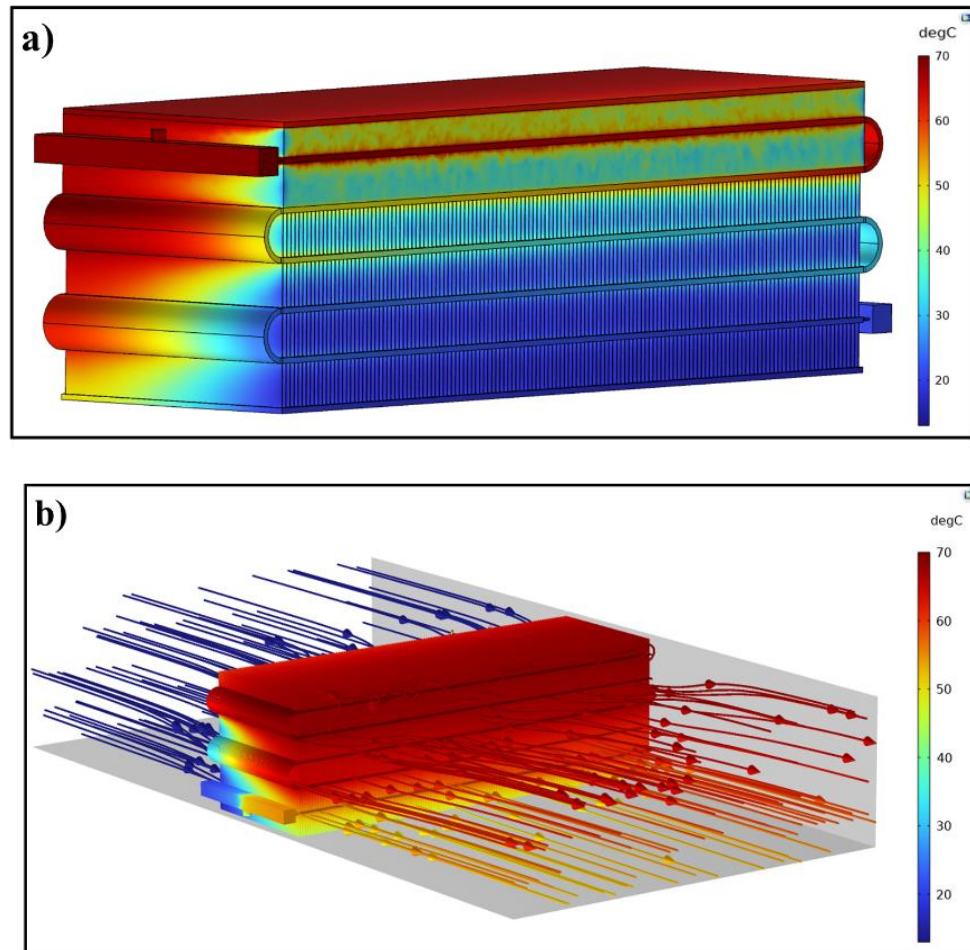


Figure 5.6. Steady state temperature distribution for the heat exchanger charging process for Case 1 (a) slabs, fins and PCM domain (b) air streamlines passing through the fins.

For a more precise outlook of the temperature distribution throughout the six rows of the heat exchanger fins during the end of the charging process, Figure 5.7 illustrates the fin temperature distribution through the front and back side of the heat exchanger for simulation Case 1.

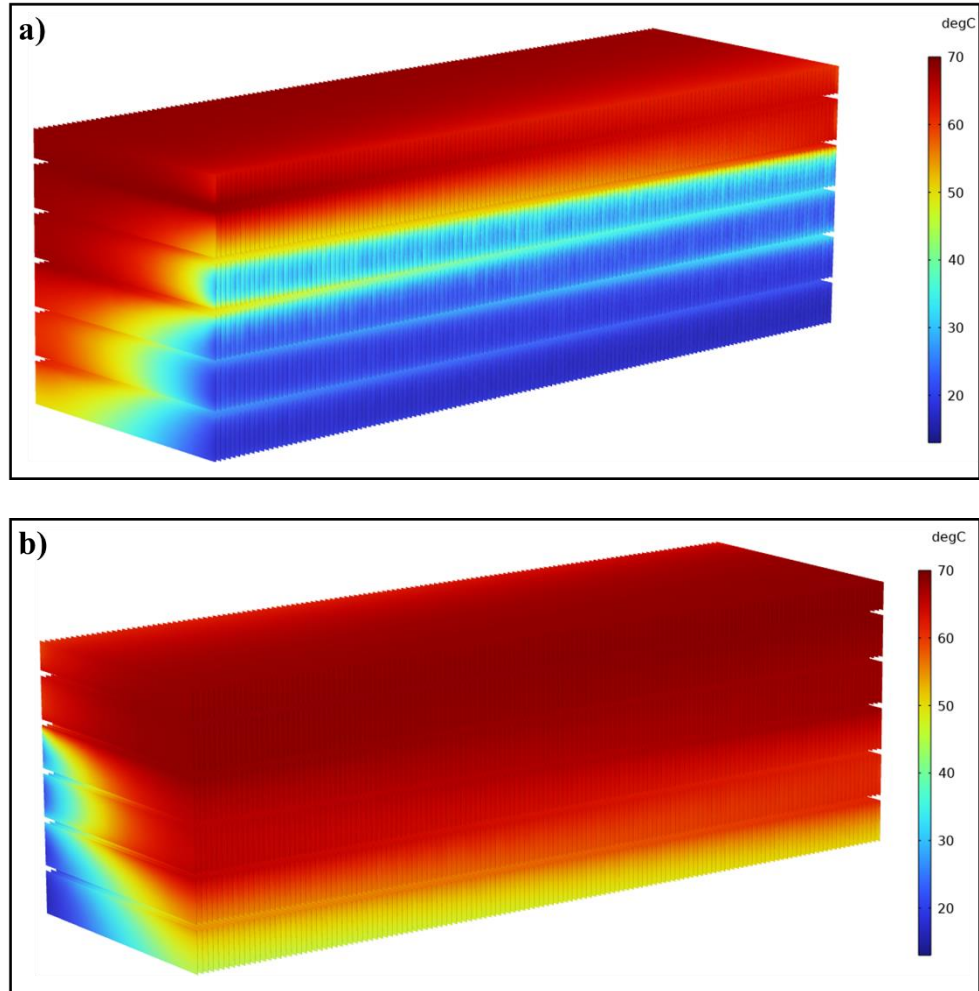


Figure 5.7. Fins temperature distribution by the end of the charging process for Case 1 (a) frontal view (b) backside view.

To further illustrate the 3D heat transfer temperature distribution of the 68 minichannel as the hot liquid domain during the end of the charging process, Figure 5.8 is represented as below.

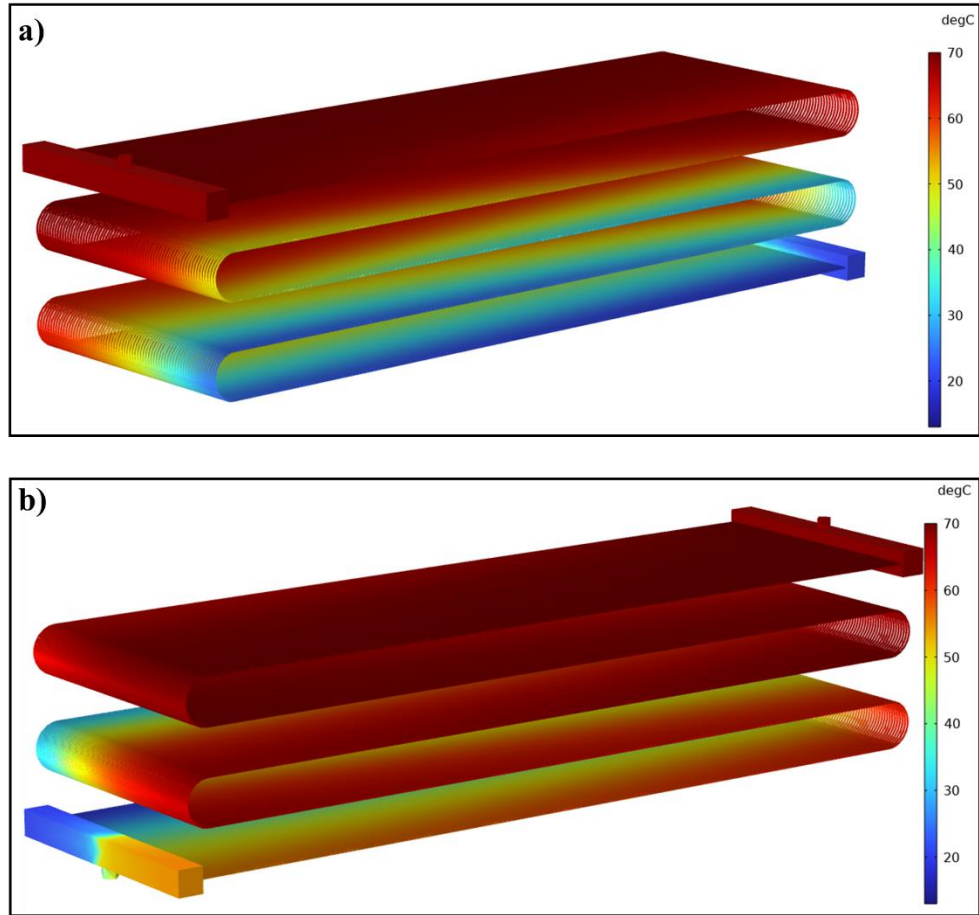


Figure 5.8. Hot heat transfer fluid minichannels temperature distribution by the end of the charging process for Case 1 (a) frontal view (b) backside view.

Figure 5.9 graphically shows the 2D cut plain temperature distribution through the middle of the heat exchanger by the end of the charging process. The temperature distribution through all domains of the heat exchanger including the hot liquid, slabs, fins, air, and PCM is precisely shown.

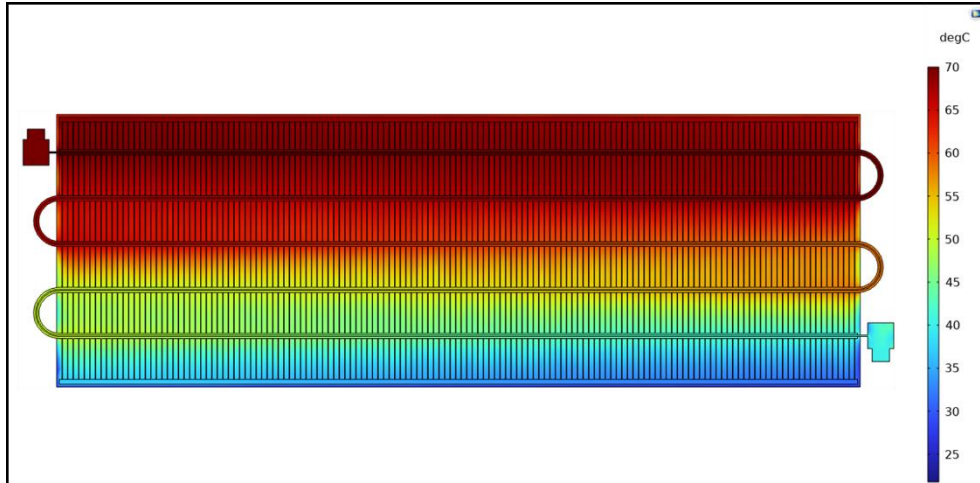


Figure 5.9. 2D Temperature distribution of the cut plain through the middle of the heat exchanger by the end of the charging process for Case 1.

5.2.1.2. Fluids Heat Transfer Rate

The transient behavior of the airside heat transfer rate during the charging and discharging process is illustrated in Figure 5.10 based on different airside mass flow rates. It is visible that in the charging process, the trend of the airside heat transfer rate is increasing. Increasing the air outlet temperature enhances the airside heat transfer, resulting in a more significant temperature differentiation between the inlet and outlet air. By the increase of the outlet temperature of the air, a greater temperature differential between the inlet and outlet air is reached, resulting in the enhancement of the airside heat transfer. It is observed that this rise is more significant for higher air mass flow rates. Increasing the air mass flow rate results in higher heat transfer in the charging process.

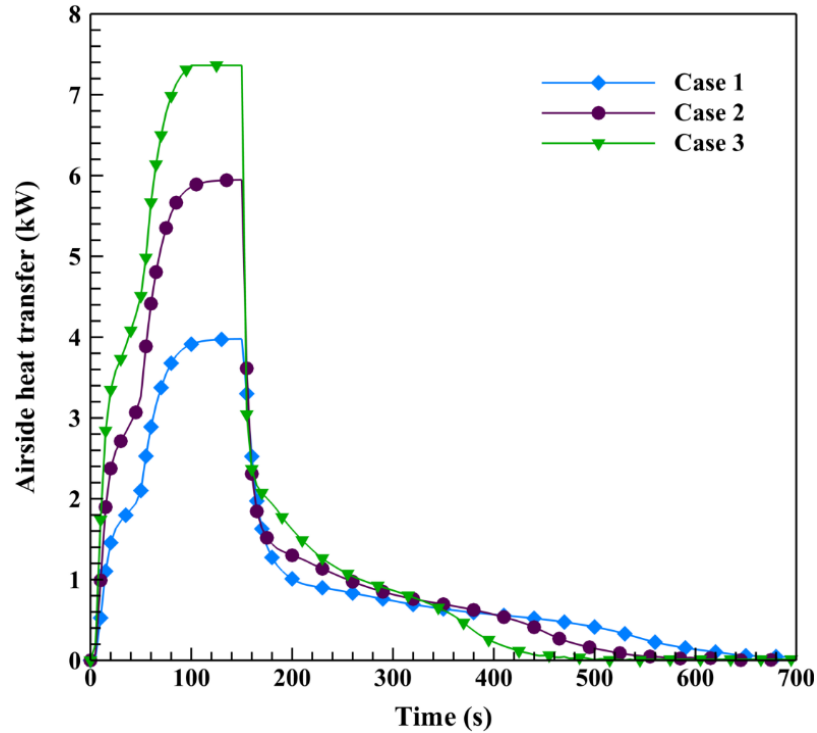


Figure 5.10. Airside heat transfer rate during the charging and discharging process.

In the discharging process, after the water fluid shutdown, there is a sharp drop in the heat transfer rate due to the PCM being within its sensible heat transfer range. When latent heat takes place, a slope change occurs for the heat transfer rate curve. The latent heat transfer range takes place faster for higher airflows leading to more heat rates for the curve. After the PCM solidifies completely, latent heat is completed, and another slope change occurs, leading to a cross appearing between the curve cases in the discharging process. Overall, in the discharging process, the total discharge heat transfer, considered the area under the curves, decreases with the mass flow rate. Askar et al. [33] attained similar results on their experimental heat exchanger; from their figure, it was observed that an increase in airside mass flow led to a decrease in air heat transfer in the discharging process. Also, this effect was diminished at higher mass flow rates.

Figure 5.11 dynamically compares the heat transfer loss in the waterside in the charging process at different airflow rates. In higher air mass flow rates, overall, the water-side heat transfer loss is increased between the cases. Due to the heat rate plots, a higher loss of heat transfer for lower air mass flow rates is observed for the waterside charging process. As seen and discussed in the previous section, the water outlet temperature drops more

significantly at higher air mass flow rates, leading to a higher water temperature differentiation, resulting in more heat drop in the water side.

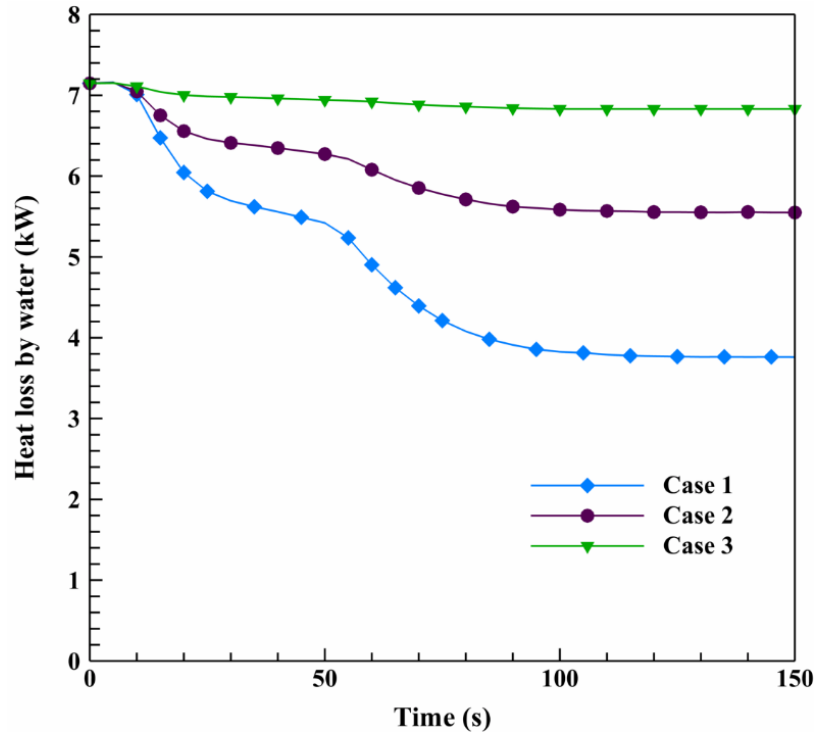


Figure 5.11. Water side heat transfer rate for the charging process.

5.2.1.3. Share of PCM Latent Heat During Discharging Process

In this section, the trend of latent heat rate throughout the PCM discharge procedure is computed to attain the share of latent heat at each time. In the charging process, the PCM extracts heat from the hot fluid, which charges the PCM to its full latent heat capacity. This energy is to be released into the air in the discharging process as passive heating for the system. The PCM mass is reported as 0.62 kg, considering a uniform mass for the domain. Thus, the total latent heat that the PCM stored during the charging process is calculated as 150.8 kJ based on the PCM latent heat specifications. The dynamic drop of the stored latent heat of the PCM in the discharging process for the three simulation cases is reported in Figure 5.12. The graph is plotted for discharge time starting at $t = 150$ s. As the PCM steadily solidifies and the liquid fraction drops, the amount of stored latent heat of the PCM drops in the figure for all cases. The drop rate is more significant for higher mass flow rates, as the higher airside mass flow has a faster PCM discharge time. When the latent

heat drops to zero, the PCM is fully solidified, and the latent heat transfer from PCM to air is completed.

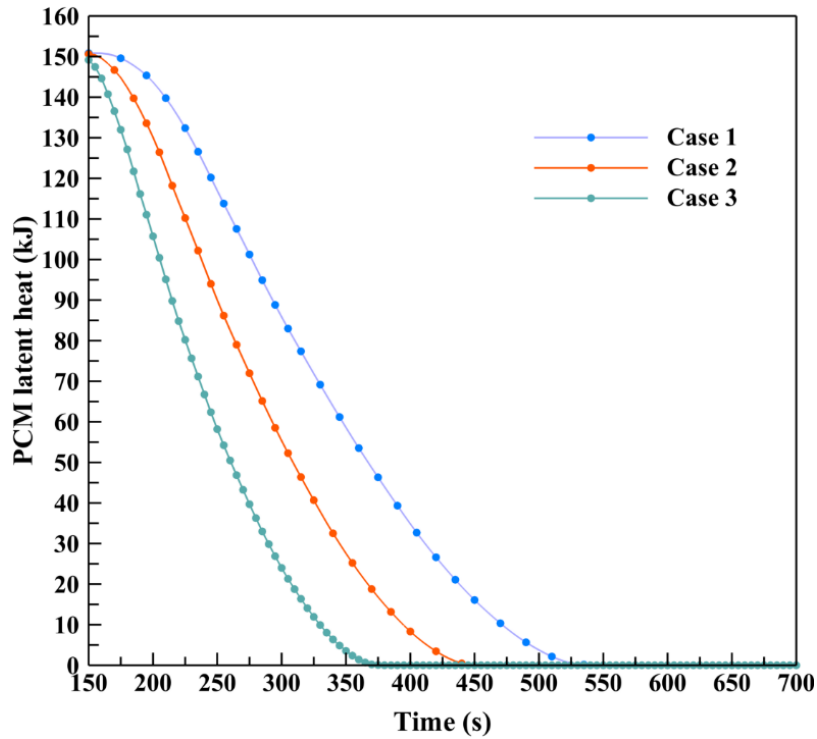


Figure 5.12. Release of the stored latent heat in the discharge process for different simulation cases.

During the discharge process, it is assumed that all the air's energy comes from the PCM, and the minor heat that is gained from the heat exchanger's body is neglected. Hence, the total discharge heat transfer refers to the amount of energy that is gained from the PCM by the airflow, represented as the airside heat rate in Figure 5.10. The rate of latent heat drop during the discharge process is attained by the derivation of the latent heat curves in Figure 5.12. The portion of sensible heat transfer from PCM to air is thus calculated by the subtraction of the latent heat rate from the total discharge rate. The total discharge heat rate, along with the latent and sensible heat rate for simulation Case 1, is presented in Figure 5.13. The share of latent heat is calculated by the percentage share of the latent heat to the total heat rate. As observed from the figure, initially, low latent heat is provided to the airside by the PCM, leading to a sharp drop in the total heat transfer rate. The reason that the latent heat rate starts from zero and the low value of latent heat share in the initial periods of the discharging process is that the PCM average temperature is above its fusion

temperature. Thus, mostly sensible heat is exploited over that period to reduce the PCM average temperature to its solidification point. In the following, the PCM latent heat share reaches its peak at more than 80%. There has been a decrease in the share of sensible heat transfer during this period, reaching its lowest values. The latent heat drop follows this while most of the PCM is discharged, increasing the sensible heat rate. After the PCM has fully melted, latent heat reaches zero, while only sensible heat is occurring, leading the system to reach a steady state.

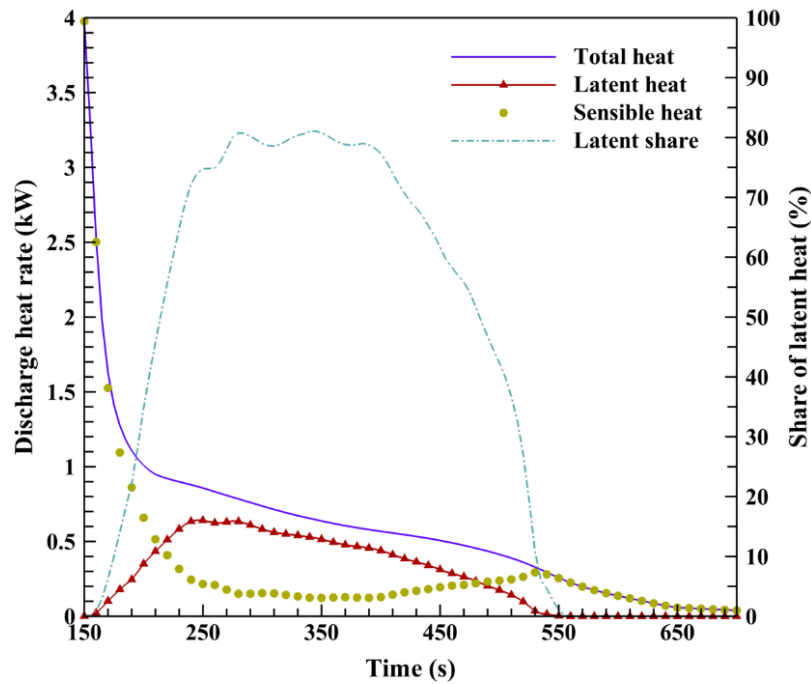


Figure 5.13. Latent and sensible heat rate trends through the discharge process for simulation Case 1.

5.2.2. PCM Phase Transition Procedure

An illustration of the solidification and melting of the PCM domain during various stages of the charging and discharge process is argued in this section. As presented in Figure 5.14 and 15, the solid phase fraction and temperature distribution have been depicted with two-dimension (2D) contours at various slices in the PCM domain over the course of the simulation time for Case 1. The contours are derived for three different plane locations through the PCM blocks of the front ($x = 0$ mm), middle ($x = 50$ mm), and back ($x = 100$ mm). The temperature contours are plotted at higher time instants than the phase fraction for better result observance. Hot fluid passes through the heat exchanger's first

slab between the blocks of the PCM, melting the PCM in the charging process. It is observed from Figure 5.14 that the melting phenomena are initially higher around the inlet of the water, which is the left side of the contours. Convective heat transfer through fins inside the PCM domain distributes heat from the hot water [73]. The PCM gradually melts, reaching an almost fully melted position at $t = 60$ s. It is observed that the middle plane through the heat exchanger melts faster than the front and back of the domain. Also, the lower PCM block takes more time to melt as it is a larger domain. The trend comparison shows that the front side of the PCM has a slightly higher solid fraction distribution among other domain locations. This is because cool airflow is in contact with the PCM's front surface, leading to slower melting. This difference, however, is not significant throughout the charging process. Looking at the temperature distribution of these surfaces during the charging process in Figure 5.15 (a), it is evident that the temperature distribution in the process of charging and discharging is coordinated with the phase fraction plots. The regions which reach higher temperatures are reaching lower solid fractions faster. It is evident that the top right part of the PCM block melted slower due to its lower temperature. Also, it is seen that the middle plane reaches a uniform temperature distribution faster than other locations. Besides, the cool airflow's effect on the front plane's temperature distribution is more evident.

Regarding the discharge process, it is seen from Figure 5.14 that while air flows underneath the PCM block, the solidification process happens gradually from the lower to the higher part of the domain. Convective heat transfer is distributed inside the PCM block through the fins from the air facing the front and under the domain. The front section of the PCM is clearly solidifying significantly faster than the rest. At simulation time $t = 450$ s, the front and middle sections of the domain are solidified to a large extent, while the back region has not been melted abundantly. It is clear from the illustration that the top PCM block takes longer to solidify after the bottom region is fully solidified. Due to the discharge temperature plots presented in Figure 15 (b), it is observed that the front surface possesses lower temperatures in the discharging process while the back has higher temperatures due to airflow. Also, in all cut planes, the lower region has cooler temperatures. At a simulation time of $t = 550$ s, the front along the middle side of the PCM reaches a uniformly cool temperature distribution.

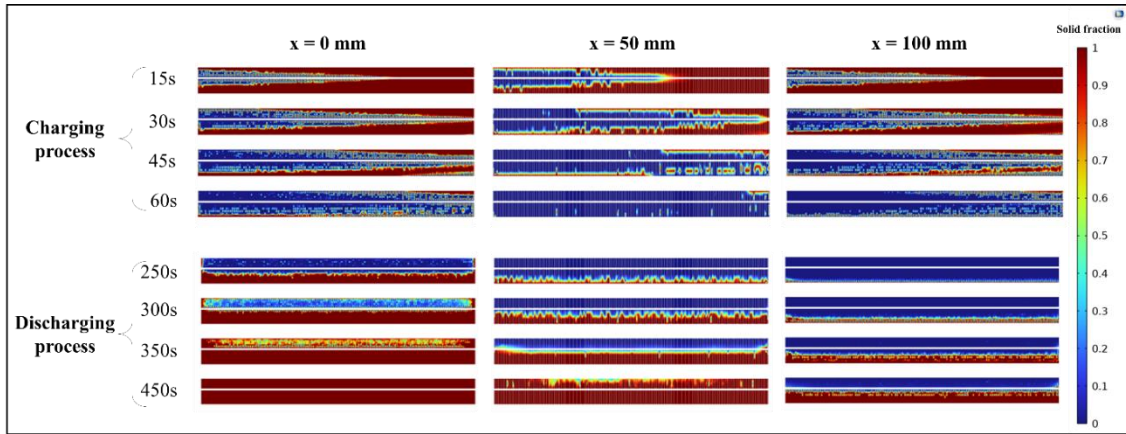


Figure 5.14. 2D solid phase contours of the PCM melting and solidification for Case 1 simulation.

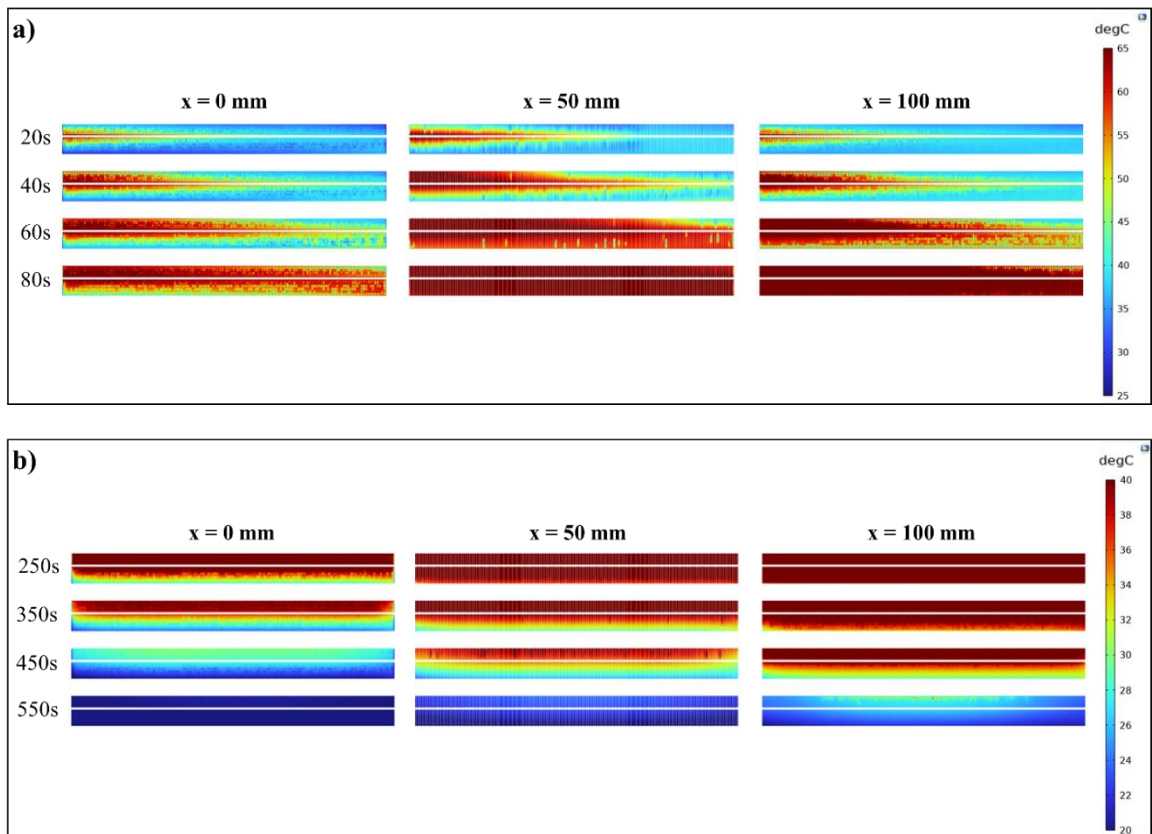


Figure 5.15. 2D PCM temperature contours for Case 1 simulation (a) charging process (b) discharging process.

5.2.3. Energy Gain Through PCM Passive Air Heating

This section presents the effect of using PCM while releasing the stored energy in the discharge process as an efficient heat gain method. Figure 5.16 compares the airside heat transfer rate (total discharge heat transfer rate) during the discharge process for simulation Case 1 with and without implementing PCM. It is observed that the effect of PCM in providing significant extra passive heating during the fluid shutdown is evident. The PCM interrupts the increase in air outlet temperature for a period of time, allowing extra time for heat transfer and air heating to occur. Without a PCM, heat transfer is sharply reduced since by shutting off the water, the air outlet temperature increases, leading to a decrease in heat transfer. The area underneath the curves represents the total discharge heat provided by the heat exchanger. This value is attained at 323.3 kJ with PCM and 76.0 kJ without PCM implementation. Thus, the application of PCM inside the heat exchanger could result in an additional load of 247.3 kJ for air heating which is observed as the area between the curves as energy gain provided by the PCM heat storage. In addition, it has been observed that the use of PCM prolongs the period of air heating and delays the decrease in the heat transfer rate. The extra discharge heating time is considered when a change of slope happens in the discharge heating curve, and its drop is delayed due to the PCM latent heat effect. This time is defined as between the interval of the discharge time that the average temperature of the PCM reaches its solidification temperature until the time that the PCM could keep the air outlet temperature above 15 °C due to Figure 5.4. With the use of PCM, around 375 seconds of extra discharge heating time is observed to be provided for the heat exchanger. This is while for the no PCM model, the heat transfer rate drops to a low amount in around 20 seconds. This additional thermal comfort time provided by the heat exchanger is highly advantageous and reliant on the airflow rate. The total latent heat energy in the discharge process has previously been reported as 150.8 kJ. The effectiveness of the PCM is described as the percentage of the ratio between the total amount of latent heat and the total amount of discharge heat.

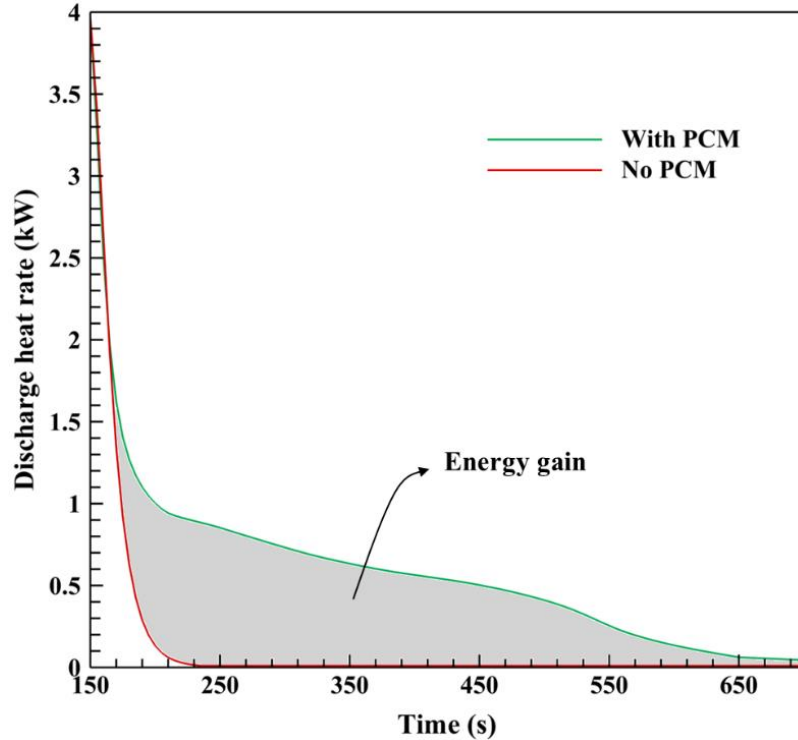


Figure 5.16. Discharge heat transfer comparison between cases with and without PCMs.

Table 5.1 compares the discharge heat, the passive heating time, and the PCM effectiveness for three simulation cases with the no PCM case. It is observed that lower air mass flow rates could provide higher discharge heat resulting in more energy gain due to having a higher discharge heating time. At lower air mass flow rates, PCM effectiveness is observed to be lower due to higher discharge heat. For Case 3, the PCM effectiveness is observed to reach 50.0%. This means that latent heat could provide around half of the heat load for the discharge process. This parameter is highly dependent on the PCM mass and melting temperature. In compact heat exchangers, increasing the PCM mass to a high amount is inefficient because it reduces the airside heat transfer area and causes lower heat transfer performance. In this study, selecting an efficient PCM with a higher melting temperature could reduce the initial sensible PCM heat transfer and the heat drop in the discharge process. It is highly recommended for future research to design an optimized PCM-to-air and liquid heat exchanger according to the PCM mass and location, higher specific latent heat, and melting point. The efficient design of LHTES could further develop thermal energy storage and release and extend the heating times.

Table 5.1. Comparison of crucial results attained from the simulation cases.

	Case 1	Case 2	Case 3	No PCM
Discharge heat (kJ)	323.3	316.2	301.3	76.0
Discharge heating time (s)	375	260	170	20
Latent heat share (%)	46.6	47.7	50.0	-

5.3. PCM Heat Exchanger Air-Cooling Results

After a precise numerical model validation, this section represents the CFD results attained by the PCM-air-liquid heat exchanger utilizing CTES for extended air cooling. Transient heat transfer thermal analysis is performed for the PCM charging and discharging processes subjected to various air mass flow rates. The thermal responses of the working fluids and the PCM are discussed in the following sections.

5.3.1. Dynamic Thermal Performance Analysis

By solving the CFD model, the PCM charging and discharging processes were simulated using three air mass flow rates of 0.08, 0.15, and 0.30 kg/s for model Case 1, Case 2, and Case 3, respectively. Effective air flow rates were selected considering the real application of automotive cabin air cooling to attain passive PCM air cooling time. The simulation charging was conducted for the time interval of 0 to 500s and 500 to 1200s for the discharging process. This time selection was to ensure the system to has reached a steady state in all simulation cases. Presented below are the dynamic results of fluids temperature and heat transfer rates, along with the PCM temperature and solid fraction plots.

5.3.1.1. Fluids and PCM Temperature Response

The dynamic results plots of the PCM charging and discharging processes for three airflow cases are represented and compared in Figures 5.17 to 5.20. The response of the air outlet temperature, liquid outlet temperature, PCM volume average temperature, and the PCM average solid phase fraction are represented. Due to the initial temperature setup, all domain's temperature are taken as 30 °C at 0s, where the PCM is initially at a fully melted condition. During the charging process, the cold HTF flows inside the heat exchanger channels performing two main tasks: solidifying the PCM and cooling the hot airflow simultaneously. These tasks are accomplished through effective heat transfer through the fins that are distributed in the airflow between the slabs. During the discharging process,

the cold HTF is shutdown, allowing passive air cooling by extracting the thermal energy stored in the PCM. Due to the uniform connection between the aluminum fins and the heat exchanger slabs, the thermal energy is transferred from the airside to the PCM domain effectively.

By observing the temperature response plots of air, cold HTF, and PCM in Figures 5.17 to 5.19, it is seen that in the charging process, the outlet fluids and PCM temperatures drop sharply from their initial value then to reach to a steady state for all airflow rate cases. In this process, while the PCM is being cooled to its solidification temperature, latent heat is activated, and solidification occurs at a constant temperature within the PCM. While the PCM is within its solidification temperature range, a slope change occurs concurrently within the PCM and fluid outlet temperatures based on Figures 5.17 to 5.19. The reason for that is because of PCM's thermal energy extraction through latent heat at constant temperature. After this period, the PCM is completely solidified, and a drop in temperature is seen due to the sensible heat until reaching a final steady state. Comparing the studied cases, the airside mass flow rate considerably affects the final fluid outlet temperatures during the charging process. In this process, the fluids' final outlet temperature increases due to higher airflow rates. This is explained by the fact that in higher airflow rates, air has less time for thermal energy transfer from the cold HTF through the heat exchanger body and fins.

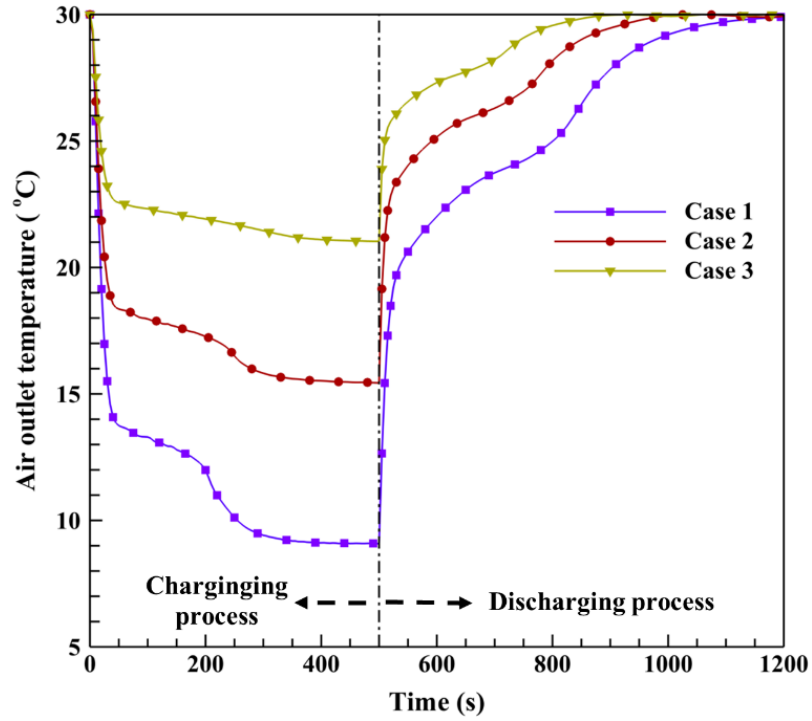


Figure 5.17. Dynamic air outlet temperature responses during the charging and discharging processes for three simulation cases.

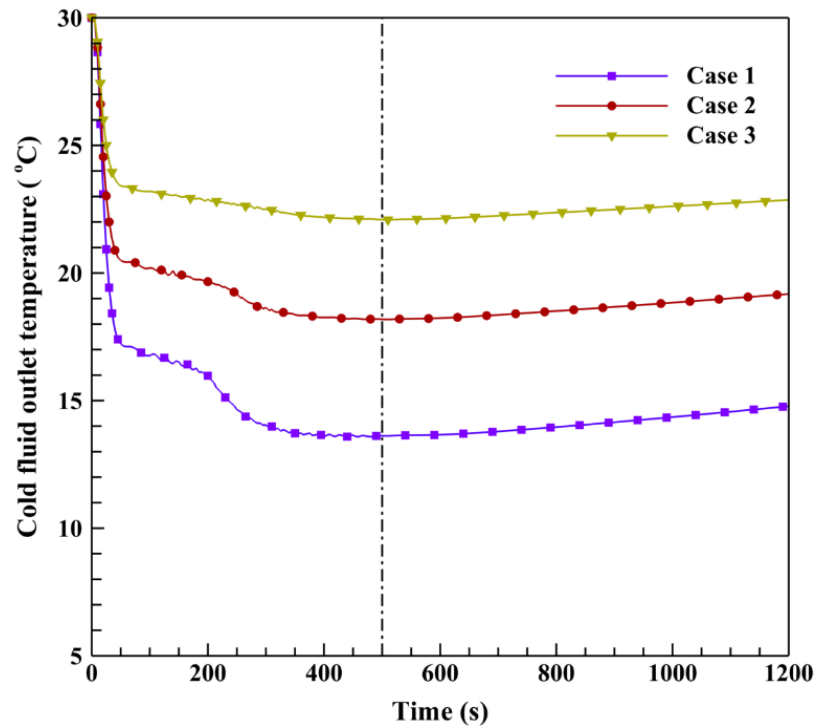


Figure 5.18. Cold fluid outlet temperature.

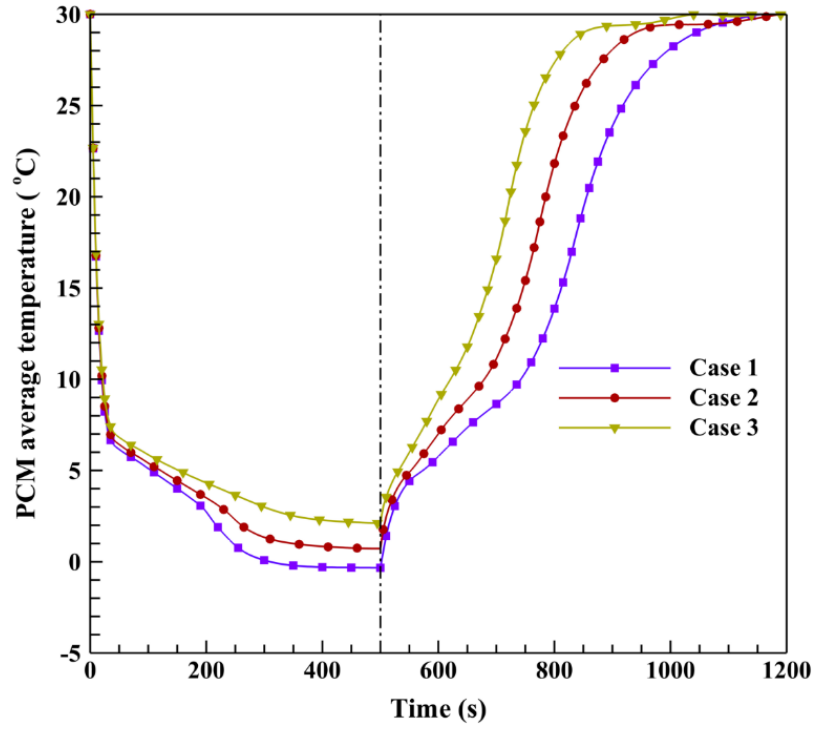


Figure 5.19. PCM average temperature.

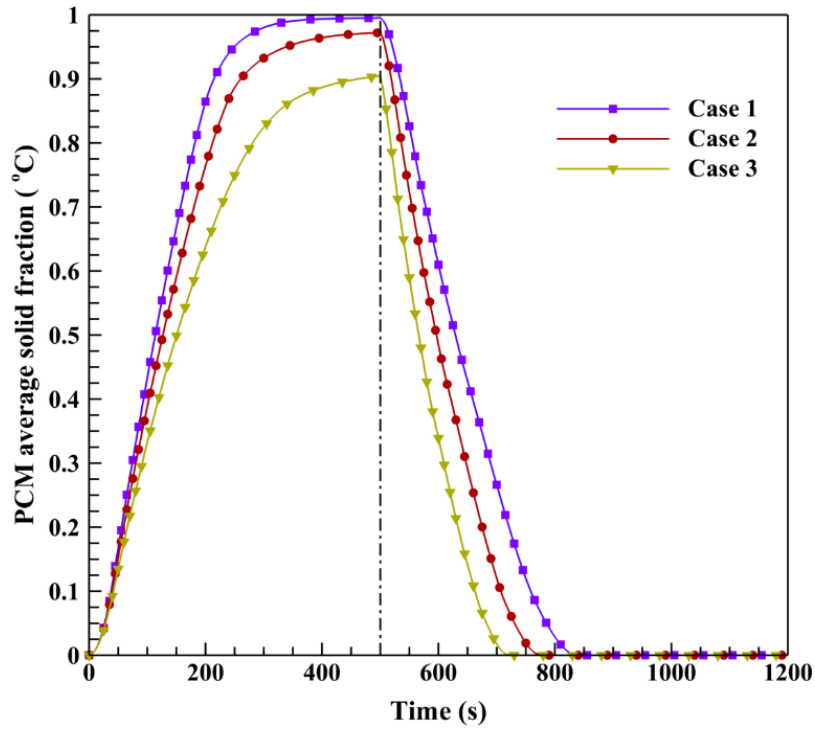


Figure 5.20. PCM average solid phase fraction transition.

In the case of the liquid stream, raising the air mass flow rate results in a greater cold fluid outlet temperature rise. This is because the velocity increase of the airstreams results in a higher convective heat transfer coefficient leading to more heat transfer in the liquid side and a rise in the cold HTF outlet temperature. In the simulated Case 1, the air and cold fluid outlet temperatures reach 9.08 and 13.62 °C at the end of the charging process at 500s. Figure 5.21 shows the 3D graphic representation of the temperature distribution for the fluid flow and the fins of the heat exchanger at this time. The airflow is shown as streamlines with direction arrows passing through the heat exchanger fins. The temperature distribution is observed in the heat exchanger. The cold liquid stream is gradually heated by the hot air streams while they pass the heat exchanger slabs. The frontal heat exchanger body exhibits higher temperatures due to being in contact with the hot airstream. The airstreams leaving the slabs and fins of the heat exchanger is cooled, with lower temperatures observed from the streams leaving top slabs.

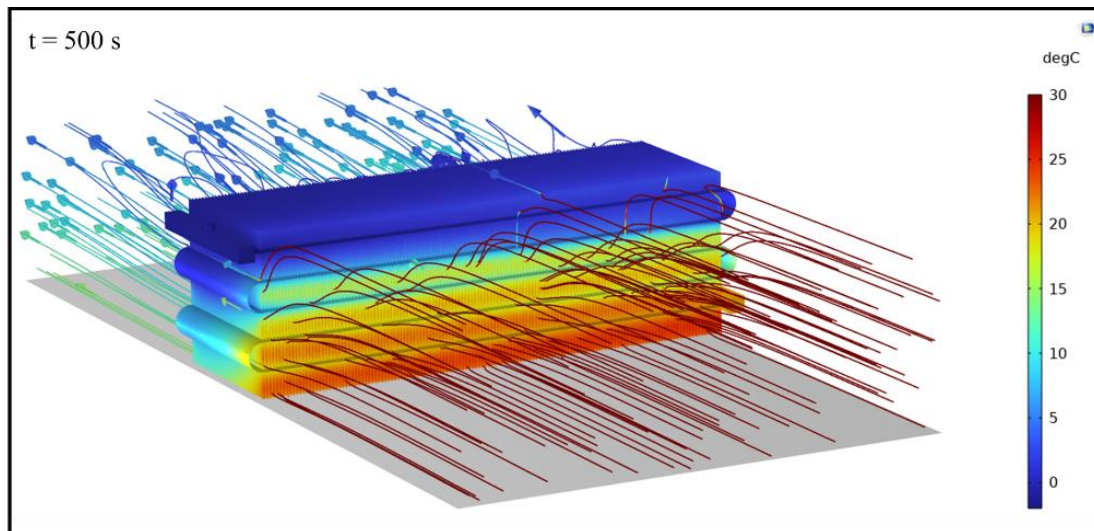


Figure 5.21. Graphic temperature distribution of the PCM-HEX at the end of the charging process for simulation Case 1.

During the charging process and observing the PCM average temperature and phase fraction plots in Figures 5.19 and 5.20, it is seen that the increase in airflow rate slightly affects the PCM final temperature, solid fraction, and solidification time. The average PCM temperature reaches to -0.33 °C for simulation Case 1 in the charging process, and the average solid fraction reaches 0.99 in an almost fully solidified situation at 350s. The increase in airflow rate disturbs the PCM solidification process and leads to an increase in

temperature and has a diminish effect on the solid fraction of the PCM. The average solid fraction reaches to 0.97 and 0.90 for Cases 2 and 3, respectively, at the final stage of the charging process. This is due to the reduction of the share of cooling load for the PCM domain in higher airflow rates. After this process, the PCM is charged with a vast majority of the capable latent heat activated to provide for the discharging process.

Figure 5.22 illustrates the fin temperature distribution through the front and back of the heat exchanger during simulation Case 1, giving a more precise view of the temperature distribution throughout the six rows of the heat exchanger fins during the end of the charging process.

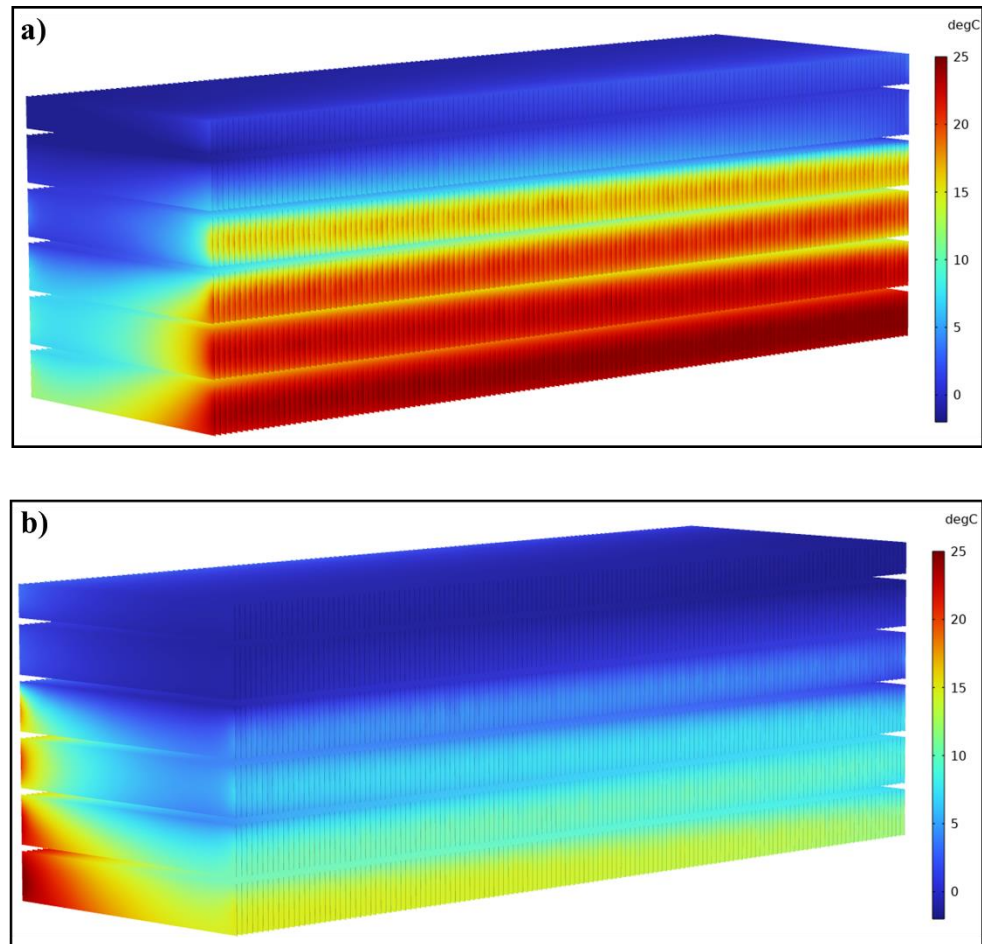


Figure 5.22. Fins temperature distribution by the end of the charging process for Case 1 (a) frontal view (b) backside view.

As an illustration of the 3D heat transfer temperature distribution of the cold liquid domain in the 68 minichannel during the end of the charging process, Figure 5.23 is presented below.

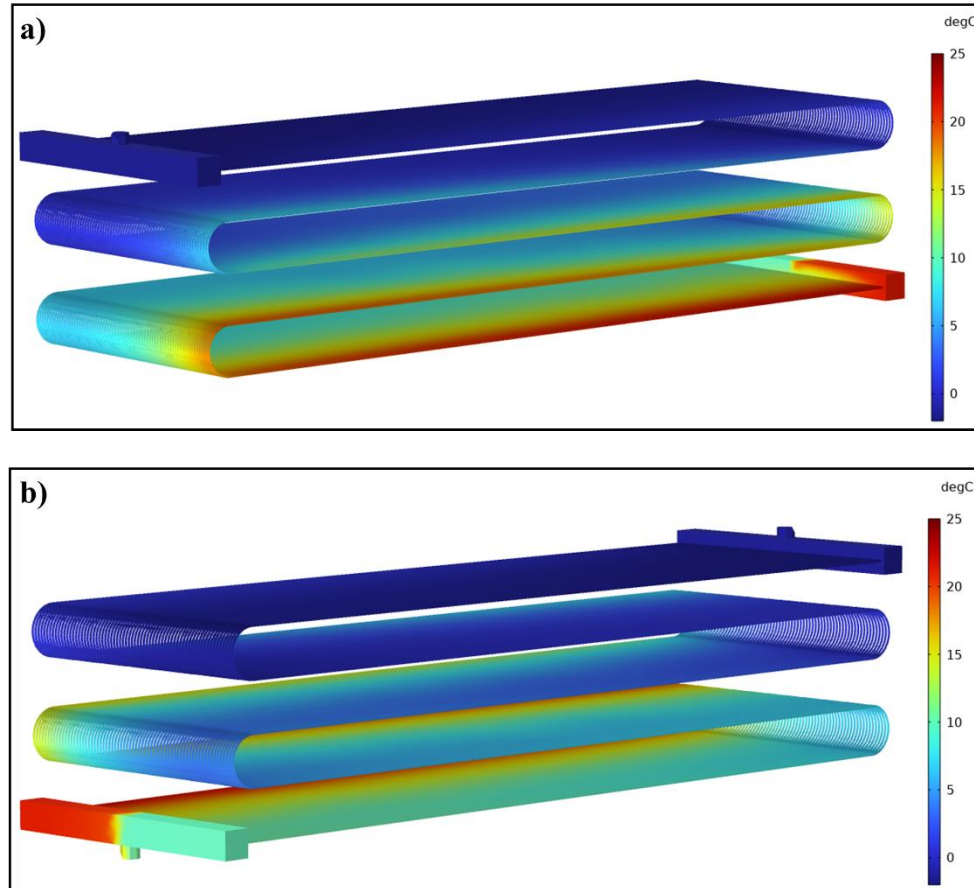


Figure 5.23. Cold heat transfer fluid minichannels temperature distribution by the end of the charging process for Case 1 (a) frontal view (b) backside view.

Following the charging process, the discharging process begins by shutting down the cold HTF at 500s. Based on the Figures 5.17 and 5.19, the outlet air and PCM temperatures initially rise with a sharp slope. This is because the average temperature of the PCM is below its melting point at this point, and there is mostly sensible heat transfer occurring between the PCM and airflow. When any specific point in the PCM reaches to its melting temperature range, a latent heat transfer occurs, enabling a prolonged heat transfer to the air, and delaying the airside temperature rise. As a result of this delay, additional air cooling could be provided during the cold fluid shutdown period. It is observed that extra thermal comfort by air cooling is provided at lower air mass flow rates. The discharged air cooling

time is defined by the time that the air outlet temperature remains below 29.5 °C in the discharging process. This value is attained 550, 410, and 290 seconds for the simulation cases, respectively. The cold liquid is shutdown in the discharging process and its heat transfer parameters are not analyzed for this process. As can be seen from both PCM plots, the PCM temperature rise and melting process occur faster with an increase in air mass flow rate. The melting point of the PCM, where the average solid fraction reaches to 0, is approached at simulation times of 845, 780, and 725s for the three cases, respectively. For effective PCM phase melting process and in order to provide sufficient cooling time during the discharging process, PCM-HEXs should be designed with an effective air flow rate.

5.3.1.2. Fluids Heat Transfer Rates

In Figure 5.24 the transient behavior of the rate of the airside cooling heat transfer rate during the charging and discharging processes is illustrated. The airside cooling rate appears to be increasing during the charging process. As the temperature of the outlet air reduces, a greater air temperature difference between the inlet and outlet is achieved, resulting in a rise in the airside heat transfer. The rise in the air heat transfer rate is observed to be more noticeable for higher air mass flow rates. When the air mass flow rate is increased, a greater amount of heat transfer is attained in the charging process. During the discharging process, the airside heat transfer rate drops sharply after the cold fluid is shutdown. The reason is that the cold fluid is shutdown and therefore the PCM is initially operating within its sensible heat transfer range. The slope of the heat transfer rate curve changes when the average PCM temperature is within its melting temperature range and transferring latent heat. For higher airflows, the latent heat transfer occurs faster, leading to a faster change of slope and higher heat rate trend during this period. As soon as the PCM is melted with complete latent heat transfer, another change of slope occurs for the curves with a sharp drop in the heat transfer rates, which results in a cross appearing between the curve cases during the discharging process. Once all the CTES stored in the PCM is extracted to the airside, the airside heat transfer is reached zero. The area under each curve in Figure 5.24 for the discharge process, indicates the total discharged heat transfer, which decreases with increasing mass flow rate during the discharging process. This result is confirmed with the experimental results attained by Askar et al. [33]. They observed a similar relationship between airside mass flow rate and air heat transfer with an

increase in airside flow rate in their experimental heat exchanger. Furthermore, this effect was diminished with increasing airflow rates based on their experimental results.

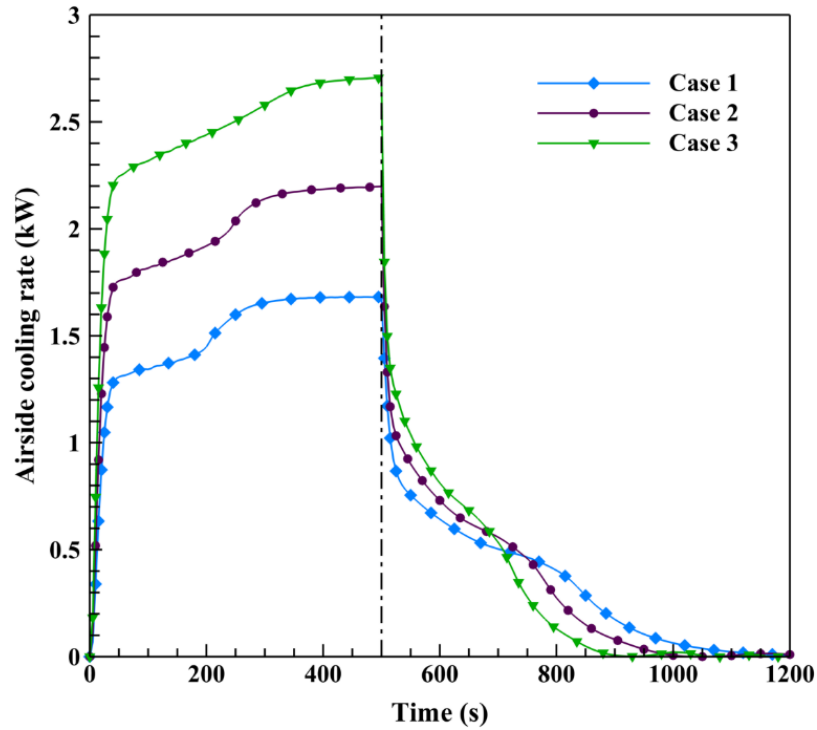


Figure 5.24. Airside heat transfer rates during the charging and discharging processes.

The heat transfer rate by the cold HTF in the charging process is represented dynamically in Figure 5.25. In the charging process, the coolant gains heat by providing cold thermal energy to the airstream and the PCM. Overall, the cold HTF heat rate drops in the charging process to reach to a steady state according to its outlet temperature behavior. It is seen that the cold liquid heat transfer rate is higher at higher airflow rates. This is due to the fact that the cold fluid outlet temperature rises more significantly at higher airflow rates, as discussed in the previous section, which results in a higher temperature differentiation and greater heat transfer rate.

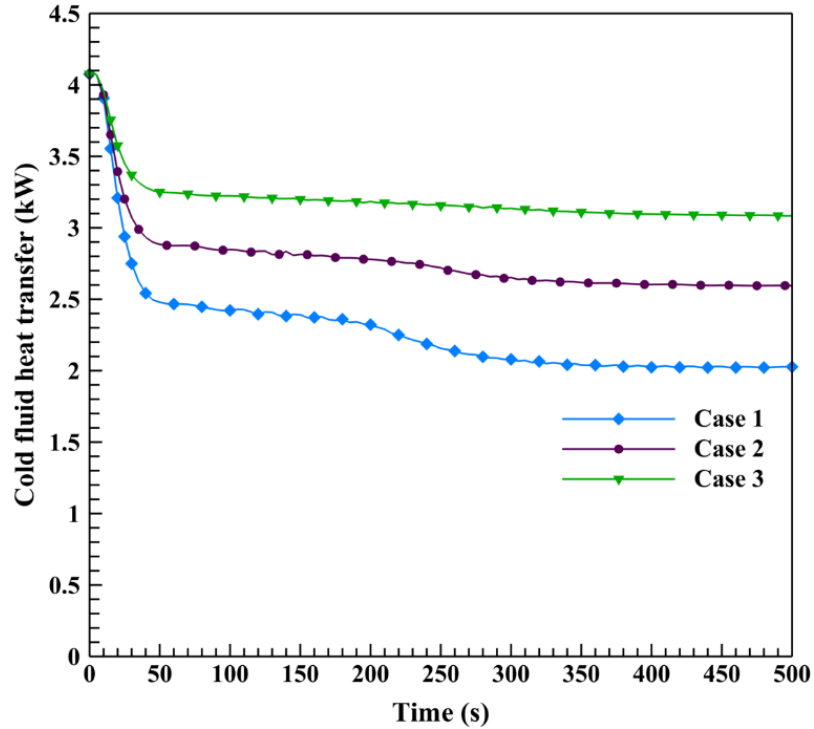


Figure 5.25. Cold fluid heat transfer rate during the charging process.

5.3.2. PCM Phase Transition Process

This section illustrates the solidification and melting processes of the PCM domain at various stages. Presented in Figures 5.26 and 5.27 are 3D contours of the solid phase fraction and temperature distribution of the PCM domain at three simulation times for simulation Case 1. The front and back views of the PCM domain are shown for a complete understanding of the PCM behavior at the incoming and outgoing of the air stream. The PCM domain is represented by two blocks that contain the PCM between the fins at the top of the heat exchanger. The cold fluid runs through the slab and channels located between the two blocks which works on charging the PCM. In the discharging process, the cold fluid is shutdown and the presence of fins in the airstream and the in the PCM plays a vital role in transferring the thermal energy through the heat exchanger body and fins to the PCM to initiate the melting process. Effective fin distribution inside the PCM domain allows suitable convective heat transfer from air and liquid to the PCM, thus proper phase transition is enabled. The PCM initial temperature is 30 °C at a solid fraction of 0 at the time of 0s.

It is observed from Figure 5.26 that at the time of 100s, the solidification is uniform at areas close to the inlet (left side) along the cold fluid flow and back of the heat exchanger. The solidification is higher on the back side of the heat exchanger due to the flow of hot air at the front which disturbs the solidification. Similar conclusion can be said to the bottom side of the PCM domain. The lower PCM block solidifies slower as it is larger than the top block. At this time of 100s, around 43% of the PCM is solidified with an average PCM temperature of 5.10 °C. At the end of the charging process, at 500s, most of the PCM block, of around 99% based on Figure 5.20, is solidified except for a small front and side regions due to direct contact with air. Looking at the temperature contours in Figure 5.27, it is evident that the temperature distribution is coordinated with the PCM phase transition process. The regions which possess lower temperatures correspond to higher solid fractions. It is seen that the regions facing the hot airflow have higher temperatures, and the regions closer to the liquid inlet possess lower temperatures in the charging process.

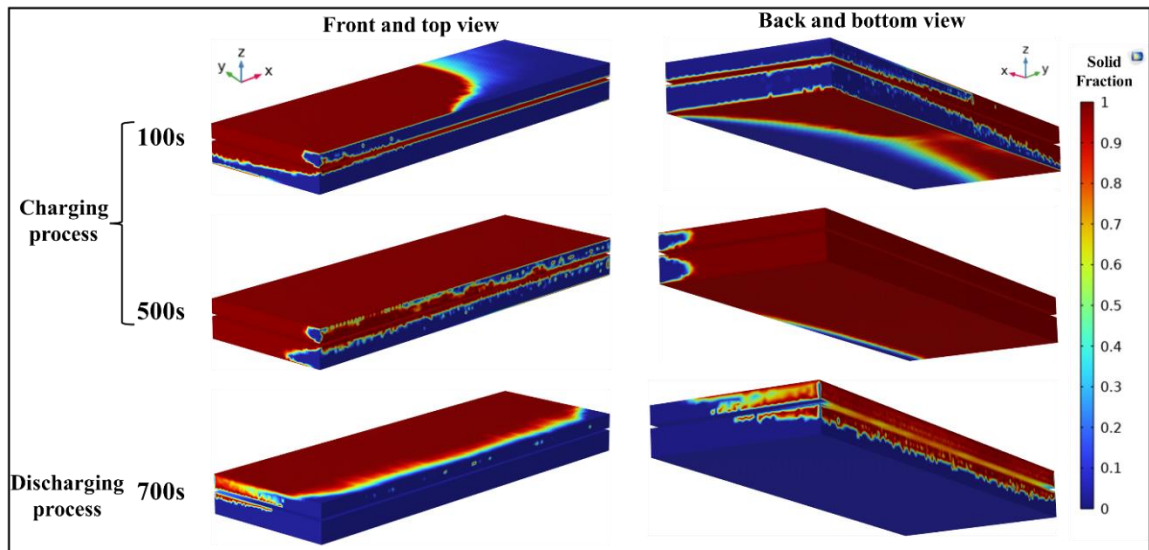


Figure 5.26. Phase fraction contours of the PCM domain during the charging and discharging processes for Case1

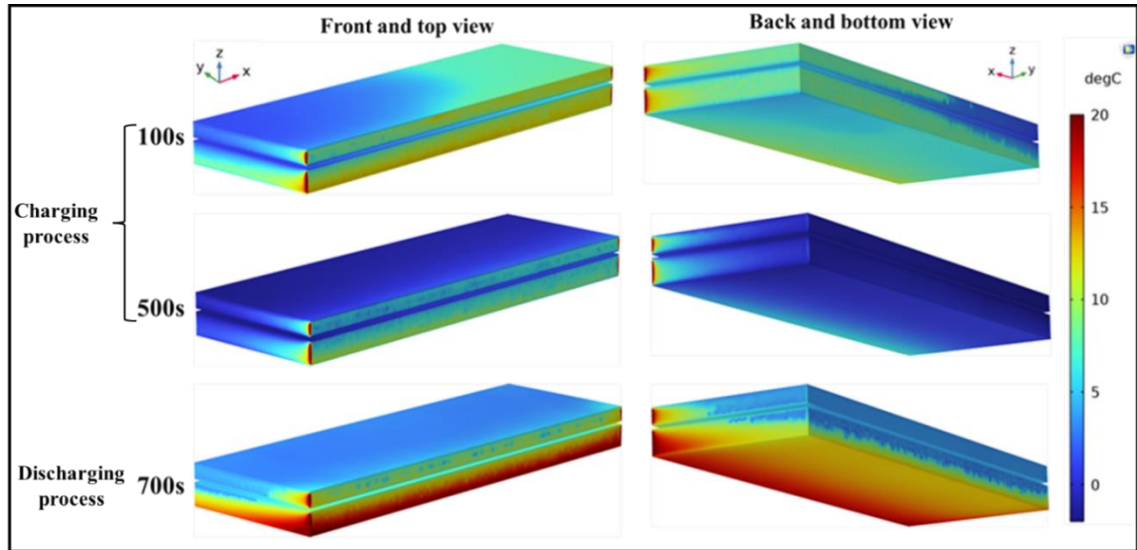


Figure 5.27. Temperature distribution through the PCM block for Case1.

The discharging process on the other hand is faster than the charging as seen in the phase fraction plots in Figure 5.20. The discharging process is shown in Figure 5.26 at the time of 700s where the PCM melts and releases its stored thermal energy. The heat is transferred from the hot air passing underneath the PCM blocks through the heat exchanger body and fins to the PCM. The fins distributed along the PCM blocks help in transferring the heat and melts the PCM. Therefore, the areas where the melting process starts are close to the bottom of the PCM blocks and the front side. The front and underneath sections of the PCM are clearly having higher temperatures and melt faster than other parts, while some areas in the back and top are still not melted. At this time at 700s, around 73% of the PCM is melted with an average PCM temperature of 8.64 °C. The melting process continues till the end of the discharging process at the time of 1200s at which the PCM is fully melted with an average solid fraction of 0 and temperature of around 30 °C.

5.3.3. Effective Passive Air Cooling Through PCM CTES

In this section, the effect of PCM usage as the main cooling source for the PCM-HEX in the discharging process is represented. Through CTES, valuable extra cooling load is provided in the discharging process, which enables extensive passive air cooling time for the heat exchanger.

5.3.3.1. PCM air cooling performance

The PCM effect on the air outlet temperature during the discharging process for simulation Case 1 is shown in Figure 5.28, where with and without PCM cases are compared. The No PCM model represents the heat exchanger and the fluids at the same operating conditions with the exclusion of the PCM domain in the top part. After the cold fluid shutdown, the air outlet temperature starts rising and the PCM is triggered to discharge. The No PCM case initially starts from a lower temperature due to more cooling provided to the airside in the charging process compared to the case of with PCM. It is seen that a temperature of 29.5 °C takes 550s to attain for the case of with PCM compared to only 80s for the case of No PCM. It can be concluded that the use of PCM extends cooling time by 470s thus delays the rise in air outlet temperature.

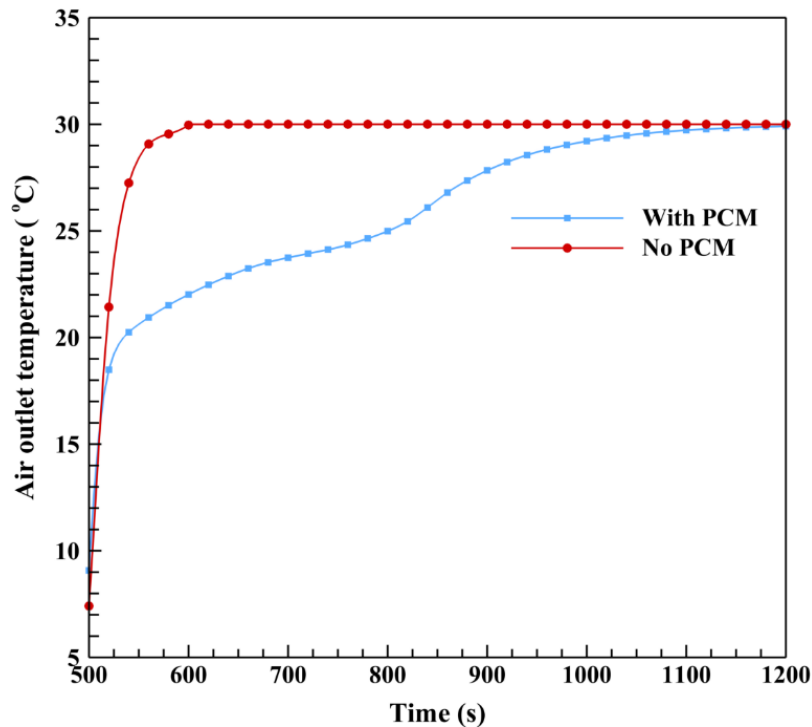


Figure 5.28. Discharged air outlet temperature comparison for Case 1 of with and without PCM.

The cooling rate provided to the airside during the discharging process is attained based on air inlet and outlet temperature difference, as presented and discussed in Figure 5.24. It is assumed that all the air's cooling energy comes from the PCM during the discharging process, thus ignoring the heat that is lost from the heat exchanger's body. Accordingly, the total discharged cooling heat transfer rate corresponds to the amount of cooling energy

gained from the PCM by the airflow. In Figure 5.29, the air-cooling heat transfer rate in the discharging process for simulation Case 1 is compared for the cases of with and without PCM. The heat transfer rate is sharply reduced in the case of the No PCM, as the air outlet temperature increases when the coolant is shutdown, resulting in smaller airside temperature difference. It is evident from the graph that the PCM has a significant effect in providing extra cooling load during the coolant shutdown. The PCM extends the air cooling period and delays the rise in air outlet temperature. Throughout the graphs in Fig. 14, the area beneath the curves represents the total amount of cooling load discharged by the PCM for air cooling. This value is achieved by integration at 231.23 kJ when PCM is implemented and at 42.98 kJ when PCM is not implemented. Consequently, by integrating the areas between the No PCM and with PCM curves, 188.25 kJ of energy is released from the PCM as cold thermal energy, which is used to cool the hot air. This area is colored between the curves for clear representation.

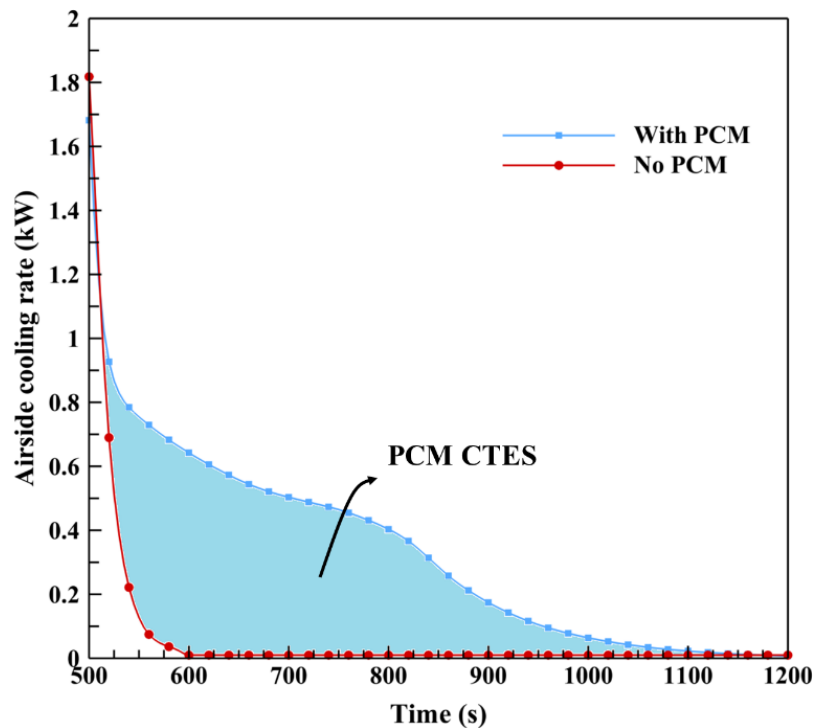


Figure 5.29. PCM effect on the discharged air-cooling rate for Case 1.

Table 5.2 compares key energy results attained for the three PCM simulation cases and the No PCM case during the discharging process. The air-cooling time discharged cooling load, and the share of PCM latent heat are presented. The air-cooling time was shown in previous sections based on the air outlet temperature discussed in Figure 5.17. It is noted that lower airflow rates can provide a higher discharged cooling load, resulting in a longer air-cooling time. The latent heat share is calculated based on the ratio percentage between the total amount of latent heat provided by the PCM in the discharging process to the total amount of discharged cooling load. The total latent heat stored in the PCM is calculated by multiplying the PCM mass by its specific latent heat of fusion, attained as 120.90 kJ. The PCM mass is reported as 0.58 kg by space integration through its volume, considering a uniform mass. It is observed that at lower air mass flow rates, the share of latent heat is attained slightly lower due to the higher discharged cooling load. This parameter is found to be over 50% for all simulation cases, with an average of 53.59% discharged latent heat share observed for the simulation cases. In the next section, the dynamic behavior of the share of PCM sensible and latent heat during the discharging process is presented.

Table 5.2. Key PCM air cooling results attained during the discharging process for different simulation cases.

	Case 1	Case 2	Case 3	No PCM
Air cooling time (s)	550	410	290	80
Discharged cooling load (kJ)	231.23	226.98	218.93	42.98
Latent heat share (%)	52.29	53.26	55.22	-

5.3.3.2. Latent heat transfer analysis

The trend of PCM latent heat rate in the discharging process is computed in this section in order to determine the dynamic share of latent heat in the discharging process. It was seen that at the initial state of the discharging process, 120.90 kJ of latent heat was stored in the PCM. This latent heat drops gradually coordinated with its solid fraction seen in Figure 5.20. By plotting the latent heat trend in the discharging process, the rate of the latent heat is attained by the derivation of the heat-time plot. The total discharged cooling rate, along with the latent and sensible heat rates for simulation Case 1 is presented in Figure 5.30. The sensible portion of discharged heat transfer is calculated by the subtraction of the latent heat rate from the total cooling rate. The dynamic share of latent heat is calculated and

plotted by the percentage of the share of latent heat to the total cooling rate. As observed, initially, the rate of latent heat provided by the PCM for air cooling starts at a low value. This is because the average volume temperature of the PCM is initially below its melting point, meaning that mostly sensible heat transfer occurs in most of the PCM domain to reach to the melting point. This causes a sharp drop in the cooling heat rate, which heat is mostly transferred by sensible heat from the PCM to the airside. During this stage, the PCM absorbs heat until the majority of the PCM reaches its melting temperature, and the latent heat transfer rate along with the share of latent heat reaches its maximum value. As a glimpse of the melting transition, assuming an interval between 540 and 760s, where maximum melting is occurring, an average heat rate of 0.58 kW for latent and 0.16 kW for sensible heat transfer is observed. The share of latent heat is within its peak during this process, with an average value of 72.86% attained. In the following, the latent heat drops while most of the PCM is discharged, and the sensible heat rate overtakes. After the PCM is fully melted, latent heat transfer ends, and sensible heat transfer overlaps the total heat rate plot until the thermal system reaches to a steady state.

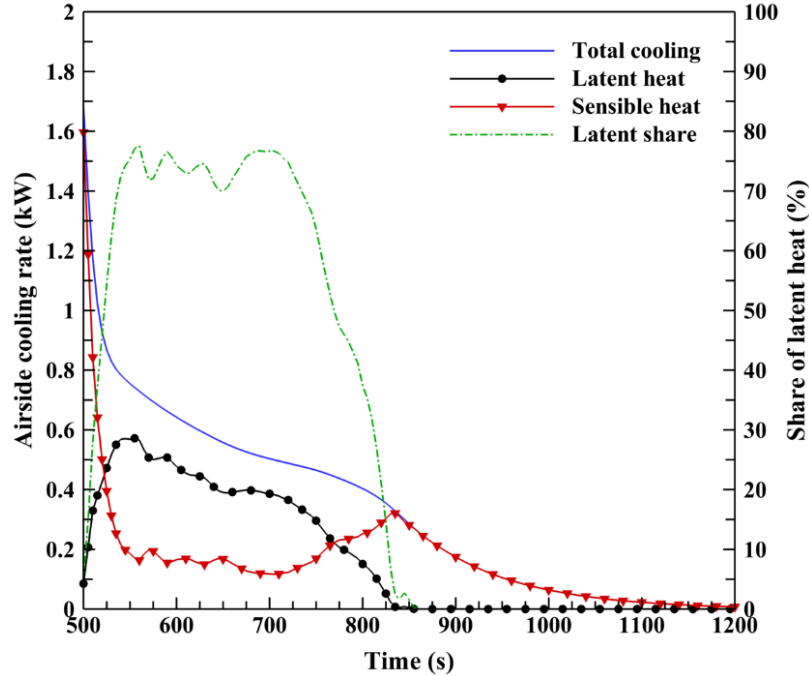


Figure 5.30. Trends of PCM sensible and latent heat rates in Case 1 discharging process.

Latent heat analysis is a crucial factor in representing the performance of the PCM in thermal systems. Designing compact PCM-HEXs which could operate with a high share of latent heat is ideal. It is recommended for further research focus on designing optimized PCM-air-liquid heat exchangers based on the PCM mass and location, as well as the higher specific latent heat and proper melting points. Effective design of LHTES systems could further develop TES and extend the amount of cooling/heating periods in PCM-HEXs.

CHAPTER 6

CONCLUSIONS AND RECOMMENDATIONS

6.1. Conclusions

In this study, an innovative PCM heat exchanger based on air and liquid flow is studied with the purpose of storage and release of thermal energy to provide extra heating and cooling time for the airside during liquid heat transfer fluid shutdown periods. The PCM is integrated into a compact cross flow heat exchanger having minichannel liquid flow. In order to improve the PCM's thermal performance and efficiently transfer thermal energy stored in the PCM to the airflow, fins are distributed inside the PCM medium and throughout the heat exchanger. A numerical heat transfer and fluid flow analysis is conducted based on a 3D CFD simulation to investigate the heat exchanger's dynamic response during the PCM charging and discharging processes. The numerical model was validated with the experimental setup with the same geometry and operating conditions. Three studies were performed on two heat exchanger design models. The heat exchangers' dynamic performance was analyzed and compared through three air mass flow rates at 0.08, 0.15, and 0.30 kg/s. The significant attained results in the research are presented in the following:

6.1.1. Air heating study

- During the PCM charging process, the PCM is fully melted with a latent heat energy storage of 151 kJ. In this process, increasing the airflow rate causes a drop in the fluids' outlet temperature while it increases the PCM melting time and the fluids' heat transfer rate.
- In the PCM discharging process, the PCM solidification time decreases by increasing the airflow rate. Lower discharged thermal energy and heating time are observed by increasing the airflow rate.
- By PCM thermal energy storage, in contrast to without PCM implementation, the heat exchanger provides an additional heat load of 247 kJ released to the airside in the discharging process. This heating load results in 355 seconds of additional air heating time attained.

- The share of latent heat provided by the PCM to the total heat transfer in the discharging process is considered the PCM effectiveness. This share is slightly enhanced by the increase in airflow rate from 47 to 50% between the simulation cases.

6.1.2. Air cooling study

- During the PCM charging process, the vast majority of the PCM was solidified, resulting in 121 kJ storage of latent cold thermal energy.
- In the PCM discharging process, faster PCM melting time was found with the increase in air mass flow rate. Also, lower cold thermal energy and cooling time for PCM air cooling resulted.
- The use of PCM resulted in over 9 minutes of extra passive air-cooling time and a cold thermal energy release of 188 kJ during the discharging process for simulation Case 1.
- The total share of latent heat provided by the PCM in the discharging process was increased by higher air mass flow rates and attained an average of 54% of the total heat transfer for the simulation cases.

The results found in this study provide a robust basis for understanding the advantage of the designed system. The PCM-air-liquid heat exchanger provides additional air heating/cooling time, potentially reducing fuel consumption, and attaining environmental benefits. The proposed system is a viable solution for the real-world application of cabin thermal comfort in hybrid and electric vehicles to increase system performance and attain air heating/cooling during short periods of engine shutdown.

6.2. Recommendations

This study provides valuable and detailed insights into the current limited knowledge about heat transfer performance analysis in compact PCM heat exchangers. The use of a thermal energy storage of PCM into a compact two-fluid heat exchanger has rarely been studied numerically due to numerical complexity of design and multiphysics simulation of the study. These highly beneficial results enrich the data base of such studies and develop a basis for future researchers to advance the study further. Below are some recommendations for future study:

- Incorporating enhanced types of PCMs for improved thermal performance, with increased latent heat or improved thermal conductivity.
- Examining the effects of different fin specifications on the charging and discharging processes as well as the thermal properties of the PCM.
- Enhancing fluid heat transfer properties by adding nanoparticles to the liquid.
- Optimizing the PCM heat exchanger with attaining maximum latent heat share of heat transfer from the PCM to the airside.
- Improvements to the design of the heat exchanger that incorporate the PCM. The PCM could be implemented between the heat exchanger slabs or inside the fins.

REFERENCES

- [1] U.S.E.I.A.O.o.E. Analysis. International Energy Outlook EIA 2019 with projections to 2050., 20585. U.S. Department of Energy, Washington, DC2019.
- [2] N.R. Canada. Canada Energy factbook. (2020-2021).
- [3] I.E.A. IEA. Cooling on the Move, the future of air conditioning in vehicles. 2019.
- [4] M. Simion, L. Socaciu, P. Unguresan. Factors which Influence the Thermal Comfort Inside of Vehicles. *Energy Procedia*. 85 (2016) 472-80.
- [5] a.S.D.P. Shah R. K. Fundamentals of heat exchanger design". Hoboken,. John Wiley & Sons. (2003).
- [6] M.-u.G.K. Mohammed Ismail, Amir Fartaj. Numerical Investigation on Heat Transfer and Fluid Flow Behaviors of Viscous Fluids through Minichannel Heat Exchanger. University of Windsor2012.
- [7] S. Fotowat, S. Askar, A. Fartaj. Transient response of a meso heat exchanger with temperature step variation. *International Journal of Heat and Mass Transfer*. 122 (2018) 1172-81.
- [8] W.-T. Yan, C. Li, W.-B. Ye. Numerical investigation of hydrodynamic and heat transfer performances of nanofluids in a fractal microchannel heat sink. *Heat Transfer—Asian Research*. 48 (2019) 2329-49.
- [9] C.K. Mangrulkar, A.S. Dhoble, S. Chamoli, A. Gupta, V.B. Gawande. Recent advancement in heat transfer and fluid flow characteristics in cross flow heat exchangers. *Renewable and Sustainable Energy Reviews*. 113 (2019) 109220.
- [10] H. Li, N. Wang, B. Zhao, H. Feng, K. Han, S. He, et al. Simulation study on the effect of fins on the heat transfer performance of horizontal dual-inner-tube latent thermal energy storage heat exchangers. *Journal of Energy Storage*. 49 (2022) 104125.
- [11] L. Kalapala, J.K. Devanuri. Influence of operational and design parameters on the performance of a PCM based heat exchanger for thermal energy storage – A review. *Journal of Energy Storage*. 20 (2018) 497-519.
- [12] L. Yang, X. Jin, Y. Zhang, K. Du. Recent development on heat transfer and various applications of phase-change materials. *Journal of Cleaner Production*. 287 (2021) 124432.
- [13] A.S. Fleischer. *Thermal Energy Storage Using Phase Change Materials*. Springer Cham 2015.
- [14] A. Sharma, V.V. Tyagi, C.R. Chen, D. Buddhi. Review on thermal energy storage with phase change materials and applications. *Renewable and Sustainable Energy Reviews*. 13 (2009) 318-45.
- [15] S. Askar. Transient experimental study of a latent heat thermal energy storage in a phase change material-air-liquid heat exchanger. University of Windsor2022.
- [16] K. Faraj, M. Khaled, J. Faraj, F. Hachem, C. Castelain. Phase change material thermal energy storage systems for cooling applications in buildings: A review. *Renewable and Sustainable Energy Reviews*. 119 (2020) 109579.
- [17] F. Souayfane, F. Fardoun, P.-H. Biwole. Phase change materials (PCM) for cooling applications in buildings: A review. *Energy and Buildings*. 129 (2016) 396-431.
- [18] J. Albadr, S. Tayal, M. Alasadi. Heat transfer through heat exchanger using Al₂O₃ nanofluid at different concentrations. *Case Studies in Thermal Engineering*. 1 (2013) 38-44.

- [19] G. Huminic, A. Huminic. Application of nanofluids in heat exchangers: A review. *Renewable and Sustainable Energy Reviews*. 16 (2012) 5625-38.
- [20] M. Ismail, S. Fotowat, A. Fartaj. Effect of Channel Size on Heat Transfer and Pressure Drop in Thin Slabs Minichannel Heat Exchanger. *International Journal of Mechanical Engineering and Mechatronics*. 2 (2014) 33-42.
- [21] P. Moorthy, A.N. Oumer, M. Ishak. Experimental Investigation on Effect of Fin Shape on the Thermal-Hydraulic Performance of Compact Fin-and-Tube Heat Exchangers. *IOP Conference Series: Materials Science and Engineering*. 318 (2018) 012070.
- [22] S. Basavarajappa, G. Manavendra, S.B. Prakash. A review on performance study of finned tube heat exchanger. *Journal of Physics: Conference Series*. 1473 (2020) 012030.
- [23] M.M. Altwieb, R.; Aliyu, A.M.; Kubiak, K.J. Heat Transfer Enhancement by Perforated and Louvred Fin Heat Exchangers. *Energies* (2022).
- [24] A.K. Saleem, M.-H. Inside Thermal Performance of Louvered Fin Flat-Tube Heat Exchangers with Different Redirection Louvers. *Energies* (2022).
- [25] A. Ereğ, B. Özerdem, L. Bilir, Z. İlken. Effect of geometrical parameters on heat transfer and pressure drop characteristics of plate fin and tube heat exchangers. *Applied Thermal Engineering*. 25 (2005) 2421-31.
- [26] F.A. Siddiqui, E.S. Dasgupta, A. Fartaj. Experimental investigation of air side heat transfer and fluid flow performances of multi-port serpentine cross-flow mesochannel heat exchanger. *International Journal of Heat and Fluid Flow*. 33 (2012) 207-19.
- [27] S.A. Shahram Fotowat, Amir Fartaj. Transient Response Comparison of a Conventional and a Meso Heat Exchanger under Mass Flow and Temperature Step Changes. *Journal of Fluid Flow, Heat and Mass Transfer*. 8 (2021).
- [28] S. Fotowat, S. Askar, A. Fartaj. Experimental transient response of a minichannel heat exchanger with step flow variation. *Experimental Thermal and Fluid Science*. 89 (2017) 128-39.
- [29] S. Abdallah, S. Rooke. Transient Response of a Serpentine Finned-Tube Cross-Flow Heat Exchanger to a Step Change in Inlet Temperature. *Heat Transfer Engineering*. 18 (1997) 51-60.
- [30] G. Yalcin, O. Ataer. Effect of Fins on Transient Behavior of Cross-Flow Air-Liquid Heat Exchangers. *Iif - iir*. (1988).
- [31] K. Silaipillayarputhur, S.A. Idem. Transient Response of a Cross Flow Heat Exchanger Subjected to Temperature and Flow Perturbations. 2015.
- [32] S. Alotaibi, M. Sen, B. Goodwine, K.T. Yang. NUMERICAL SIMULATION OF THE THERMAL CONTROL OF HEAT EXCHANGERS. *Numerical Heat Transfer, Part A: Applications*. 41 (2002) 229-44.
- [33] S. Askar, S. Fotowat, A. Fartaj. Transient experimental investigation of airside heat transfer in a crossflow heat exchanger. *Applied Thermal Engineering*. 199 (2021) 117516.
- [34] M. Mishra, P.K. Das, S. Sarangi. Transient behaviour of crossflow heat exchangers due to perturbations in temperature and flow. *International Journal of Heat and Mass Transfer*. 49 (2006) 1083-9.
- [35] M. del Valle, A. Ortega. Experimental Characterization of the Transient Response of Air/Water Crossflow Heat Exchangers for Data Center Cooling Systems 2015.
- [36] T. Gao, B. Sammakia, J. Geer. Dynamic response and control analysis of cross flow heat exchangers under variable temperature and flow rate conditions. *International Journal of Heat and Mass Transfer*. 81 (2015) 542-53.

- [37] A. Shahsavari, A. Shaham, Ç. Yıldız, M. Arıcı. Entropy generation characteristics of phase change material in a variable wavy walled triplex tube latent heat storage unit for battery thermal management system. *Journal of Energy Storage*. 51 (2022) 104374.
- [38] Ç. Susantez. Numerical investigation of latent heat thermal energy storage unit with different configurations and phase change materials. *Journal of Energy Storage*. 54 (2022) 105279.
- [39] I. Sarbu, C. Sebarchievici. *A Comprehensive Review of Thermal Energy Storage*. Sustainability 2018.
- [40] S. Chavan, R. Rudrapati, S. Manickam. A comprehensive review on current advances of thermal energy storage and its applications. *Alexandria Engineering Journal*. 61 (2022) 5455-63.
- [41] W. Wang, X. Yang, Y. Fang, J. Ding, J. Yan. Enhanced thermal conductivity and thermal performance of form-stable composite phase change materials by using β -Aluminum nitride. *Applied Energy*. 86 (2009) 1196-200.
- [42] L. Fan, J.M. Khodadadi. Thermal conductivity enhancement of phase change materials for thermal energy storage: A review. *Renewable and Sustainable Energy Reviews*. 15 (2011) 24-46.
- [43] T.-P. Teng, C.-C. Yu. Characteristics of phase-change materials containing oxide nano-additives for thermal storage. *Nanoscale Research Letters*. 7 (2012) 611.
- [44] H. Ji, D.P. Sellan, M.T. Pettes, X. Kong, J. Ji, L. Shi, et al. Enhanced thermal conductivity of phase change materials with ultrathin-graphite foams for thermal energy storage. *Energy & Environmental Science*. 7 (2014) 1185-92.
- [45] P. Sivasamy, A. Devaraju, S. Harikrishnan. Review on Heat Transfer Enhancement of Phase Change Materials (PCMs). *Materials Today: Proceedings*. 5 (2018) 14423-31.
- [46] S. Rana, M. Zunaid, R. Kumar. CFD analysis for heat transfer comparison in circular, rectangular and elliptical tube heat exchangers filled with PCM. *Materials Today: Proceedings*. 56 (2022) 637-44.
- [47] M. Rahimi, A.A. Ranjbar, D.D. Ganji, K. Sedighi, M.J. Hosseini. Experimental Investigation of Phase Change inside a Finned-Tube Heat Exchanger. *Journal of Engineering*. 2014 (2014) 641954.
- [48] M. Akgün, O. Aydın, K. Kaygusuz. Experimental study on melting/solidification characteristics of a paraffin as PCM. *Energy Conversion and Management*. 48 (2007) 669-78.
- [49] M. Gorzin, M.J. Hosseini, M. Rahimi, R. Bahrapoury. Nano-enhancement of phase change material in a shell and multi-PCM-tube heat exchanger. *Journal of Energy Storage*. 22 (2019) 88-97.
- [50] K.Y. Leong, S. Hasbi, B.A. Gurunathan. State of art review on the solidification and melting characteristics of phase change material in triplex-tube thermal energy storage. *Journal of Energy Storage*. 41 (2021) 102932.
- [51] M. Mozafari, A. Lee, S. Cheng. Simultaneous energy storage and recovery in triplex-tube heat exchanger using multiple phase change materials with nanoparticles. *Journal of Energy Storage*. 49 (2022) 104164.
- [52] M. Teggari, S.S.M. Ajarostaghi, Ç. Yıldız, M. Arıcı, K.A.R. Ismail, H. Niyas, et al. Performance enhancement of latent heat storage systems by using extended surfaces and porous materials: A state-of-the-art review. *Journal of Energy Storage*. 44 (2021) 103340.

- [53] N. Bianco, A. Fragnito, M. Iasiello, G.M. Mauro, L. Mongibello. Multi-objective optimization of a phase change material-based shell-and-tube heat exchanger for cold thermal energy storage: experiments and numerical modeling. *Applied Thermal Engineering*. 215 (2022) 119047.
- [54] M. Medrano, M.O. Yilmaz, M. Nogués, I. Martorell, J. Roca, L.F. Cabeza. Experimental evaluation of commercial heat exchangers for use as PCM thermal storage systems. *Applied Energy*. 86 (2009) 2047-55.
- [55] M.E.H. Amagour, A. Rachek, M. Bennajah, M. Ebn Touhami. Experimental investigation and comparative performance analysis of a compact finned-tube heat exchanger uniformly filled with a phase change material for thermal energy storage. *Energy Conversion and Management*. 165 (2018) 137-51.
- [56] M.E.H. Amagour, M. Bennajah, A. Rachek. Numerical investigation and experimental validation of the thermal performance enhancement of a compact finned-tube heat exchanger for efficient latent heat thermal energy storage. *Journal of Cleaner Production*. 280 (2021) 124238.
- [57] Y. He, W. Yuan, J. Cao, L. Li, Z. Ling. Compact latent heat exchanger for the fast supply of hot water with serpentine tubes in shape-stabilized composite phase change material and auxiliary electric heating. *Applied Thermal Engineering*. 211 (2022) 118469.
- [58] M. Ouzzane, M. Bady. Investigation of an innovative Canadian well system combined with a frozen water/PCM heat exchanger for air-cooling in hot climate. *Applied Thermal Engineering*. 213 (2022) 118737.
- [59] F. Herbinger, M. Bhourri, D. Groulx. Investigation of heat transfer inside a PCM-air heat exchanger: a numerical parametric study. *Heat and Mass Transfer*. 54 (2018) 2433-42.
- [60] S. Askar, S. Fotowat, M. Momeni, A. Fartaj. Transient experimental study of a latent heat thermal energy storage in a heat exchanger for effective thermal management. *Journal of Energy Storage*. 55 (2022) 105680.
- [61] S. Kahwaji, M.B. Johnson, A.C. Kheirabadi, D. Groulx, M.A. White. A comprehensive study of properties of paraffin phase change materials for solar thermal energy storage and thermal management applications. *Energy*. 162 (2018) 1169-82.
- [62] W.-B. Ye, C. Li, S. Gong, Y. Hong, S.-M. Huang, S. Xu. STUDY ON THERMAL UNIFORMITY AND IMPROVEMENT FOR THE DRYING OF LITHIUM-ION BATTERIES. 46 (2019) 487-98.
- [63] W.-B. Ye. Thermal simulation and evaluation for non-uniformity detection of electrode. *Applied Thermal Engineering*. 96 (2016) 583-92.
- [64] W.-B. Ye, C. Li, S.-M. Huang, Y. Hong. VALIDATION OF THERMAL MODELING OF UNSTEADY HEAT SOURCE GENERATED IN A RECTANGULAR LITHIUM-ION POWER BATTERY. 50 (2019) 233-41.
- [65] J. Du, Y. Hong, S. Wang, W.-B. Ye, S.-M. Huang. Experimental thermal and flow characteristics in a traverse corrugated tube fitted with regularly spaced modified wire coils. *International Journal of Thermal Sciences*. 133 (2018) 330-40.
- [66] B. Rivière. Discontinuous Galerkin methods for solving elliptic and parabolic equations. *Society for Industrial and Applied Mathematics*. (2008).
- [67] E. Süli, D.F. Mayers. *An Introduction to Numerical Analysis*. Cambridge University Press, Cambridge, 2003.

- [68] N. Nigro, M. Storti, S. Idelsohn, T. Tezduyar. Physics based GMRES preconditioner for compressible and incompressible Navier-Stokes equations. *Computer Methods in Applied Mechanics and Engineering*. 154 (1998) 203-28.
- [69] O. Schenk, K. Gärtner. Solving unsymmetric sparse systems of linear equations with PARDISO. *Future Generation Computer Systems*. 20 (2004) 475-87.
- [70] A.D. Brent, V.R. Voller, K.J. Reid. ENTHALPY-POROSITY TECHNIQUE FOR MODELING CONVECTION-DIFFUSION PHASE CHANGE: APPLICATION TO THE MELTING OF A PURE METAL. *Numerical Heat Transfer*. 13 (1988) 297-318.
- [71] A. Bejan. *Convection Heat Transfer*. John Wiley & Sons 2013.
- [72] H. Niyas, S. Prasad, P. Muthukumar. Performance investigation of a lab-scale latent heat storage prototype – Numerical results. *Energy Conversion and Management*. 135 (2017) 188-99.
- [73] W.-T. Yan, W.-B. Ye, C. Li. Effect of aspect ratio on saturated boiling flow in microchannels with nonuniform heat flux. *Heat Transfer—Asian Research*. 48 (2019) 3312-27.

VITA AUCTORIS

NAME: Mahdi Momeni

PLACE OF BIRTH: Arak, Iran

YEAR OF BIRTH: 1997

EDUCATION: Nemooneh High School, Arak, Iran, 2015

K.N. Toosi University of Technology, B.Sc.,
Tehran, Iran, 2020

University of Windsor, M.Sc., Windsor, ON, 2023

ProQuest Number: 30248104

INFORMATION TO ALL USERS

The quality and completeness of this reproduction is dependent on the quality and completeness of the copy made available to ProQuest.



Distributed by ProQuest LLC (2023).

Copyright of the Dissertation is held by the Author unless otherwise noted.

This work may be used in accordance with the terms of the Creative Commons license or other rights statement, as indicated in the copyright statement or in the metadata associated with this work. Unless otherwise specified in the copyright statement or the metadata, all rights are reserved by the copyright holder.

This work is protected against unauthorized copying under Title 17, United States Code and other applicable copyright laws.

Microform Edition where available © ProQuest LLC. No reproduction or digitization of the Microform Edition is authorized without permission of ProQuest LLC.

ProQuest LLC
789 East Eisenhower Parkway
P.O. Box 1346
Ann Arbor, MI 48106 - 1346 USA